Active Network Management and Uncertainty Analysis in Distribution Networks

Zhou, Lin

Award date:
2015

Awarding institution:
University of Bath

Active Network Management and Uncertainty Analysis in Distribution Networks

By
Lin Zhou
BEng, SMIEEE

The thesis submitted for the degree of

Doctor of Philosophy

in
The Department of
Electronic and Electrical Engineering
University of Bath

June 2015

Signature:…… Date:……

ABSTRACT

In distribution networks, the traditional way to eliminate network stresses caused by increasing generation and demand is to reinforce the primary network assets. A cheaper alternative is active network management (ANM) which refers to real-time network control to resolve power flow, voltage, fault current and security issues.

However, there are two limitations in ANM. First, previous ANM strategies investigated generation side and demand side management separately. The generation side management evaluates the value from ANM in terms of economic generation curtailment. It does not consider the potential benefits from integrating demand side response such as economically shifting flexible load over time. Second, enhancing generation side management with load shifting requires the prediction of network stress whose accuracy will decrease as the lead time increases. The uncertain prediction implies the potential failure of reaching expected operational benefits. However, there is very limited investigation into the trade-offs between operational benefit and its potential risk.

In order to tackle the challenges, there are two aspects of research work in this thesis.

1) Enhanced ANM. It proposes the use of electric vehicles (EVs) as responsive demand to complement generation curtailment strategies in relieving network stress. This is achieved by shifting flexible EV charging demand over time to absorb excessive wind generation when they cannot be exported to the supply network.

2) Uncertainty management. It adopts Sharpe Ratio and Risk Adjust Return On Capital concepts from financial risk management to help the enhanced ANM make operational decisions when both operational benefit and its associated risk are considered. Copula theory is applied to further integrate correlations of forecasting errors between nodal power injections (caused by wind and load forecasting) into uncertainty management.

The enhanced ANM can further improve network efficiency of the existing distribution networks to accommodate increasing renewable generation. The cost-benefit assessment informs distribution network operators of the trade-off between investment in ANM strategy and in the primary network assets, thus helping them to make cost-effective investment decisions. The uncertainty management allows the impact of risks that arise from network stress prediction on the expected operational benefits to be properly assessed, thus extending the traditional deterministic cost-benefit assessment to cost-benefit-risk assessment. Moreover, it is scalable to other systems in any size with low computational burden, which is the major contribution of this thesis.

CONTENT

ACKNOWLEDGEMENT

Firstly, I would like to express my deepest appreciation to my supervisor Prof. Furong Li for her helpful guidance and support during my PhD life.

I would like to take this opportunity to express my ultimate gratitude to my family for their endless support and encouragement.

I would also like to thank my colleagues, Mr. Xing Tong, Dr. Chenghong Gu, Dr. Ignacio Hernando Gil, Dr. Rohit Bhakar, Dr. Kang Ma, Miss Jie Yan, Dr. Ran Li, Mr. Jiangtao Li, Miss Chen Zhao, Mr. Zhipeng Zhang, Mr. Heng Shi, Mr. Minghao Xu, Miss Wei Wei, Miss Heather Wyman-Pain for discussing with me, and sharing knowledge and useful resources with me.

I would also like to express my heartfelt gratefulness to my previous fellow colleagues, Dr. Chenchen Yuan, Dr. Zhimin Wang, Dr. Zhanghua Zheng, Dr. Yan Zhang and Dr. Bo Li who gave me much inspiration, and many constructive suggestions.

And, I would also thank all my friends in the University of Bath, including Mr. Huiming Zhang, Mr. Maomao Zhang, Miss Lifen Chen, Miss Hui Tang, Miss Jiangning Gao for their help during my PhD life.

Special thanks also to Dr. Zechun Hu from Tsinghua University and Dr. Shufeng Dong from Zhejiang University for their support during my research.

In addition, I am sincerely grateful for the Graduate School Scholarship that University of Bath provided me for my three year PhD study.

LIST OF ABBREVIATION

AC	Alternate Current
ANM	Active Network Management
AuRA-NMS	Autonomous Regional Active Network Management System
CDF	Cumulative Distribution Function
CO2	Carbon Dioxide
CSP	Constraint Satisfaction Problem
DC	Direct Current
DECC	Department of Energy & Climate Change
DG	Distributed Generator
DNOs	Distribution Network Operators
DSM	Demand Side Management
EVs	Electric Vehicles
IRR	Internal Rate of Return
LIFO	Last-In-First-Off
LTDF	Load Transfer Distribution Factor
NPV	Net Present Value
PS	Probabilistic Sequence
PTDF	Power Transfer Distribution Factor
RAROC	Risk Adjusted Return On Capital
SR	Sharpe Ratio
UK	the United Kingdom
VAR	Value At Risk

LIST OF FIGURE

LIST OF TABLE

LIST OF MATHEMATICAL SYMBOLS

i	Busbar Number i
l	Overloaded Line Number l
t	Timeslot
P_{gi}	Generation Output at Busbar i
P_{di}	Load Demand at Busbar i
ΔP_{gi}	Generation Curtailment at Busbar i
P_{gi}^{min}	Lower Limit of the Generation Output at Busbar i
P_{gi}^{max}	Upper Limit of the Generation Output at Busbar i
PTDF(l,i)	PTDF Value between Line l and Busbar i
P_{l}^{max}	Line Rating of Line l
L	Set of Lines in the Network
NG	Set of Generation in the Network
NB	Set of all Busbars in the Network
i_s	The Slack Bus
P_l	Power Flow on Line l
P_{ndi}	New Load Demand at Busbar i
ND	Set of Busbars with Load Demand
$\Delta P_{di,t}$	Load Shifting Capability at Busbar i at Timeslot t
$EV_{i,t}$	Flexibility of EVs at Busbar i at Timeslot t
LTDF(l,i)	LTDF Value between Line l and Busbar i
CN_i	Customer Number on Busbar i
D_i	Annual Load Demand on Busbar i
η_i	Percentage of Domestic Consumption on Busbar i
ADD_i	Average Domestic Electricity Consumption on Busbar i
B_c	Typical EV Battery Capacity
$S_{v,t}$	the State-of-energy of Vehicle v at Timeslot t

δ_{min}	Minimum Coefficient of Battery Capacity
δ_{max}	Maximum Coefficient of Battery Capacity
$S_{t,min}$	Minimum State-of-energy of Batteries at Timeslot t
$S_{t,max}$	Maximum State-of-energy of Batteries at Timeslot t
$C_{t,min}$	Minimum EV Charging Demand at Timeslot t
$C_{t,max}$	Maximum EV Charging Demand at Timeslot t
NEV	Number of EVs on Individual Busbar
$S_{t-1,min}$	Minimum State-of-energy of Batteries at Timeslot t-1
$S_{t-1,max}$	Maximum State-of-energy of Batteries at Timeslot t-1
$P_{dr,t+1}$	Driving Electricity Consumption of EVs over Timeslot t+1
P_{ch}	Charging Rate of EVs
$N_{undrv,t}$	Number of EVs that are Stopped at Timeslot t
$S_{1,min}$	Minimum State-of-energy at the End of 1^{st} Hour
$S_{1,max}$	Maximum State-of-energy at the End of 1^{st} Hour
$P_{dr,2}$	Driving Electricity Consumption in 2^{nd} Hour
S_t	State-of-energy of a Large Fleet of EVs
C_t	Charging Amount of a Large Fleet of EVs
y	Year y
B_y	Operational Benefit in Year y
EP_y	Electricity Price in Year y
GC_y	Annual Generation Curtailment Reduction in Year y
C_y	Network Investment Cost in Year y
AC_y	Cost of Asset Investment in Year y
ANM_y	Cost of Investing ANM in Year y
DSM_y	Cost of DSM in Year y
PV	Present Value of Future Investment
d	Discount Rate

Asset	Modern Equivalent Assets Cost
n	Time to Reinforce Network
y_0	Year 2011
T	Shifting EV Load Based on the Congestion at Timeslot T (Trial T)
$GC_{T,t}$	Generation Curtailment at Timeslot t after Implementing Trial T
$GC_{0,t}$	Generation Curtailment at Timeslot t without EV Load Shifting
GCR_T	Generation Curtailment Reduction of Trial T
TWS	Time-window Scale
$Priority_t$	Shifting Priority of Timeslot t
$OL_{l,t}$	Line Overloading on Line l at Timeslot t
w_{EV}	Weight of EV Flexibility
w_{OL}	Weight of Line Overloading
ΔR	the Profit/Loss of a Portfolio over a Fixed Horizon
IC	Initial Investment Cost
R	the Future Rate of Return
μ_R	Mean Rate of Return
σ_R	Standard Deviation (Volatility) of Rate of Return
R_F	Risk-free Rate of Return
$\{x_t\}$	Raw Data Sequence of Observations
$\{s_t\}$	Smoothed Output Statistics
α	Smoothing Factor
$\{x_{t-1}\}$	Previous Observation
$\{s_{t-1}\}$	Previous Smoothed Statistic
$\{X_{t+m}\}$	Output of Double Exponential Smoothing Method
m	Lead Time of Forecasting
a_t	Estimated Level at Timeslot t
b_t	Estimated Trend at Timeslot t
$\{x_{w,t}\}$	Sequential Actual Real-time Data of Wind Generation

$f(PF_{T,t,l})$	Probability Density Function of Power Flow on Line l at Timeslot t
$\otimes$	Convolution Symbol
$\mu_{P_{T,t,i}}$	Mean Value of Power Injection on Busbar i at Timeslot t in Trial T
$\mu_{PF_{T,t,l}}$	Mean Value of Power Flow on Line l at Timeslot t in Trial T
$\sigma_{P_{T,t,i}}$	Standard Deviation of Power Injection on Busbar i at Timeslot t
$\sigma_{PF_{T,t,l}}$	Standard Deviation of Power Flow on Line l at Timeslot t in Trial T
$\mu_{OL_{T,t,l}}$	Mean Value of Line Overloading of Line l at Timeslot t
$\sigma_{OL_{T,t,l}}$	Standard Deviation of Line Overloading of Line l at Timeslot t
$\mu_{GC_{0,t}}$	Mean Value of $GC_{0,t}$
$\sigma_{GC_{0,t}}$	Standard Deviation of $GC_{0,t}$
$\mu_{GC_{T,t}}$	Mean Value of $GC_{T,t}$
$\sigma_{GC_{T,t}}$	Standard Deviation of $GC_{T,t}$
$\mu_{GC_{T,t,l,i}}$	Mean Value of Generation Curtailment on Busbar i Caused by Line l at Timeslot t
$\sigma_{GC_{T,t,l,i}}$	Standard Deviation of Generation Curtailment on Busbar i Caused by Line l at Timeslot t
$\mu_{GC_{T,t,l}}$	Mean Value of Generation Curtailment Caused by Line l at Timeslot t
$\sigma_{GC_{T,t,l}}$	Standard Deviation of Generation Curtailment Caused by Line l at Timeslot t
CN	Busbars with Generation Curtailment
M	Set of Overloaded Lines
$GCR_T^{'}$	Generation Curtailment Reduction of Trial T when Uncertainty is Considered
GCR’	Generation Curtailment Reduction when Uncertainty is Considered
LP	Typical Load Pattern Set
M_{ij}	Transfer Matrix of Load Pattern from the Reference Day to Forecasted Day
$\{X_{L,t+m}\}$	Sequential Forecasting Data of Load Demand

$\{X_{W,t+m}\}$	Sequential Forecasting Data of Wind Generation
$\{E_{P,t+m}\}$	Sequential Forecasting Errors of Nodal Power Injections
$f_a(a)$	Probability Density Function of Variable a
$f_b(b)$	Probability Density Function of Variable B
Δd	Discretisation Interval
A(i)	Discrete Probability Sequences of Variable a
B(i)	Discrete Probability Sequences of Variable b
N_a	Maximum Integer Less than $a_{max}/\Delta d$
N_b	Maximum Integer Less than $b_{max}/\Delta d$
c	Confidence Level
$f(PF_{0,t,l})$	Probability Density Distribution of Power Flow on Line l at Timeslot t without Load Shifting
$VAR_{PF_{0,t,l}}$	VAR of Power Flow on Line l at Timeslot t without Load Shifting
$VAR_{GC_{0,t}}$	VAR of Generation Curtailment at Timeslot t without Load Shifting
$VAR_{GC_{0,t,l}}$	VAR of Generation Curtailment to Relieve Line Overloading on Line l at Timeslot t without Load Shifting
$VAR_{GC_{T,t}}$	VAR of Generation Curtailment at Timeslot t in Trial T
$RAROC_T$	RAROC value of Trial T
$F_a(a)$	Cumulative Distribution Function of Variable a
$F_b(b)$	Cumulative Distribution Function of Variable b
$f_{ab}(a,b)$	Joint Probability Density Function of Variable a and b
$F_{ab}(a,b)$	Joint Probability Function of Variable a and b
$C(\cdot)$	Copula Function
$c(\cdot)$	Probabilistic Density Function of $C(\cdot)$
$\emptyset^{-1}(\cdot)$	Inverse Function of Standard Normal Distribution
ρ	Correlation Parameter
τ	Kendall Rank Correlation Coefficient

CHAPTER 1. INTRODUCTION

This chapter briefly introduces the background, motivation, challenges, objectives, and contributions of this thesis. It also provides an outline of the thesis.

1.1. New Environment for Power System

Countries over world are promoting increasing proportion of energy sourcing from renewable sources. The main drivers are global awareness of environmental pollution caused by Carbon Dioxide (CO2) emissions, depletion of domestic fossil fuels reserves and significant global energy demand growth. The United Kingdom (UK) has set up a target of 15% of energy from renewables by 2020 [1]. The binding target is expressed as a percentage of total energy use, including electricity, heat and transport. Fig. 1-1 displays the renewable generation from 2008 to 2012 in the UK, and makes estimations of renewable generation required to meet the 2020 target.

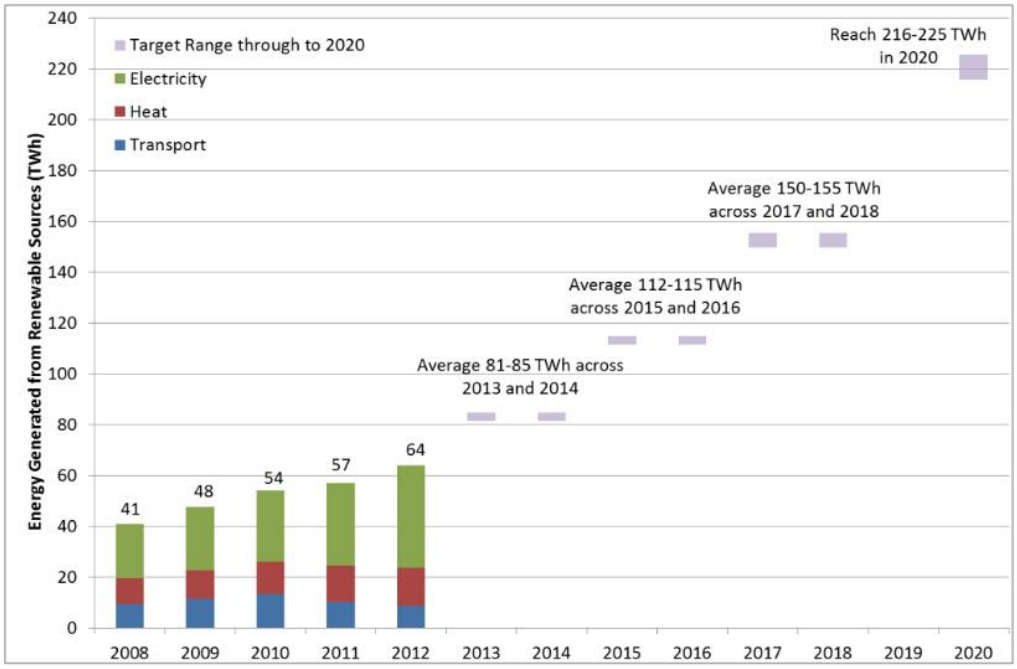

Figure 1-1 Progress in Renewable Electricity, Heat and Transport [1]

Driven by the 2020 renewable target, a massive increase in renewable distributed generation is required in the existing UK distribution network. The UK currently has 4GW of operational onshore wind capacity to generate around 7TWh of electricity annually, contributing to 1.95% of the total electricity generation. The government document indicates that onshore wind could contribute up to around 13GW by 2020 [2] .

Beyond the renewable distributed generation, electrification of vehicles and heating is also expected to grow substantially in the future, particularly from 2030 onwards, to

help meet the 15% target. By the year 2030, the number of Electric Vehicles (EVs) would reach 2.142 million in the UK [3]. It is predicted that electrification of vehicles and heating could add an additional ~5-15% to electricity demand in 2030. The government has set up a transport sub-target of 10% of its energy usage for all forms of transport be sourced from renewable sources by 2020.

The distribution networks are traditionally designed to deliver energy from grid supply points to end customers. They have limited capacity to accommodate significantly increasing renewable generation and load demand. This can lead to severe network pressure and significant energy losses during peak times in the current passive distribution network, particularly for areas dominated by renewable generation. For example, excessive generation will lead to reverse power flow, and cause the power flow to exceed the existing line capacity at times.

The traditional approach to increase network capacity for accommodating generation and demand growth is to reinforce the present network or build new lines, which is costly, time-consuming and environmentally unfriendly. In addition, very limited control is applied in the existing network. For instance, currently in the UK, constraint management for power flow management generally follows the Last-In-First-Off (LIFO) rule [4]. It means the last-in distributed generator (DG) will be the first to be tripped off or curtailed once an overloading is detected, regardless of its ability to alleviate network pressure. This results in unnecessary waste of renewable generation [5]. Thus, Smart Grid concept is becoming a hot issue, being promoted by many governments around the world. Being equipped with interactive communication systems, smart sensing and metering, remote measurement infrastructure, a smart grid will transform the current system to deliver energy more efficiently, securely and reliably [6].

In the UK, Distribution Network Operators (DNOs), which are licensed companies for electrical energy distribution authorized by the Office of Gas and Electricity Markets, play an important role in actively looking for alternative Active Network Management (ANM) to accommodate the increasing DGs with lower network investment. By enhancing system operational control and better utilising of the existing network capacity, ANM can improve the efficiency of existing network, maintain the security of

supply and defer new assets investment when accommodating increasing DGs [7].

1.2. Research Motivation

1.2.1. Motivation 1

ANMs are promoted to undertake active control of the network, acting upon real-time information, to resolve voltage, power flow, fault current and network security issues caused by increasing DGs. From a technical perspective, ANM strategies can be classified into four categories [8-13]:

1) Demand side management;
2) Voltage and power flow management;
3) Fault current management;
4) Advanced distribution protection.

This thesis focuses on power flow management to relive network congestion, i.e. congestion management. 'Congestion management' means to manage the outputs of DGs so that the line ratings will not be exceeded due to the connection of DGs. The goal of congestion management is to minimise system operation costs or maximise the connected DG capacity, subject to system operating constraints such as power balance, generation loading limits and network capacity constraints [4, 14-22].

However, previous congestion management strategies are only implemented on the generation side. The operational benefits are determined by transferring the reduction amount of annual generation curtailment into economic perspective. Previous strategies did not consider the potential benefit from demand side responses, particularly from flexible demand such as EVs.

Some demand side management (DSM) strategies have taken advantage of the flexibility of EVs' charging/discharging mode to optimise network operation since EVs can be regarded as energy storages that can smooth intermittency of renewable energy. If EVs' charging demand can be coordinately shifted to absorb excess renewable generation before generation constraint management, the load curve could be optimised

to align with both intermittent wind generation curve and power flow condition in the network, resulting in more local renewable energy being used to support local customers.

1.2.2. Motivation 2

Previous congestion management strategies use real-time network data to control the generation devices determinately in time sequence. When it is enhanced through integrating DSM, i.e. economically shifting flexible load demand over time, it requires the prediction of network stress.

In practice, due to the intermittency of wind, inaccuracy of wind forecasting cannot be neglected even for one-hour ahead forecasting. Average reported error for the wind forecasting is in the order of 10%~20% of the installed power for a 24-hour ahead forecasting [23]. Although load forecasting error is much smaller than wind [23], the network condition will still be dramatically influenced since load is an important network parameter.

Therefore, there are significant uncertainties in predicting network stress due to the uncertain wind and load. Traditional deterministic network operation approaches are not sufficient to capture the impact of network uncertainties on system operation. An appropriate uncertainty management should be established to understand and quantify the impacts of wind and load forecasting errors on the enhanced congestion management.

1.3. Research Challenges

1.3.1. Enhancing Congestion Management by Integrating Intelligent EV Charging

The DSM strategies of EVs can be classified into three categories according to their different objectives: technical, economic and combined techno-economic objectives

[24]. In this thesis, in order to alleviate network stresses, the optimal EV charging will be determined to minimise network generation curtailment, which belongs to technical objective. The most efficient busbar to relieve network stress should be determined for EV load shifting. The constraints concerning EV battery characteristics and customer driving behaviours should also be considered in the optimal EV load shifting.

1.3.2. Cost-Benefit Assessment of the Enhanced Congestion Management

An appropriate way to assess the cost-benefit of combining previous congestion management with intelligent EV charging should be established. The impacts of the enhanced congestion management on the long-term network planning should also be evaluated, providing evidence for DNOs to make economic investment decisions. In long-term network planning, the operational benefits in different years should be converted into an equivalent present value to help DNOs make final network investment decisions.

1.3.3. Uncertainty Management in the Enhanced Congestion Management

Since intelligent EV charging refers to economically shifting EV demand over time, when congestion management is enhanced by intelligent EV charging, it requires the prediction of network stress. The prediction of network stress will be highly uncertain due to wind and load forecasting errors. The characteristics of wind and load forecasting errors are not the same. In general, the error scale of wind forecasting is higher than load [23]. In addition, wind forecasting error increases as forecasting time horizon increases, while load forecasting error does not always increase with the lead time.

Thus, it is challenging to appropriately define the characteristics of wind and load forecasting errors and convert them into the errors in network stress prediction. Moreover, since network stresses predicted under differing lead time have varying uncertainty levels, it becomes difficult to optimally shift EV load demand over time

when both operational benefit and its associated risk should be considered.

1.3.4. Integrating Correlations between Nodal Power Injections into Uncertainty Management

Since wind forecasting is strongly dependent on weather condition in an area, the wind forecasting errors on different busbars in the area have strong correlations. The load forecasting errors on different busbars somehow also have correlations since weather do influence the electricity consumption pattern. Thus, forecasting errors of the nodal power injections between busbars are correlated.

However, in the calculation of deterministic power flow, the nodal power injections are assumed to be independent. Therefore, the correlations introduced from wind and load forecasting should be properly defined, expressed in a mathematical way and integrated into the uncertainty management strategy to increase the accuracy of network stress forecasting.

1.4. Research Objectives

This thesis attempts to achieve the following targets:

1) To enhance the previous congestion management by integrating demand side responses, i.e. by incorporating intelligent EV charging into generation curtailment strategy, so that the generation curtailment could be further minimised, and the security of supply can be maintained at a lower cost;

2) To assess the cost-benefit of the enhanced congestion management, so that evidence for cost-effective long-term network planning that strike the right balance between operational benefits and investment cost could be provided to DNOs;

3) To establish a proper uncertainty management strategy to extend the traditional deterministic cost-benefit assessment to cost-benefit-risk assessment, so that the

errors from wind and load forecasting could be properly incorporated into the enhanced congestion management;

4) To improve the uncertainty management by integrating the correlations between nodal power injections (caused by wind and load forecasting), so that the prediction of network stress could be more accurate.

1.5. Main Contributions

The main contributions of this thesis are listed as follows:

1) Applying DSM realized by intelligently shifting flexible EV load demand over time to the previous congestion management, where cost-benefit assessment is implemented to evaluate its performance and alternative network planning suggestions are given;

2) Enhancing intelligent EV charging with bi-directional charging optimisation strategy and more comprehensive charging constraints;

3) Proposing an uncertainty management strategy based on Sharpe Ratio (SR) method to allow the impact of risks that arise from network stress prediction on the expected operational benefits to be properly assessed, thus extending the traditional deterministic cost-benefit assessment to cost-benefit-risk assessment. The proposed strategy is scalable to any systems with low computational burden, which is the major contribution of this thesis.

4) Proposing enhanced uncertainty management method called Risk Adjusted Return On Capital (RAROC) to evaluate the effects of both wind and load forecasting errors on the enhanced congestion management, where the forecasting errors are allowed to be in any distribution;

5) Applying Copula theory to integrate the effects of correlations between nodal power injections into RAROC method, giving more accurate network stress prediction and a more convincing stochastic congestion management strategy.

1.6. Thesis Outline

The rest of the thesis is organised as follows.

Chapter two gives an overview of low carbon distribution network in the near future, where the development of renewable distributed generation and EVs are estimated. The chapter also introduces the development of ANM strategies in the UK distribution networks, followed by detailed explanation of the previous congestion management.

Chapter Three describes how the previous congestion management could be improved by adding intelligent EV charging. The charging strategy is operated by optimally shifting flexible EV charging demand over time to maximally reduce network stress as well as generation curtailment to the maximum possible extent. A case study is presented to model the future of the 33kV Aberystwyth network. The simulation results are analysed to assess the cost-benefit of the enhanced congestion management in the distribution network and its influence on network planning.

Chapter Four improves the intelligent EV charging model by optimising EV charging to be bi-directional and enhancing the EV flexibility with network power flow constraint. The simulation results prove that with the two improvements, EV charging model can reduce network pressure and generation curtailment further to a larger extent.

Chapter Five proposes an uncertainty management strategy for the enhanced congestion management by adopting SR concept from financial sector. The uncertainty in this chapter only refers to wind forecasting error, which is also assumed to follow normal distribution. Monte Carlo Simulation is utilised to justify the normal distribution assumption. The results indicate that SR method is straight forward and scalable. It can properly extend the traditional deterministic cost-benefit assessment to cost-benefit-risk assessment, so that the errors from wind forecasting could be incorporated into the enhanced congestion management.

Chapter Six adopts an enhanced financial concept RAROC based on SR to address the limitation in SR method, i.e. the distribution of variables must be normal distribution.

Independent sequence operation theory is applied to derive the uncertain power flow when both wind and load forecasting errors are considered. RAROC method extends the feasibility of uncertainty management by allowing the forecasting errors to be in any distribution.

Chapter Seven utilises Copula theory to define and visualise the impacts of correlations between nodal power injections (caused by the correlations in wind and load forecasting) on the enhanced congestion management. Dependent operation theory is used to integrate the correlations in the calculation of uncertain power flow. A case study is well-analysed to prove that integrating correlations can give more accurate network stress prediction and a more convincing stochastic congestion management strategy.

Chapter Eight summarises the key findings and the major contributions of this thesis. Some potential research topics are presented as future work.

CHAPTER 2. BACKGROUND AND LITERATURE REVIEW

This chapter gives an overview of the development and new challenges in future low carbon distribution networks. The state-of-art of the existing ANM strategies are reviewed and the key limitations are identified.

2.1. Introduction

Nowadays, the global climate change raises concerns of environmental pollution caused by greenhouse gas emissions from fossil fuel. Hence, the world now encourages the utilisation of renewable energy in society to reduce CO2 emission. A majority of renewable generators are expected to be connected to the existing distribution networks which are traditionally designed to deliver energy from grid supply points to end customers. They have limited capacity to accommodate significant renewables. This can lead to severe network pressure and significant energy losses during generation peak times, particularly for areas dominated by renewable generation. The traditional way to provide the extra network capacity is to reinforce the capacity of existing circuits or to construct new circuits, which is expensive, time-consuming, and environmentally unfriendly.

ANM has emerged as a cheaper alternative to accommodate growing generation and demand. ANM refers to coordinated control of multiple network components in real-time to resolve power flow, voltage, fault current and security issues caused by increasing embedded generation in distribution networks. Through better utilisation of existing network capacity, ANM can strike the right trade-offs between building new network assets and enhancing system operational performance.

This chapter reviews the development of low carbon distribution networks in the near future and a range of existing ANM strategies. This thesis focuses on active congestion management. Previous congestion management evaluates the value of ANM only in terms of economic generation curtailment. If the congestion management could be further improved by using flexible load demand as responsive demand to complement network stress relief, both the network stresses and waste of green energy can be significantly reduced, providing smarter distribution networks.

2.2. Renewable Energy Generation

The UK has signed the European Union Renewable Energy Directive, which includes a UK target of 15% of energy from renewables by 2020. This target is equivalent to a

seven-fold increase in UK renewable energy consumption from 2008 levels [25]. To meet the targets for that proportion of renewable energy in the UK energy mix, government needs to maximise the utilisation of renewable energy generation. Several kinds of renewable energy, such as wind, solar, biomass, incremental hydro and close–loop thermal energy, are under development with governments' support. In capacity term, wind power dominates the renewable energy market most at present. As shown in [26], the total operating wind power capacity in the world has grown from 2GW in 1990 to over 74GW by the end of year 2006. The operating wind power capacity is predicted to be 260GW by the end of year 2020. Paper [27] gives the international rankings of wind power capacity as shown in Table 2-1. Now, the United State and China rank at the first two positions in terms of both installed wind power capacity and cumulative wind power capacity.

Table 2-1 International Rankings of Wind Power Capacity

Annual Capacity (2009, MW)		**Cumulative Capacity (end of 2009, MW)**	
China	13,750	the United State	35,155
the United State	9,994	China	25,853
Spain	2,331	Germany	25,813
Germany	1,917	Spain	18,784
India	1,172	India	10,827
Italy	1,114	Italy	4,845
France	1,104	France	4,775
U.K.	1,077	U.K.	4,340
Canada	950	Portugal	3,474
Portugal	645	Denmark	3,408
Rest of World	4,121	Rest of World	22,806
Total	**38,175**	**Total**	**160,080**

According to the government document [2], the UK now has more than 4GW of installed onshore wind capacity in operation which generate approximately 7TWh of electricity every year. Most wind farms are established in Scotland (~2.5GW) because of its abundant wind resource, followed by England (~0.9GW), Wales (~0.4GW) and Northern Ireland (~0.3GW). Onshore wind is predicted to contribute up to around 13GW by 2020 as shown in Fig. 2-1, which requires an annual growth rate of 13%.

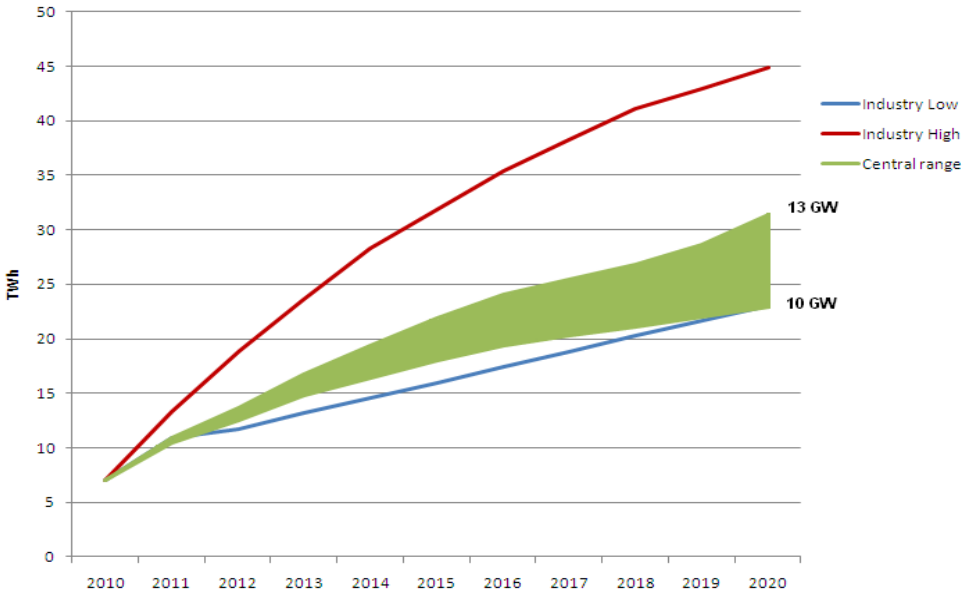

Figure 2-1 Deployment Potential to 2020 for Onshore Wind [2]

Document [2] also gives some data about UK's offshore wind generation. Now the UK is global leader for offshore wind energy. It has 1.3GW of operational capacity across 15 wind farms, which generated over 3TWh of electricity during 2010. The UK will keep this lead role till 2020 and beyond. Fig. 2-2 from [2] indicates that up to 18GW of capacity could be deployed by 2020. Beyond 2020, the country has a very high probability to generate over 40TWh of electricity from offshore wind by 2030.

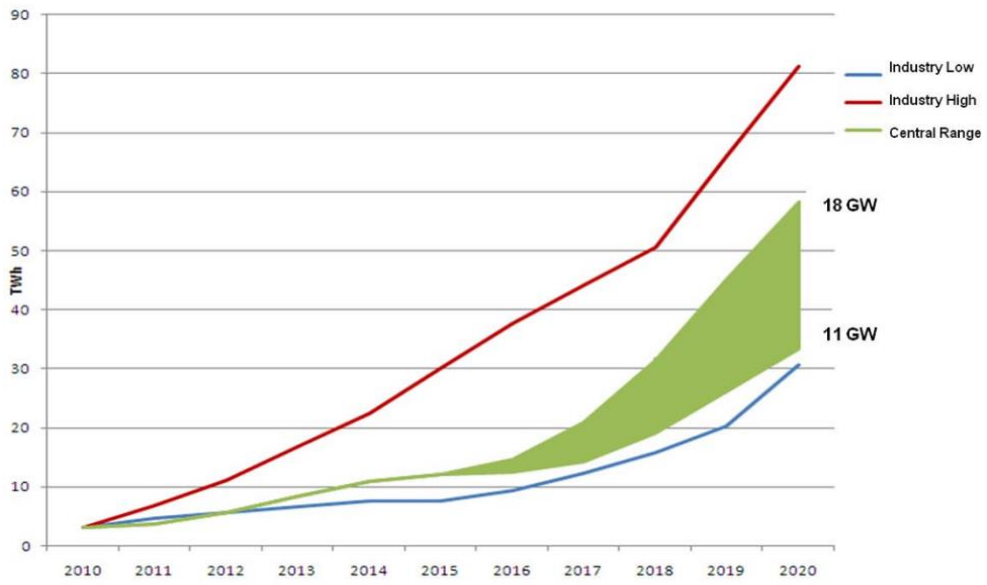

Figure 2-2 Deployment Potential to 2020 for Offshore Wind [2]

2.3. Active Network Management

With the increasing renewable generation connected to the distribution networks, although the CO2 emission can be reduced to a large extent, the generation will burden the existing distribution systems.

Distribution networks are traditionally designed to be unidirectional for only connecting and supplying demand. They supply a large amount of customers with electricity from a few central power generators. So the network operation is passive. The existing networks follow the so called "fit and forget" policy to connect DGs, which means that control problems should be solved at the planning stage by providing adequate network capacity [28]. Once the circuit is constructed, and energised, it is left to operate in isolation. Although voltages and currents may be monitored, there will be minimal follow up action in the control timeframe to alter the network based on these measurements [12]. Thus, increasing renewable DGs introduce new challenges to distribution system operators in operating and planning their networks, particularly how can they maintain security of supply at a value to their customers.

There are four main interconnected technical issues [8-12]:

1) Power flow management. With the increasing DGs, the total installed generation could surpass the local load demand and start exporting power back to the main grid. The power flow changes from unidirectional to bidirectional, resulting in network congestion and a failure risk in equipment's thermal ratings;
2) Voltage control. The reversed power flow caused by the connection of DGs will lead to voltage rise effect, particularly in rural networks;
3) Fault level. The connection of DG may lead to breach of circuit breaker ratings when network is operating close to its fault level ;
4) Network security. The power quality of intermittent generation sources poses a big challenge to maintain the high level of power quality customers demanded.

The traditional way to address network stresses is to construct new circuits or reinforce the capacity of existing circuits. However, building primary network assets is expensive, time-consuming, and has a negative effect in environment, such as dust emissions and noise during construction and upgrading activities. In addition to the cost, seeing any

network reinforcement through the appropriate planning processes can also be a discouragement.

Therefore, the necessity for distribution network evolving from the usual passive unidirectional flow network to active distribution networks is being proposed [7, 10, 29, 30]. Active distribution network has been defined as 'a network where real-time management of voltage, power flows and even fault levels is achieved through a control system either on site or through a communication system between the network operator and the control devices' [31]. In one word, active distribution networks have systems in place to control a combination of distributed energy resources (generators, loads and storage) [10].

Report [32] gives a long definition for ANM: 'ANM is understood to mean systems that operate to take action automatically to maintain networks within their normal operating parameters. For example, this may be controlling generator output, reactive power flow, use of dynamic ratings, island operation and automatic synchronisation. The lines between automation, protection and ANM are blurred. However, at a simplistic level, the protection is to manage fault situations safely and automation is to return the network to normal operation once the fault is cleared. ANM operates pre-emptive action to maintain networks within their normal operating parameters. ANM is of greater use as the level of distributed generation increases and the number of possible variables increases. ANM may also involve variables that up to now have not been controlled such as managing demand. Existing network protection is not considered part of ANM however ANM could have an impact on the operation of protection and therefore this work further seeks to ascertain what protection schemes are available'.

In short, ANM can be defined as coordinated control of multiple network components in real-time to resolve power flow, voltage, fault current and security issues caused by the increasing embedded generation to ensure the regulatory status of distribution networks.

Previous work in [9, 33] introduced associated research challenges, potential solutions and the corresponding impact of ANM on distribution networks. ANM plays a

significant role in maximizing the utilisation of existing network capacity to meet demand growth and national targets for renewable energy. Its benefits are being recognised by governments and the electricity supply sectors. Paper [33] claimed that ANM can potentially accommodate up to three time as much generation.

Paper [13] classifies completed and ongoing active management projects into 11 key technical areas: Active Management Planning, Communications and Control, Demand Side Management, Fault Level Management, Future Technologies, Modelling and Analysis, Power Flow Management, Power Quality, Protection Systems, Storage and Voltage Control. These areas can be further sorted out in four categories:

1) Voltage and power flow management;
2) Demand side management;
3) Fault current management;
4) Advanced distribution protection.

2.3.1. Voltage Control and Power Flow Management

2.3.1.1. Voltage Control

Traditionally, voltage problems are avoided by selecting line reactance and resistance carefully in the planning stages [9]. Currently, coordinated management of the voltage level at the substation, voltage profile on the network (e.g. voltage drop) and generation curtailment appears to be the most efficient solution to support both generation and demand in the distribution networks without significant capital expenditure [34-37].

Report [33] deals with voltage rise effects caused by the connection of DGs through: 1) active power generation curtailment; 2) reactive power management; 3) area based coordinated voltage control of On Load Tap Changing Transformers; and 4) application of voltage regulators. Through the active voltage control, the most distant customer can be kept above the lower voltage limit under the maximum load condition and all customers can be kept below the upper voltage limit under the minimum load condition. The load conditions are neglected.

2.3.1.2. Power Flow Management

Power flow management, i.e. congestion management, means to manage the ouputs of DGs so that the line ratings will not be exceeded due to the connection of DGs. The strategies for power flow management can come under one of three categories: pre-fault constraints, post-fault constraints and real-time control of generation [38]. The current advanced management requires generator control to be dependent on reliable real-time measurements and robust Supervisory Control And Data Acquisition [9]. Paper [14] has demonstrated that power flow management such as generator output curtailment under certain network conditions can accommodate the needs of more DG connections within the conventional power system planning strategies, and more economic than paying for network reinforcement.

An approach is introduced to define the operating margins required to trigger generator output regulation (trimming) and tripping for the provision of network security [14, 22]. Coordinated voltage control, adaptive power factor control and energy curtailment are integrated in basic optimal power flow management to maximise the wind power capacity in [21]. Power flow sensitivity factors (the mathematical relationship between changes in network power flows because of changes in DG power outputs) are used to coordinate the power outputs of DGs in order to ensure there is no thermal overloading occurs in [4, 15, 16].

Paper [17] presents two techniques, i.e. current-tracing technique and constraint satisfaction problem (CSP) technique, for the management of power flows within static thermal constraints. It is shown that the current-tracing technique can marginally achieve the least DG real power curtailment but the CSP technique is more computationally efficient and allows contractual constraints to be considered [17]. Modelling power flow management problem as a CSP involves the determination of the controllable network devices (denoted as variables), the parameters of the variable's control (denoted as domains) and the constraints of the problem. The variables refer to the controllable DG units, with the respective domains being the bands that restrict their outputs. The constraints includes power flow constraints, contractual constraints between the host DNO and the generator, and preference constraints from the objective function [18-20, 39].

2.3.2. Demand Side Management

2.3.2.1. Overview of DSM

The objective of DSM is to dynamically balance the load demand between peak time and off-peak time of network congestion, reducing the operational and planning cost of the whole system [40-43]. In the distribution networks, DSM could bring a spectrum of potential benefits [42]:

1) Reducing the generation margin. Through identifying households that would be willing (for a fee) to give up consumption relatively infrequently, DSM can provide an alternative cheaper form of reserve to traditional generation reserve.
2) Improving transmission grid investment and operation efficiency. Through curtailing some loads at appropriate locations, DSM could reduce the system operating costs and the capacity of network and generation in order to make sure the transmission network security.
3) Improving distribution network investment efficiency. DSM could also be used to manage network constraints at the distribution level through unlocking unused network capacity and the provision of system support services, bring in benefits such as deferring new network investment, increasing the connection of distributed generation, relieving voltage-constrained power transfer problems, relieving congestion in distribution substations, and enhancing the quality and security of supply to critical load customers;
4) Managing demand supply balance in systems with intermittent renewables. The application of DSM, as a form of standing reserve could reduce the energy gap when high wind conditions coincide with low demand.

Paper [42] also gives a brief introduction of DSM techniques: night-time heating with load switching, direct-load control, load limiters, commercial/industrial programmes (supporting the system following outages of generation or network facilities), frequency regulation, time-of-use pricing, demand bidding, and smart metering and appliances.

As explained in [40], six main DSM categories as shown in Fig. 2-3. Peak clipping and valley filling are methods to reduce the difference between the peak load level and the valley load level so that the distribution network is more stable and safe. Load shifting is used to shift load from peak time to off-peak time to smooth the demand curve.

Conservation is an approach to cut off the load demand by reducing the energy sales. So the DNOs have to think about the incentives to encourage the customers to reduce the electricity consumption at the peak time. Load building is a reverse way of conservation. It is based on increasing the market share of loads supported by energy conversion and storage systems or decentralized energy resources. Flexible load shape requires DNOs to identify customers with the flexible loads who are willing to be controlled in critical periods in exchange for various incentives.

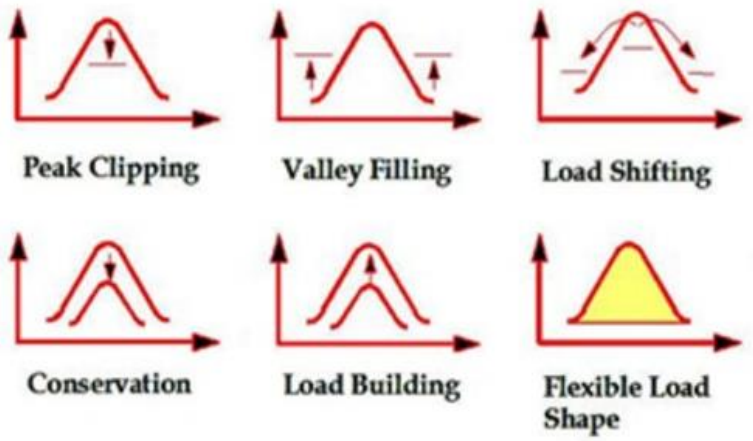

Figure 2-3 DSM Load Shape Categories [40]

This thesis focuses on load shifting category, where demands that can be shifted typically belong to one of the following categories [44].

1) Inert thermal processes (heating, cooling).
2) Inert diffusion processes (ventilation, irrigation, etc.).
3) Mass transport (pumps with tanks, conveyor belts, etc.).
4) Logistics (schedules, dependencies, lunch-breaks, etc.).

2.3.2.2. Development of EVs

To help meet the ambitions for renewables and carbon reduction, electrification of vehicles and heating is expected to grow substantially in the future, particularly from 2030 onwards. Report [3] indicates that in the year 2030, the UK will have 11.9 million of vehicle sales and 18% of them are EVs. The total electricity consumption will reach 411TWh, where the EV electricity consumption will take up 5%.

However, as said in [45], without any coordinating control, uncontrolled charging of EVs can have the following detrimental effects:

1) Increases the loss in distribution transformers;
2) Reduces life span of the transformers by thermal loading on them;
3) Increases voltage deviations;
4) Increases harmonic distortions;
5) Increases necessitating additional investments on distribution side reinforcements due to peak demand.

However, since charging and discharging mode of EVs is flexible, they can also be regarded as energy storage devices that can smooth the intermittency of renewable energy sources like wind. If EVs' charging can be controlled to accompany with the valley portion in demand curve, they can not only help the demand avoid peak periods but also accommodate excessive wind power, reducing wind curtailment. The potential benefits existing in "wind-EV" complementation are shown in [46, 47].

1) Wind energy is a clean resource for EV's charging.
2) Coordinated EV recharging reduces the abandoned wind energy.
3) The benefits will increase with increasing EV battery capacity, increasing EV ownership, larger capacity of transmission lines, and bidirectional charging modes.

Paper [24] gives a literature overview of coordinated EV charging. Different objectives define different EV charging strategies. They can be classified into technical, economic and combined techno-economic objectives.

Technical objectives focus on physical grid infrastructures which include minimising energy losses, minimising voltage deviations, reducing peak power demand, balancing power supply and demand, supporting higher penetration of renewable energy, and increasing robustness [48, 49]. A DSM strategy that considers customers' preference, comfort level, and load priority is proposed in [48] to accommodate EV charging while keeping the peak demand unchanged. Paper [49] establishes a single EV charging demand model and then employs queuing theory to describe the behaviour of multiple EVs.

Economic objectives are related with the energy market-related stakeholders (consumers, producers, and retailers), e.g. dual-tariff schemes, real-time pricing [50, 51]. Price mechanisms in the form of time-of-use electricity tariffs are employed in [50] to encourage commuters to recharge EVs during off-peak hours. For two different charging rates (120 VAC and 240 VAC) and charging times (day and night charging), paper [51] evaluates the economic EV charging under different electricity pricing options considering the influence on demand factor, load factor and utilisation factor.

Coupled techno-economic objectives combine both technical constraints and economic objectives. The commercial part is implemented by balancing demand and supply of electricity on electricity trading markets. The technical part concentrates on the primary system assets and the location. Paper [52] shows a novel method to plan EV charging, achieved by minimising bid volumes first, and then constraining with electricity grid constraints, namely both voltage and power.

2.4. Autonomous Regional Active Network Management System

One of ANM projects called Autonomous Regional Active Network Management System (AuRA-NMS) is introduced in [39] to address new industrial challenges created by new DGs in distribution networks. It involves seven universities in UK, two DNOs and a major manufacturer [53]. Although AuRA-NMS is heuristic and non-optimal, the utilisation of sensitivity analysis makes its results similar with other optimisation algorithms.

'Autonomous and regional' in AuRA-NMS reflects that the algorithm is decentralized and devolved from a network control centre, and operation crosses a region not just a feeder. The word 'active' means that it aims to enhance the utilisation of primary infrastructure and integration of distributed generation, to incorporate new control opportunities such as energy storage, and to create flexibility for different future use. [54]. In AuRA-NMS, a number of network controls, either autonomous or cooperative, are carried out to deal with a set of network operational problems such as a fault, an

out-of-tolerance voltage or a generator whose output is being limited by certain network constraints. In order to provide a hardware platform for these controls, various regional controllers across the distribution networks need to be combined with reliable and flexible communication channels.

AuRA-NMS is a part of the drive to develop 'intelligent' or 'smart' networks. As [55] explained, AuRA-NMS is also designed to be both flexible and extensible. Flexibility denotes the ability to easily rebuild the control system in the event of:

1) Changes to network topology and plant ratings;
2) Connection of new generation or energy storage;
3) Removal of generation or energy storage;
4) Changes to protection and control equipment;
5) Installation of new measurement and monitoring equipment;
6) Removal of measurement and monitoring equipment.
7) Changes to the regulatory framework in which the DNOs operate, and the markets in which generators connected to the network participate.

Extensibility, on the other hand, indicates the ability to easily:

1) Add additional network control and management functionality in the future;
2) Replace existing functionality when improved network control and management techniques or algorithms are developed.

In the long run, flexibility and extensibility are essential in future active network management systems.

From a technical perspective, AuRA-NMS has following four main controls: power flow management, steady state voltage control, automatic restoration and implementation of network performance optimization strategies [53]. This thesis focuses on the power flow management aspect to eliminate the network congestions, i.e. congestion management.

In the UK, currently, the congestion management follows the LIFO rule. The rule implies that the last-in DG will be the first to be tripped off or curtailed once overloading occurs in a network [4]. The drawback of this rule is that the last-in DG may not have significant effects in mitigating the overloading. In the worst scenario, it may not have any effect at all, which results in unnecessary energy waste.

Unlike the LIFO rule that often results in excessive curtailment of wind generation, the congestion management in AuRA-NMS allows real-time states to be obtained and used to select the most sensitive busbar to alleviate network congestion [4, 15, 16]. The congestions can be eliminated with the least amount of generation curtailment or load shedding. The concept of congestion management is illustrated in Fig. 2-4.

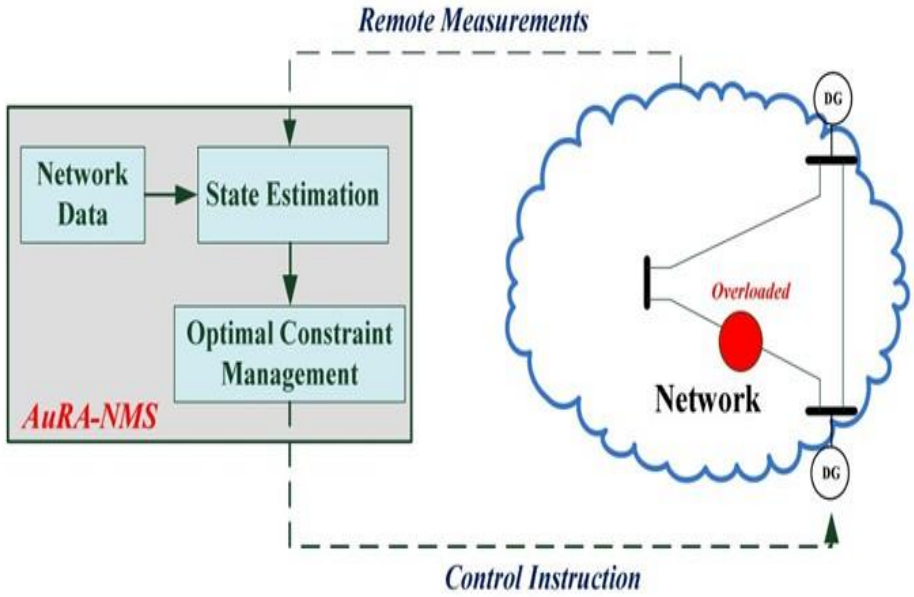

Figure 2-4 Schematic Illustration of AuRA-NMS Congestion Management [15]

Once an overloading state is detected, AuRA-NMS will receive the information through remote measurements. Then, with the help of real-time data, the system will find the most sensitive generator to reduce its output to remove the stress. After the optimal congestion management is found, the system will give the control instruction back to the network. It is assumed that it is equipped with state estimation software.

As ANM strategies normally consider the generation side and demand side management in isolation, the main drawback in AuRA-NMS congestion management is that it investigated system optimisation only in generation side. More generation curtailment could be reduced if congestion management can be enhanced with DSM, particularly by taking advantage of flexible demand such as EVs.

2.5. Chapter Summary

This chapter gives an overview of new challenges in future low carbon distribution networks. The challenges are introduced from increasing renewable distributed generation and new demand from electrification. ANM is being developed as a cheaper alternative to traditional ways to address these challenges. ANM strategies can mitigate the network pressure in distribution networks as well as help to meet the CO2 mitigation target.

This thesis focuses on congestion management aspect of ANM. Previous research evaluated the value of congestion management in terms of economic generation curtailment, which did not include the potential operational benefits from demand side response, particularly from flexible load demand. If previous congestion management could be improved by adding DSM, network congestion could be alleviated to a large extent before curtailing DGs, resulting in more network stresses being relieved and more renewable generation being utilised.

CHAPTER 3. CONGESTION MANAGEMENT WITH INTELLIGENT EV CHARGING

This chapter improves the previous congestion management by integrating intelligent EV charging. Cost-benefit assessment is implemented to evaluate the performance of the enhanced congestion management. Alternative network planning suggestions are also given.

3.1. Introduction

As mentioned in last chapter, ANM is an efficient way to accommodate increasing renewable generation and load demand in distribution networks with minimal needs in reinforcing network or building new lines. This chapter proposes an enhanced ANM strategy by integrating intelligent EV charging into the previous congestion management. In this thesis, Intelligent EV charging refers to shifting flexible EV load demand from congestion peak time to congestion off-peak time to relieve network pressure.

A concept called Time-Window Scale is used to restrain time horizon in EV load shifting. When, where and how much should the EV charging demand be shifted is determined by network power flow. The shifting level will be limited by the flexibility of EV charging demand which is constrained by number of EVs, battery characteristics and road travel behaviour.

The chapter is organized as follows: Section 3.2 introduces the enhanced congestion management strategy, where intelligent EV charging is added; Section 3.3 discusses a case study of 33kV Aberystwyth network; Section 3.4 assesses the cost-benefit of the enhanced congestion management strategy in distribution network planning; Section 3.5 analyses the effects of electricity prices on network planning; some comparisons between the enhanced congestion management and other existing ANM are discussed in Section 3.6; finally, the conclusion is drawn in Section 3.7.

3.2. The Enhanced Congestion Management

3.2.1. Previous Congestion Management

The optimal decision in previous congestion management is formulated as the following linear programming problem [15].

Objective:

$$\min \sum_{i \in NG} \Delta P_{gi} \tag{3-1}$$

Subject to:

$$\left| \sum_{i=1}^{NB} PTDF(l,i) \times (P_{gi} - \Delta P_{gi} - P_{di}) \right| \leq P_l^{max}, l \in L \tag{3-2}$$

$$P_{gi}^{min} \leq \Delta P_{gi} \leq P_{gi}^{max}, i \in NG \tag{3-3}$$

Where, P_{gi} and P_{di} are the power generation and load demand at busbar i, respectively. ΔP_{gi} stands for the generation curtailment at busbar i. P_{gi}^{min} and P_{gi}^{max} are the lower and upper limits of the generation output at busbar i. PTDF(l,i) is an element of sensitivity matrix called Power Transfer Distribution Factor (PTDF), which is a matrix of line flow l to power injection on busbar i. P_l^{max} is the line rating of line l. L ,NG and NB represent the set of lines, generation and all busbars in the network, respectively.

When an overloading state is detected, the system will first pick out the most overloaded line l. PTDF matrix is the reference to select the most efficient busbar to line l. It is a sensitivity matrix of line active power flow with respect to nodal injections based on direct current (DC) power flow equations. Appendix B gives the detailed derivation of the PTDF matrix. The matrix indicates that the relationship between power injection on busbar and power flow on network branch is linear.

The quantity of wind generation that needs to be curtailed can be determined by the following equation where i_s is the slack bus and P_l is the power flow on line l. Dividing the overloading amount of line l by the nodal sensitivity achieves the required quantity of generation curtailment to completely mitigate line overloading. However, ΔP_{gi} is limited by the generation availability on busbar i at specific timeslot, i.e. it cannot exceed the amount of nodal produced generation P_{gi}. Thus, a minimisation equation is used to get the final ΔP_{gi} .

$$\Delta P_{gi} = \min \left\{ \frac{|P_l - P_l^{max}|}{PTDF(l, i) - PTDF(l, i_s)}, P_{gi} \right\}, i \in NG \tag{3-4}$$

3.2.2. Proposed Intelligent EV Charging Model

3.2.2.1. Constraints for Intelligent EV Charging

In order to calculate the load shifting capability, two conditions are assumed in the proposed algorithm:

1) Total energy consumption before and after load shifting on each busbar should be the same.
2) Load shifting capability is predefined, but limited by the EV flexibility on busbars which is related to number of EVs, battery characteristics, and road travel behaviour.

As noted, total energy consumption before and after DSM on each busbar should be the same and this is mathematically represented in (3-5).

$$\sum P_{di} = \sum P_{ndi}, \quad i \in ND \tag{3-5}$$

where, P_{ndi} is the new load demand at busbar i. ND stands for the set of busbars that have load demand.

The load shifting capability is described in (3-6).

$$\Delta P_{di,t} = \min \left\{ \frac{|P_l - P_l^{max}|}{LTDF(l, i) - LTDF(l, i_s)}, EV_{i,t} \right\}, \quad i \in ND \tag{3-6}$$

where, $\Delta P_{di,t}$ and $EV_{i,t}$ are the load shifting capability and the flexibility of EVs at busbar i at timeslot t, respectively. The matrix called Load Transfer Distribution Factor (LTDF) is a sensitivity matrix of nodal load perturbation to line flows based on DC power flow equations. It is derived from PTDF since load could be regarded as negative generation. It is formed as reference to select the most efficient busbar to line l. Dividing the overloading amount of line l by the nodal sensitivity achieves the required quantity of load shedding to completely mitigate line congestion. However, $\Delta P_{di,t}$ will be further limited by the EV flexibility on the busbar at specific timeslot, i.e. it cannot exceed EV flexibility $EV_{i,t}$. Thus, a minimisation equation is used to get the final $\Delta P_{di,t}$.

The flexibility of EV load demand on a busbar is related to number of EVs, battery characteristics and road trip conditions in that area [52, 56-58]. The charging boundary

is considered over a 24-hour period. It is calculated by the following three steps:

A. Determination of number of EVs;

B. EV battery characteristics;

C. Road trip limitations.

A. Determination of number of EVs

The number of EVs on a specific busbar is calculated according to EV penetration rate and the corresponding customer number. EV penetration rate is assumed to be 0.675 per customer from year 2030 to 2050 [59]. Customer number on the busbar i (CN_i) is expressed in (3-7).

$$CN_i = \frac{D_i \cdot \eta_i}{ADD_i}, \ i \in ND \tag{3-7}$$

where, D_i is the annual total load demand on specific busbar i. η_i is its corresponding percentage of domestic consumption. And ADD_i is the average domestic electricity consumption per customer.

B. EV battery characteristics

Typical EV battery capacity B_c in the UK is Nissan Leaf characterized by 24kWh. To avoid damage and premature aging, there are limitations on the battery state-of-energy $S_{v,t}$ [52] as shown below.

$$\delta_{min} B_c \leq S_{v,t} \leq \delta_{max} B_c \tag{3-8}$$

where, $S_{v,t}$ is the state-of-energy of vehicle v at timeslot t, and the minimum δ_{min} and maximum δ_{max} coefficients of the battery capacity are set to be 0.2 and 0.9, respectively.

C. Road trip limitations

To obtain the aggregated flexibility of a large number of EVs, the trip behaviour of an EV at each timeslot within 24 hours can be obtained from [57] as shown in Fig. 3-1. The average electricity consumption of an EV in use is 2.1 kW [56]. When an EV is parked at a charge station, the vehicle is assumed to be charged immediately at the maximum charging rate 4KW. Since the operation of ANM is executed on each busbar rather than each customer, this chapter considers total EVs on each busbar instead of individual EV separately. The wishes of individual EV owners are beyond the scope of this thesis. They are assumed to be responded as average.

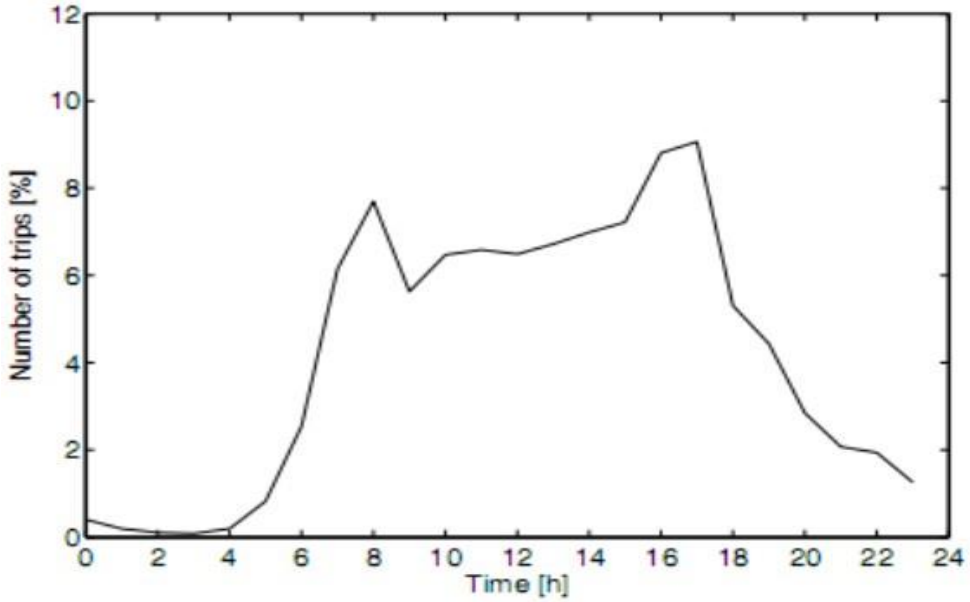

Figure 3-1 Percentage of Trips by Vehicle at Each Hour [57]

One hour prior to departure, the state-of-energy of a vehicle's battery must ensure that sufficient energy is stored to cover energy consumption over the next hour. Therefore, for a large number of EVs on a busbar, the total state-of-energy of batteries varies in the range of $[S_{t,min}, S_{t,max}]$. The upper $C_{t,max}$ and lower $C_{t,min}$ limits of EV charging at timeslot t can be expressed as:

$$C_{t,min}=\max\{P_{dr,t+1}+NEV\times\delta_{min}\times B_c-S_{t-1,max}\ ,0\},\ 1<t\leq 24 \tag{3-9}$$

$$C_{t,max}=\min\{NEV\times\delta_{max}\times B_c-S_{t-1,min}\ ,\ P_{ch}\times N_{undrv,t}\},\ 1<t\leq 24 \tag{3-10}$$

where, NEV is the total number of EVs on one busbar. $C_{t,min}$ and $C_{t,max}$ are the minimum and maximum charging levels at timeslot t, respectively. $S_{t-1,max}$ and $S_{t-1,min}$ are the maximum and minimum state-of-energy at timeslot t-1. $P_{dr,t+1}$ is the total electricity consumption of all EVs on the busbar over the next timeslot t+1 due to driving, and P_{ch} is the maximum charging rate per vehicle once it is stopped. $N_{undrv,t}$ is the number of EVs that are stopped at timeslot t.

Both energy-of-state S_t and charging amount C_t for a large fleet of EVs are unknown. But they can be derived from each other according to the recursive relationship in (3-11). In order to derive charging boundaries C_t, some initial assumption should be made for S_t as in (3-12) and (3-13).

$$S_t=S_{t-1}+C_t-P_{dr,t},1<t\leq 24 \tag{3-11}$$

$$S_{1,min}=NEV\times\delta_{min}\times B_c+P_{dr,2} \tag{3-12}$$

$$S_{1,max}=NEV\times\delta_{max}\times B_c \quad (3\text{-}13)$$

where, $S_{1,min}$ and $S_{1,max}$ are the minimum and maximum energy-of-states at the end of 1st hour. $P_{dr,2}$ is the driving energy consumption in 2nd hour.

3.2.2.2. Operation of Intelligent EV Charging

A. Concept of Time-Window Scale

In the proposed control algorithm, load demand and generation profiles are updated every hour. Time-Window Scale concept is used to constrain the time horizon for intelligent EV charging. M-Time-Window means that to relieve network stress at timeslot i, load shifting can be made in the following M-1 hours, i.e. from i+1 to i+M-1. If there is no line overloading in timeslot i, the check system will move on to the next timeslot i+1 and the dispatch of EV load demand at timeslot i stays the same with the original dispatch. Otherwise, intelligent EV charging is undertaken before system moves on to next timeslot.

For in-depth explanation, if the time-window scale is assumed to be 6 hours, then the most suitable timeslot for swapping load can only be selected in the following 5 hours as shown in shadow grids in Fig. 3-2. Constrained by the EV flexibility, if load shifting between timeslot i and timeslot i+3 can maximally reduce the line overloading in timeslot i, then the exchange will be executed between timeslots i and i+3. The EV charging at other hours in the time-window will not change.

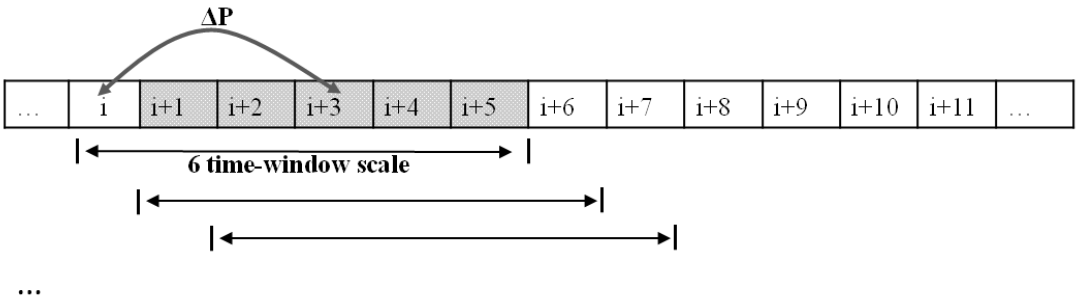

Figure 3-2 6-hour Time-window Example

B. Operation of Intelligent EV Charging

Essentially, the proposed intelligent EV charging strategy will firstly identify when and

where pressure points might arise, and their strength, secondly identify the most suitable timeslot to shift the excessive load demand and the level of shifts.

When there is line overloading occurs, the most overloaded line l is found in the same way as in previous congestion management. Then according to LTDF, the most sensitive busbar with maximum absolute LTDF value is picked out. The factor could be either negative or positive for increasing or reducing load demand, respectively. The predefined load shifting capability $\Delta P_{di,t}$ to eliminate congestion is identified as in (3-6). The next step is to find proper timeslot in the time-window scale to exchange $\Delta P_{di,t}$. As the example in Fig. 3-2, the timeslot i+3 is chosen as the most suitable timeslot because it has maximum EV flexibility. Hence, the exchange of $\Delta P_{di,t}$ is implemented between timeslot i and i+3.

If the line overloading cannot be totally eliminated, the program will look into the second sensitive node to make load shifting further. The loop will carry on until there is no available flexible EV load demand left for load shifting. After that, the network power flow is recalculated and generation curtailment is executed to eliminate the remaining overloading. The flowchart to clearly explain the intelligent EV charging is shown in Fig. 3-3.

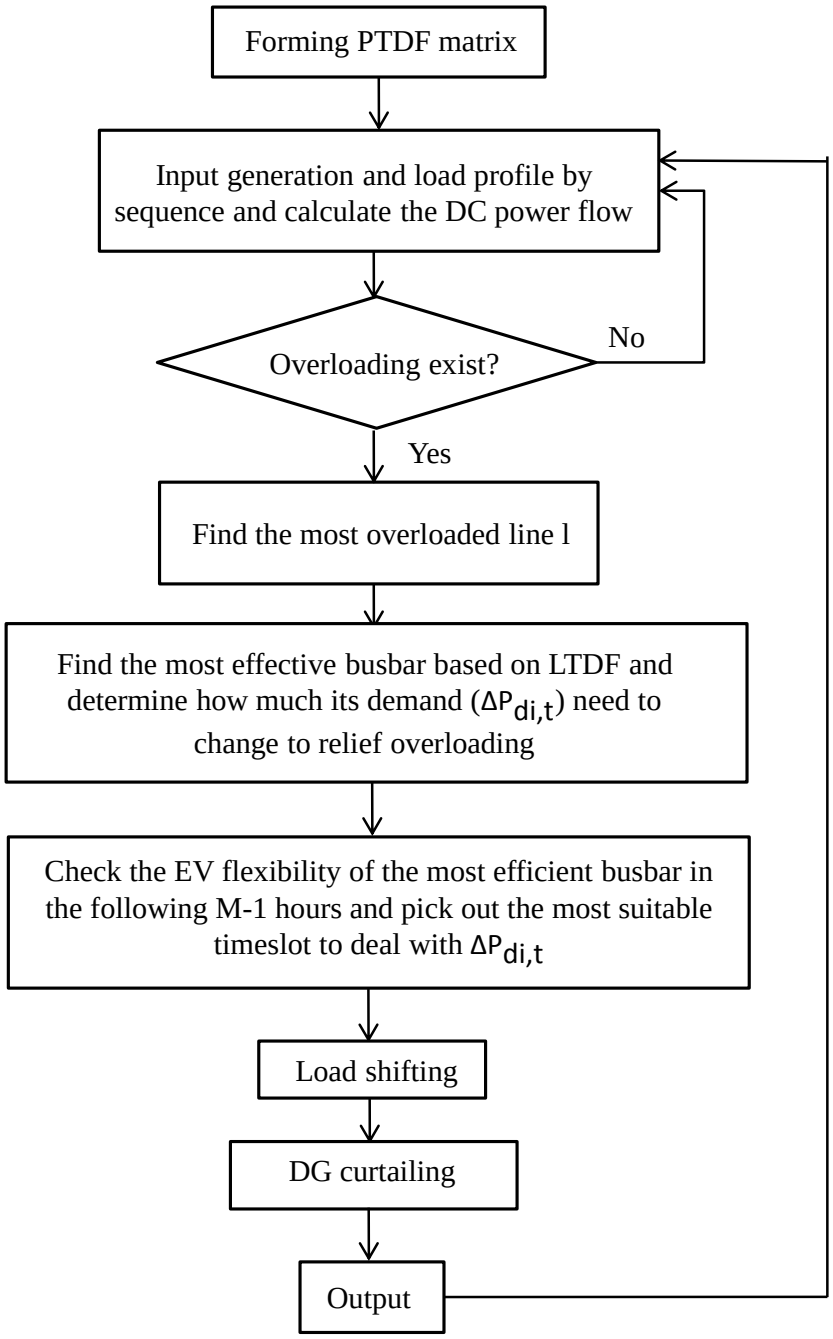

Figure 3-3 Flowchart of the Intelligent EV Charging Strategy

3.3. Test System and Case Study

3.3.1. Test System and Data Forecast

3.3.1.1. Test System

In order to analyse the benefits of the proposed algorithm, a 47-busbar network is

adopted for case study. The test system, Aberystwyth 33kV network, is a practical 132/33kV distribution network in the UK which consists of approximately 200km of overhead line and 20km of underground cable [39]. The entire network structure is shown in Appendix A. This thesis focuses on the south part of the network whose single line topology is shown in Fig. 3-4.

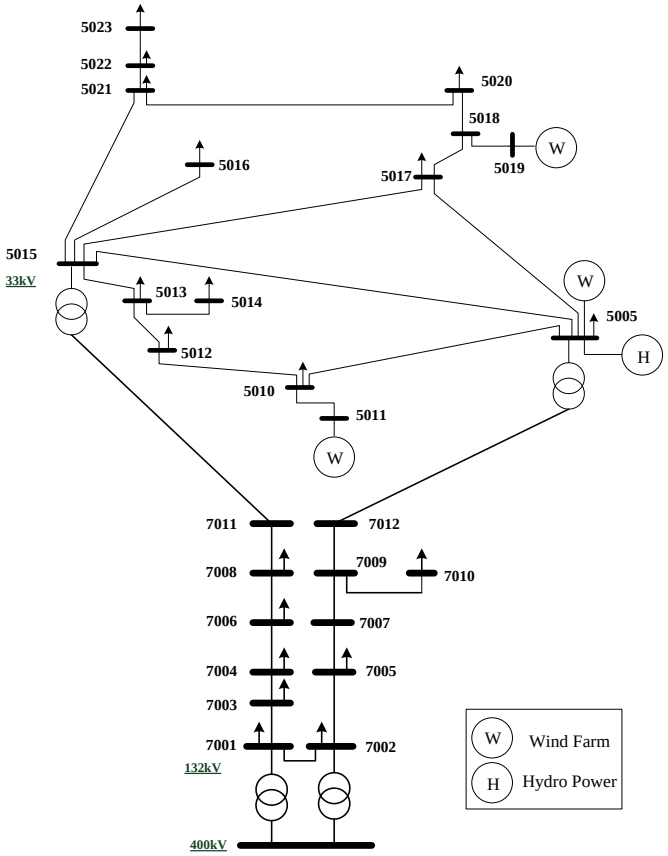

Figure 3-4 Single Diagram of the South Part of 132/33kV Network

For the south part of the network, the hourly load demand and DG outputs in year 2006 are available already. The load profile in 2006 mainly contains classical load. In year 2006, the maximum total load demand is 51.4MW and the maximum total DG output is 71.3 MW. Thus, in year 2006, the network is already suffering network congestion caused by the excessive DGs.

3.3.1.2. Data Forecasting

Considering life expectancy of existing wind farms, the year they were commissioned, the potential for increasing land use, and the potential for increasing turbine size, report

[5] gives the expansion size and time of repowering wind farms in the existing Aberystwyth 33KV network. At least 44MW of new wind capacity is planned to be added on the network by 2020 based on the current sizeable wind capacity.

Report [5] identified two streams of additional wind generation, one is repowering the existing wind farms, and the other is from new potential sites. Only the repowering stream is considered in this thesis as they are the most likely additional wind capacity to the area. Table 3-1 lists the timing and sizes of repowering in the existing wind farms [5]. And hourly DG outputs profiles in year 2013 and 2018 are available. Since the network has already experienced congestions under contingencies from renewable generation, the increasing DG output will worsen the congestion situation.

Table 3-1 Expansion Size and Time of Existing Wind Farms

Wind Farm	**Replacement Year**	**New Capacity (MW)**	**Existing Capacity (MW)**
Mynydd Gorddu WF	2013	30	9.4
Rheidol WF	2012	6.4	2.4
Llangwyryfon WF	2018	30	9.35
Cemmaes WF	2017	17.5	15.3

As indicated in [5], the repowering in 2018 has already reached the maximum wind blade size level, the wind turbines cannot be expanded any more. Therefore, the wind generation profile in the network after year 2018 will stay the same with that in 2018.

Load demand in Aberystwyth area is not expected to increase too much in the short and medium term. Thus, all future classic loads are kept same as in 2006 until 2030. When more and more EVs and heat pumps come forth, a large amount of flexible load demand will be added on the classical load. In order to use the data to do the simulation, this chapter makes EV load forecasting first for years 2030-2050.

To forecast the EV load demand on individual busbar, the number of EVs is necessary to know. For practical applications, the number of EVs in an area can be estimated analytically based on the number of electricity clients (customers) in that area. It can be calculated as shown in (3-9). The annual total load demand D_i can be obtained from company data. The percentage of domestic proportion η_i and the average domestic

demand ADD_i can be found in report [60]. The results of EV number estimation on 12 busbars which have load demand are listed in Table 3-2.

Table 3-2 Nodal EV Number Estimation

Bus Bar	Yearly Load Demand (MWh)	Domestic percentage	Average Domestic consumption (KWh)	Customer Num.	EV Num.
Bow street	26010.6	46.61%	5652	2145	1448
Machynlleth1	17109.1	43.39%	4946	1501	1013
University College Wales	29496.2	46.61%	5652	2432	1642
Aberdovey	15774.9	46.92%	5134	1442	973
Tywyn	23929.2	46.92%	5134	2187	1476
Fairbourne	14816.4	46.92%	5134	1354	914
North Road	30644.2	32.60%	3952	2528	1706
Aberystwyth	29926.0	46.61%	5652	2468	1666
Parc Y Llyn	35784.9	48.95%	4361	4017	2711
Llanilar	12792.07	46.61%	5652	1055	712
Rhydlydan	5621.5	48.95%	4361	631	426
Rhydlydan ST1	3385.1	48.95%	4361	380	257

Database in Department of Energy & Climate Change (DECC) summary of demand profiles for the UK shows that total EV electricity consumption for whole UK is predicted to be 32.2TWh and 38.4TWh for year 2030 and 2050, respectively. Linear distribution method can be used to get the annual EV electricity consumption of the whole UK from year 2030 to year 2050.

For busbar i, the prediction of annual EV electricity consumption can be estimated analytically through calculating the customer number ratio of that area, which is the ratio of the customer number CN_i in Table 3-2 to the total population occupancy in the UK [60]. With the regional customer ratio and the total EV electricity consumption of the UK, the annual EV electricity consumption on busbar i can be easily derived.

Database from DECC also gives Monte Carlo scenario of predicted EV load demand profile for the national grid in 2030 and 2050. The profile is hourly recorded. According to the general hourly EV consumption allocation in Monte Carlo scenario and the total annual EV consumption on busbar i, the hourly EV electricity consumption on busbar i from year 2030 to 2050 can be forecasted.

3.3.2. Time-series Simulation and Results

Time-series simulation is carried out by calculating network power flow. Power flow calculations are carried out for the whole year, i.e. 8760 operating states in sequence. After simulations, the curtailment results are counted and compared. It is assumed that the duration of each curtailment is one hour. The total curtailments are identified in the whole year. Overloading mainly occurs on line 5015-5017, 5010-5012, and 5018-5017 because of new DG integrations.

Before the application of intelligent EV charging, for year 2030, constraint management needs to curtail 1790.74MWh of DG when line overloading occurs in some operating states. The DG connected to 5019 is responsible for the curtailment. However, when load shifting is taken first, the curtailment amount reduces significantly.

Table 3-3 lists the details of generation curtailment reduction in different time-window scales. The annual generation curtailment amount decreases from 1672.9MWh in 2-hour time-window scale down to 1649.2MWh in 24-hour time-window scale. The reduction reaches up to 7.9%, with an average of around 7.6%. It is obvious that 24-hour time-window is the best choice which saves the maximum amount of renewable energy by 141.6MWh.

Table 3-3 Total DG Output Curtailments in Different Time-Window Scale

Time-Window Scale (Hours)	Generation Curtailment (MWh)	Curtailment Reduction (MWh)
2	1672.9	117.9
3	1667.2	123.6
4	1665.3	125.4
5	1662.0	128.7
6	1660.4	130.3
7	1657.4	133.4
8	1655.1	135.6
9	1654.1	136.6
10	1653.7	137.0
11	1654.2	136.5
12	1653.6	137.1
13	1653.7	137.0
14	1653.3	137.4
15	1653.1	137.6
16	1652.7	138.1
17	1652.2	138.6
18	1652.1	138.6
19	1651.3	139.4
20	1650.9	139.8
21	1650.9	139.9
22	1650.4	140.3
23	1650.3	140.4
24	1649.2	141.6

Fig. 3-5 shows the changing curve of curtailment quantity when time-window scale increases. The curve in Fig. 3-5 decreases significantly in the first 10 scales and becomes flatter in the remaining scales, which means most of the load shifting is done in the first 10 hours.

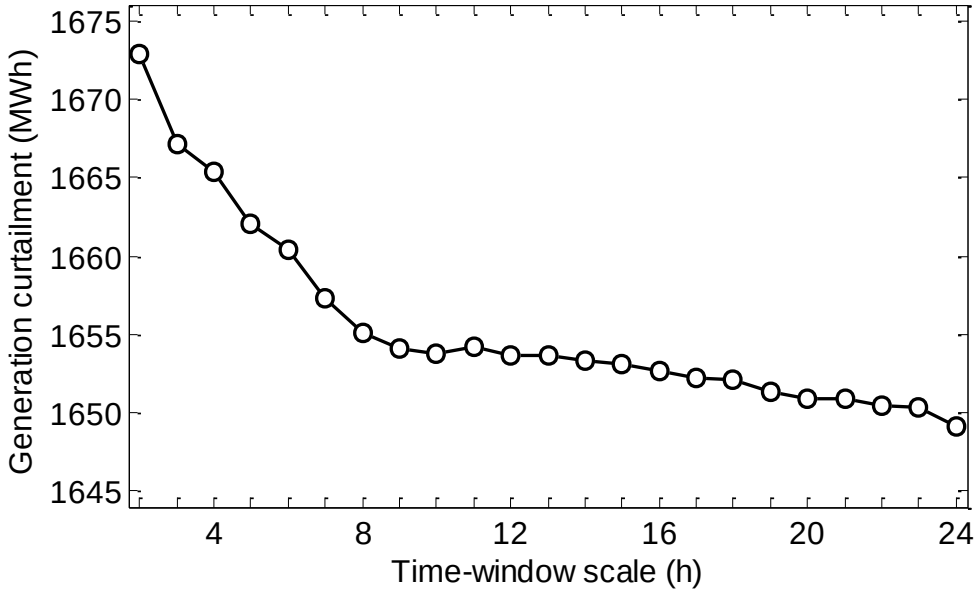

Figure 3-5 Generation Curtailment of ANM with Intelligent EV Charging under Different Time-Window Scales

Two phenomena are worth noting in Fig. 3-5. First, in most situations, the generation curtailment decreases when time-window scale increases. Thus, we argue that larger time-window scale can give better perspective of the network condition to help make a smarter load shifting decision.

Second, small fluctuations appear in the curve. Congestion management with intelligent EV charging is operated in sequence to minimise the generation curtailment in one particular hour. The operation in earlier hours may increase the power flow in later hours and make network congestion in later hours more severe. Therefore, the increased generation curtailment in later hours may be bigger than the saved generation curtailment in earlier hours, which makes the total annual generation curtailment more in the end and leads to the curve fluctuation.

Before intelligent EV charging is applied, the most serious congestion happens at 10:00 a.m. on the 340th day of the year. Hence, data on this day is chosen to analyse the change in load curve due to intelligent EV charging. The system will go through all busbars to do load shifting according to their LTDF ranking before generation curtailment. Since load shifting on one busbar is always limited and not enough to eliminate line overloading, this report analyses the total load demand of the whole network instead of just the most sensitive busbar.

Fig. 3-6 shows the change of network load curve when intelligent EV charging is added on congestion management. The difference between the blue solid curve and red curve stands for the original EV demand dispatch. The green dot line indicates the load demand distribution after intelligent EV charging. The difference between red line and dot line is EV re-dispatch in the 24 hours.

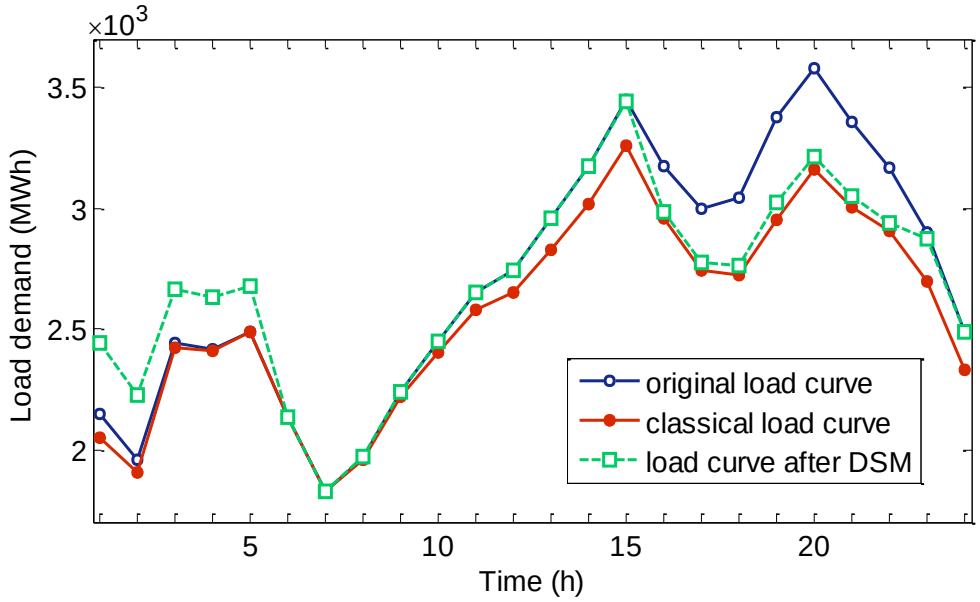

Figure 3-6 EV Re-dispatch on Peak Curtailment Day

The generation curtailments with and without intelligent EV charging are displayed in Table 3-4. Without intelligent EV charging, the total generation curtailment of the 340th day is 28.7MWh. The value could be reduced by 12% (namely 3.5MWh) when intelligent EV charging is implemented. As shown in Fig. 3-6, in the first 5 hours (from 0:00 to 5:00), the EV demand is increased to reduce the generation curtailment. The increasing EV demand mainly comes from excessive load accumulated in the previous day.

In the following 10 hours (from 5:00 to 15:00), the load curve after intelligent EV charging nearly matches the original load curve as shown in Fig. 3-6. However, one should note that this does not mean there is no load shifting on individual nodes because the curtailment values still have changes in these hours in Table 3-4. From the 16th hour on (from 15:00 to 24:00), compared with the original load curve, the load curve after DSM decreases dramatically, which is due to the slight line congestion detected in these

hours. The shaved EV demand is moved to the timeslots that need larger load demand to alleviate network pressure. Although the generation curtailment has a small increase at 22:00 in Table 3-4, the total curtailment of the whole 340th day is reduced.

Table 3-4 Generation Curtailment Comparison with and without DSM

Time	Without DSM (MWh)	After DSM (WMh)
1:00	1.35	0.64
2:00	0.38	0.00
3:00	0.30	0.00
4:00	0.00	0.00
5:00	2.57	1.98
6:00	0.75	0.75
7:00	0.98	0.98
8:00	2.47	1.98
9:00	4.31	3.86
10:00	4.46	4.07
11:00	2.27	1.90
12:00	4.31	3.98
13:00	1.97	1.67
14:00	1.69	1.73
15:00	0.88	1.18
16:00	0.00	0.00
17:00	0.00	0.00
18:00	0.00	0.00
19:00	0.00	0.00
20:00	0.00	0.00
21:00	0.00	0.00
22:00	0.01	0.44
23:00	0.00	0.00
24:00	0.00	0.00
Total	28.69	25.16

3.4. Cost-benefit Assessment

3.4.1. Investment Options

Last section has indicated the performance improvement by applying intelligent EV charging on existing congestion management and determined the best time-window scale for system operation which is 24-hour. This section will determine how the optimal trade-off between operational benefit and network investment cost might be impacted by intelligent EV charging. The alternative planning strategies for smart

distribution system are also recommended.

Investment options could be classified into three main potential planning strategies that DNOs might undertake in the light of increasing renewable penetration and EV demand:

1) Invest only in network primary assets,

2) Invest only in the ANM,

3) Invest both in network assets and ANM.

Table 3-5 lists the exhaustive investment options. Wind farm repowering in 2013 and 2018 require the new lines added in 2013 and 2018, respectively. The driver for new line in 2030 is the added load demand from EVs.

Table 3-5 Exhaustive Investment Options

Plan No.	**Investment detail**	**Plan No.**	**Investment detail**
1	2 lines in 2013	13	ANM in 2030+2 lines in 2013+2 lines in 2018
2	2 lines in 2018	14	ANM in 2030+2 lines in 2013+1 line in 2030
3	1 line in 2030	15	ANM in 2030+2 lines in 2018+1 line in 2030
4	2 lines in 2013+2 lines in 2018	16	ANM in 2030+2 lines in 2013+2 lines in 2018+1 line in 2030
5	2 lines in 2013+1 line in 2030	17	ANM in 2011& 2031+2 lines in 2013
6	2 lines in 2018+1 line in 2030	18	ANM in 2011& 2031+2 lines in 2018
7	2 lines in 2013+2 lines in 2018+1 line in 2030	19	ANM in 2011& 2031+1 line in 2030
8	ANM in 2030	20	ANM in 2011& 2031+2 lines in 2013+2 lines in 2018
9	ANM in 2011&2031	21	ANM in 2011& 2031+2 lines in 2013+1 line in 2030
10	ANM in 2030+2 lines in 2013	22	ANM in 2011& 2031+2 lines in 2018+1 line in 2030
11	ANM in 2030+2 lines in 2018	23	ANM in 2011& 2031+2 lines in 2013+2 lines in 2018+1 line in 2030
12	ANM in 2030+1 line in 2030		

3.4.2. Cost-benefit Category

For each investment option, the operational benefits mainly come from the annually saved renewable energy, which is affected by the electricity price as shown in (3-14).

$$B_y = EP_y \cdot GC_y \quad (3\text{-}14)$$

where, for the year y, B_y is the operational benefit, EP_y is the electricity price, and GC_y is the annual generation curtailment reduction.

The network investment cost considered in network planning mainly includes primary asset investment, ANM, and DSM as shown:

$$C_y = AC_y + ANM_y + DSM_y \quad (3\text{-}15)$$

where, for the year y, C_y is the network investment cost, AC_y is the cost of asset investment, ANM_y is cost of investing ANM, and DSM_y is the cost from intelligent EV charging.

For the primary asset investment, the time to invest new lines in network is determined by the year the wind farm is upgraded and the EV demand connected. The detailed information about primary assets investment is listed in Table 3-6.

Table 3-6 Time and Cost of Primary Asset Investment [5]

Number	Right of Way	Year	Cost (£m)	Present Value (£m)	Lifetime (years)
Asset 1	5015-5017 5017-5018	2013	1.33	1.14	40
Asset 2	5010-5012 5012-5013	2018	3.13	1.94	40
Asset 3	5017-5018	2030	1.25	0.33	40

The cost of existing AuRA-NMS without intelligent EV charging is £700k and its lifetime is 20 years [39]. The cost estimation for the development of DSM varies considerably from country to country, and even between networks on those countries. Therefore, it is difficult to evaluate particular cost for the operation of DSM for the purposes of generation curtailment reduction whilst ignoring other costs and benefits of DSM.

There are a number of projects currently on-going trying to ascertain the cost-benefits of the Smart Grid (including DSM). One such project is run by Scottish Power in Liverpool. In this large scale trial of Smart Grid Technology, a few thousand houses in the Liverpool area are being used as a trial for a range of technologies including energy storage, smart metering, and DSM. The cost of the trial is given in the document [61]. However, in order to test the feasibility of constraint programming approach to power flow management, a software prototype is developed to run on commercially available substation computing equipment [18]. Hence, the cost of ANM consists of hardware and software. Since existing ANM already has the ability of remote measurement and monitoring, it can remote monitor the EV consumption as well. And DSM is included in software. Therefore, in our proposed enhanced ANM, the cost of integrating DSM is minimised.

The long-term network planning in this chapter ranges from 2011 to 2050, so it is necessary to convert the profits in different years to an equivalent present year such as 2011. Therefore, the profits of different investment options can be comparable. With the assumption in [62], the present value of future reinforcement is given below.

$$PV=\frac{Asset}{(1+d)^n} \tag{3-16}$$

where, PV is present value of future investment, d is discount rate. Asset stands for modern equivalent assets cost, and n is time to reinforce a network asset.

There are two ways for assessing the performance of an investment option. One measurement is Net Present Value (NPV) [63], which can be used to compare the profits of planning options. The higher an option's NPV, the more desirable it is to be undertaken. It is calculated as shown in (3-17). However, the discount rate d should be known in advance.

$$NPV = \sum_{y=2011}^{2050} \frac{(B_y - C_y)}{(1+d)^{(y-y_0)}} \tag{3-17}$$

where, y_0 is the year 2011.

Another measurement is Internal Rate of Return (IRR). The higher an option's IRR, the more desirable it is to be undertaken. It is derived by setting the option’s NPV to be zero as:

$$NPV = \sum_{y=2011}^{2050} \frac{(B_y - C_y)}{(1+IRR)^{(y-y_0)}} = 0 \quad (3\text{-}19)$$

3.5. Network Planning Considering Electricity Prices

3.5.1. Network Planning under Constant Electricity Prices

In this section, to simplify the calculation, constant electricity prices and NPVs are adopted to evaluate the performance of different investment options. The discount rate d is assumed to be 6.9% [36]. Applying electricity prices of £40, £60, £80 and £100 per MWh to the total MWh savings, the results can be easily obtained and are shown in Fig. 3-7 and Fig. 3-8 considering depreciation.

From Fig. 3-7, one can see under previous congestion management, option 19 gives the highest profit when electricity price is set to £40/MWh. However, option 21 is the best choice when wholesale electricity price climbs to £60/MWh, £80/MWh, and £100/MWh, and the largest benefit is £31.77m. The situation is same when applying intelligent EV charging on ANM. However, its largest benefit can reach £31.83m when electricity price is £100/MWh. Furthermore, the savings of options 9, 20, and 22 are comparable to the most efficient choice.

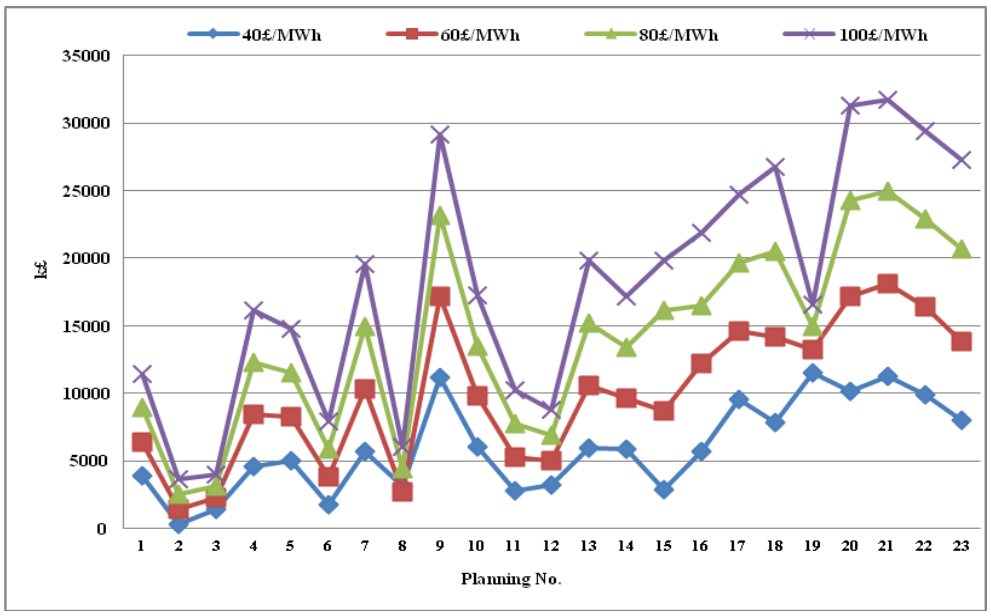

Figure 3-7 Options' NPVs in Existing ANM without DSM under Constant Electricity Price

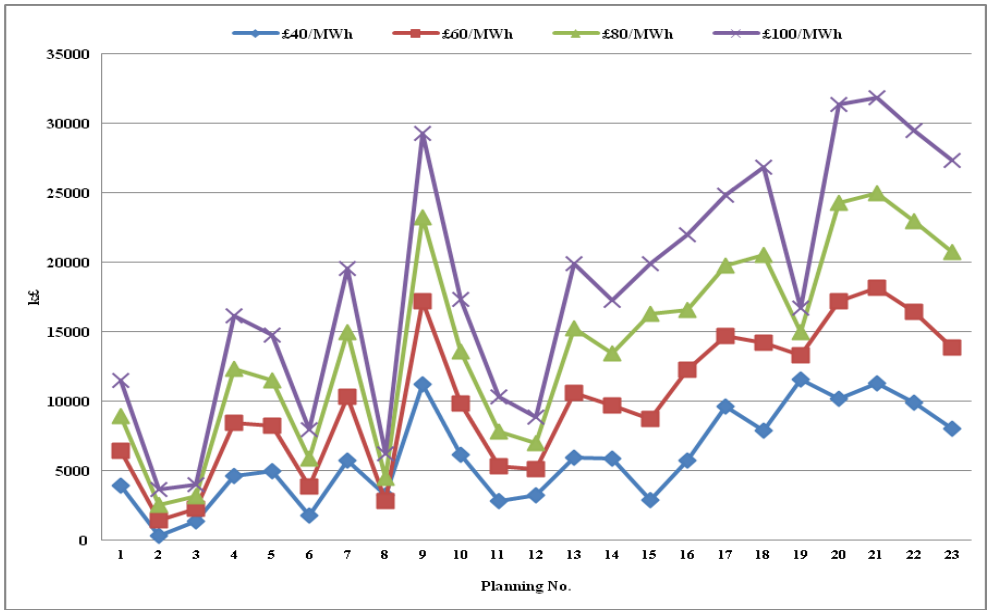

Figure 3-8 Options' NPVs in Proposed ANM with DSM under Constant Electricity Prices

The MWh saved benefits solely due to the use of intelligent EV charging are shown in Fig. 3-9. In the first 7 options, there is no difference because they are lines investment only. The other options show the benefits from intelligent EV charging clearly. The curtailment savings are same in options 8 (invest AuRA in 2030) and option 9 (invest AuRA in 2011&2031). This is because before year 2030, the load profile is assumed to stay the same and there is no EV connected into the network. The function of intelligent EV charging cannot be executed since no flexible EV is available.

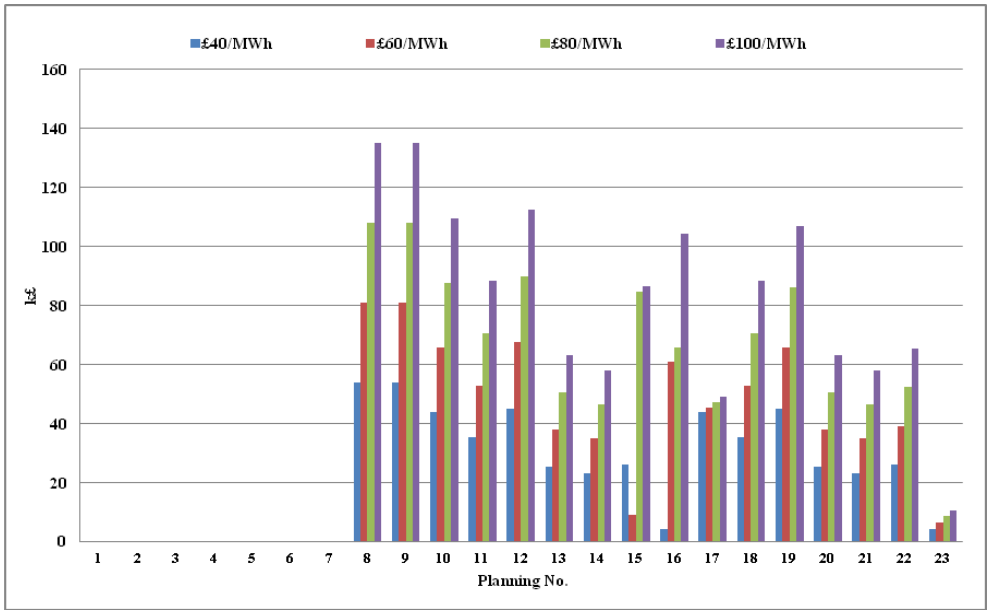

Figure 3-9 Increased NPVs by DSM under Constant Electricity Prices

3.5.2. Electricity Price Uncertainty

Cost-benefit assessment in last section is based on fixed electricity price over 40 year period. However, actual energy price will fluctuate as well as the electricity price over a longer period of time. This part takes reference from Ofgem's Project Discovery – Energy Market Scenarios to analyse the planning fluctuation caused by electricity price uncertainty.

The price curve of electricity from 2010 to 2025 is shown in Fig. 3-10. The four projected scenarios, Green Transition, Slow Growth, Green Stimulus and Dash for Energy are based on two key global drivers that will most likely shape different outcomes for the Great Britain energy markets over the next decade or so: the speed of global economic recovery and the extent of globally coordinated environmental action [64]. To investigate the impact of electricity price uncertainty, we adopt the wholesale electricity price from year 2010 to 2025 in [64] and assume the wholesale electricity price from year 2026 to 2050 will be the same with year 2025.

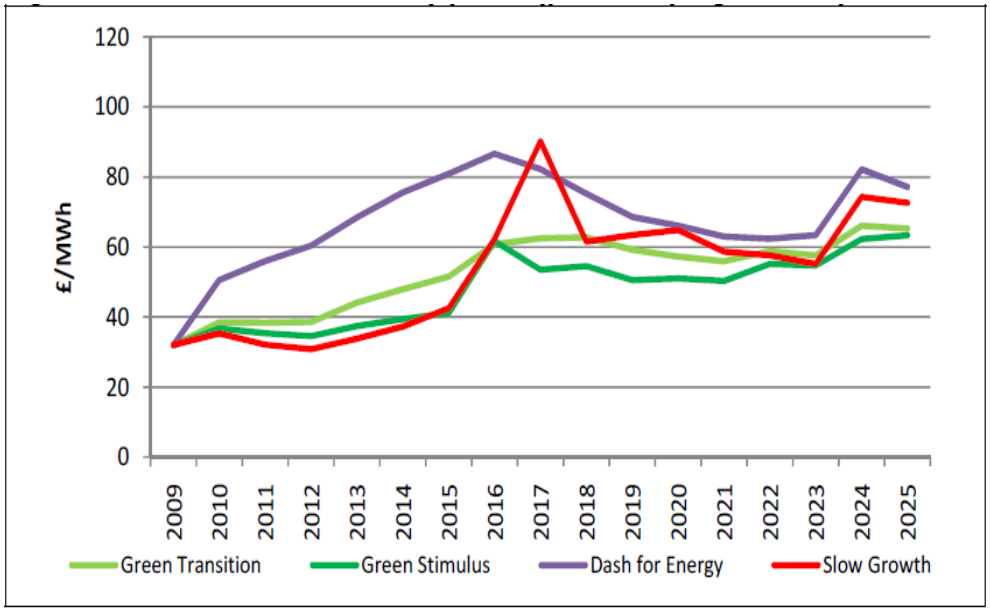

Figure 3-10 Wholesale Electricity Prices [64]

The exhaustive investment options are reduced to 15 options as listed in Table 3-7. It is because in the network planning, if ANM is invested, it is more reasonable to invest it from year 2011. Thus, option 8 (ANM in 2030) in Table 3-5 is deleted.

Table 3-7 Investment Options

Plan No.	Investment detail	Plan No.	Investment detail
1	2 lines in 2013	9	ANM in 2011& 2031+2 lines in 2013
2	2 lines in 2018	10	ANM in 2011& 2031+2 lines in 2018
3	1 line in 2030	11	ANM in 2011& 2031+1 line in 2030
4	2 lines in 2013+2 lines in 2018	12	ANM in 2011& 2031+2 lines in 2013+2 lines in 2018
5	2 lines in 2013+1 line in 2030	13	ANM in 2011& 2031+2 lines in 2013+1 line in 2030
6	2 lines in 2018+1 line in 2030	14	ANM in 2011& 2031+2 lines in 2018+1 line in 2030
7	2 lines in 2013+2 lines in 2018+1 line in 2030	15	ANM in 2011& 2031+2 lines in 2013+2 lines in 2018+1 line in 2030
8	ANM in 2011& 2031		

Since the actual discount rate is unknown in practice, IRRs is adopted in this section to do the assessment. By applying electricity prices in (3-16) and (3-17), the corresponding IRR of each investment option is calculated. Fig. 3-11 shows the IRRs under congestion management without intelligent EV charging, where the IRRs of the 15 investment options vary greatly.

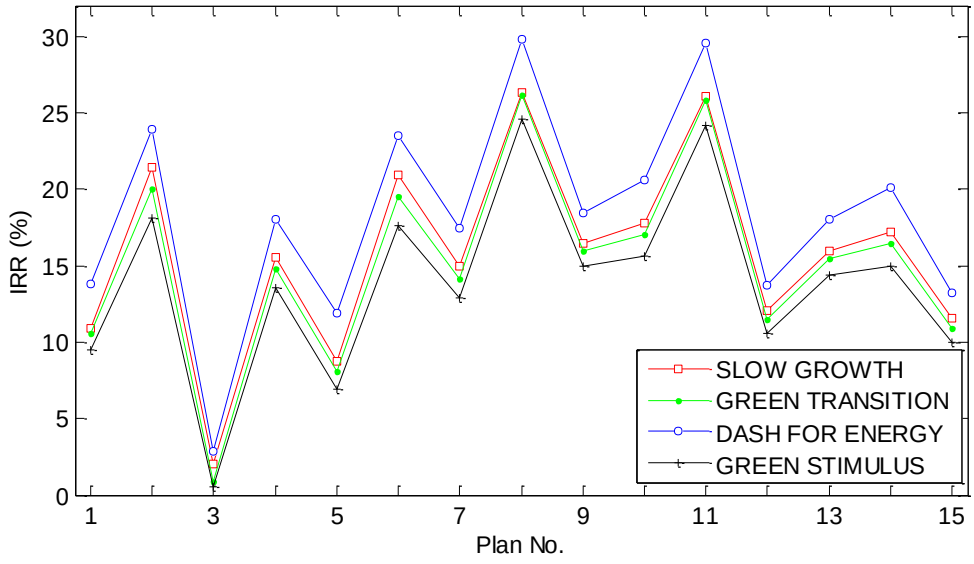

Figure 3-11 Options' IRRs in ANM without DSM

Taking GREEN STIMULUS scenario as an example, the IRRs of options range from 1% (option 3) to 24.56% (option 8). Compared with options 1 and 2 which invest two

lines, option 3 only invests one line in 2030. Options 1 and 2 build two lines earlier than option 3 according to the year of wind farm repowering, which can greatly reduce generation curtailment before 2030. After 2030, one line in option 3 is not enough to accommodate the excessive generation and demand, resulting large amount of generation curtailment. Although option 3 produces both lower cost C_y and lower operational benefit B_y, the reduction in B_y is bigger than that of C_y, leading to very small IRR value according to (3-20).

Furthermore, compared with options 8-15, only line investment is triggered in option 3. Though the cost C_y is small, network pressure will result in large quantity of generation curtailment, which reduces the benefit B_y. It is caused by that the network has to bear severe network pressure from 2013 to 2030 due to the wind farm repowering in 2013 and 2018, and form 2030 to 2050 due to both excessive generation and load growth.

The 4 scenarios produce quite similar tendency of IRRs for the 15 options but not exactly the same. It is because for each option, the electricity price only influences B_y in (3-20) while C_y is fixed for all 4 scenarios. If the electricity uncertainty is bigger than that projected in Ofgem's report, the four curves may cross with each other. In Fig. 3-11, the highest IRRs are obtained in option 8 for all scenarios (26.34% in SLOW GROWTH, 26.18% in GREEN TRANSITION, 29.77% in DASH FOR ENERGY, and 24.56% in GREEN STIMULUS). Option 11 is comparable to the most profitable option 8.

Fig. 3-12 shows the IRRs in enhanced congestion management with intelligent EV charging. The curve tendency in Fig. 3-12 is similar to that in Fig. 3-11. The reason is that when intelligent EV charging is applied, only GC_y in (3-16) is changed, which only causes B_y to vary in (3-20) with other elements unchanged. Therefore, the shapes of the curves do not change obviously. Option 8 still gets the highest profit in four scenarios. However, its largest IRRs reach 26.36%, 26.19%, 29.79% and 24.58% in scenario SLOW GROWTH, GREEN TRANSITION, DASH FOR ENERGY and GREEN STIMULUS, respectively. Fig. 3-11 and Fig. 3-12 give the recommendations in distribution network planning. However, in these two figures, it is difficult to see the increased benefit from applying intelligent EV charging.

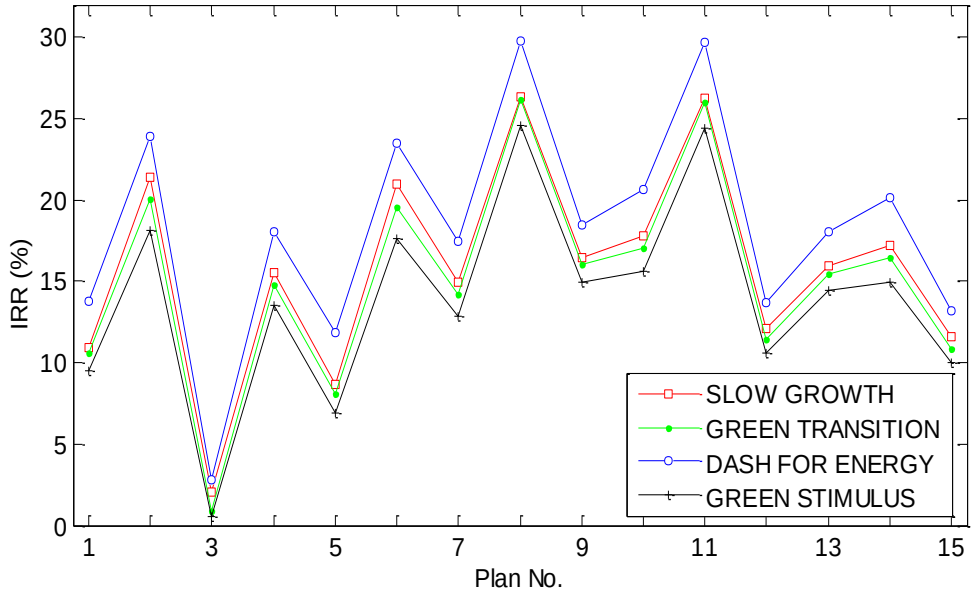

Figure 3-12 Options' IRRs in Proposed ANM with DSM

Fig. 3-13 shows the increased operational benefit from adding intelligent EV charging on congestion management. For each investment option, the increased benefit is calculated by comparing NPVs with and without intelligent EV charging. In order to obtain NPVs, the IRR in (3-20) is set to be 6.9% for all investment options.

In Fig. 3-13, options 8 to 15 show increased benefits brought from DSM, whereas options 1 to 7 show no increased benefit since they are only line investment. Option 11 (AuRA in 2011& 2031+1 line in 2030) gets the largest increased benefit from DSM (£530k in SLOW GROWTH， £478k in GREEN TRANSITION, £566k in DASH FOR ENERGY, and £463k in GREEN STIMULUS). Fig. 3-13 indicates that the operational benefits from intelligent EV charging vary with the investment options, which means integrating intelligent EV charging in congestion management will influence network planning.

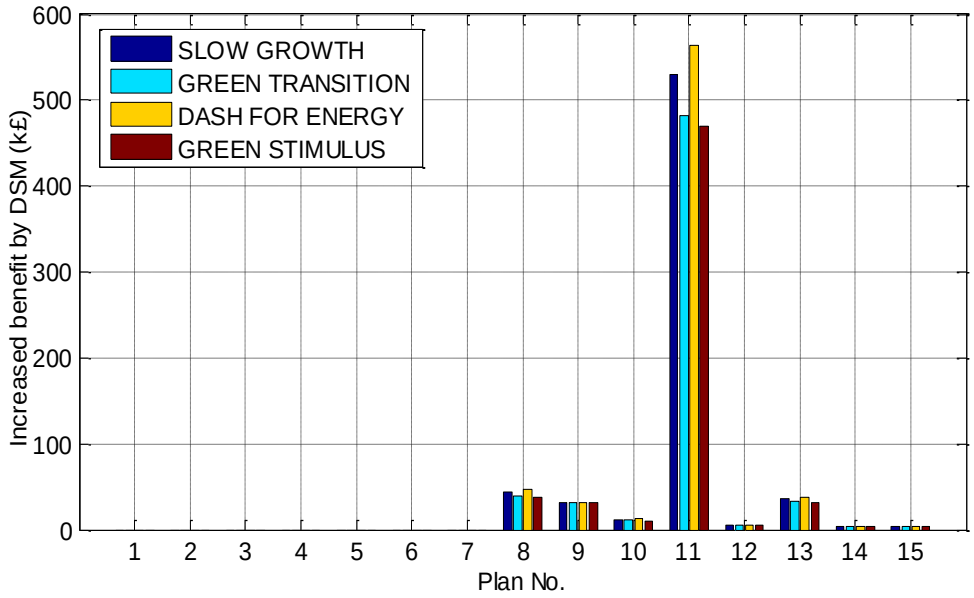

Figure 3-13 Increased Benefit from DSM

3.6. Discussions

This chapter proposes an enhanced congestion management strategy, which is achieved by augmenting existing congestion management to include intelligent EV charging. As demonstrated in the practical distribution system, combined management of generation and demand can achieve 7.9% improvement in utilising renewable energy, and subsequently increase network operational benefit by £566k.

There are many papers investigating the role of ANM on distribution network operation as discussed in Chapter 2, but from different aspects and use different methodologies. For example, paper [21] indicates that a multi-period AC optimal power flow technique is able to increase wind power penetration volume by 30% if 5% energy curtailment is allowed. Paper [22] uses active power flow management for trimming and tripping of regulated non-firm generation. It approves that the method has the potential to increase the capacity of both firm and non-firm generation by 3 times. Paper [15] compares the generation curtailment reductions by using AuRA-NMS under different additional DG capacity levels. It concludes that by using the method, 79.6% generation curtailment reduction can be realised when additional 40 MW DG is connected.

These papers did not consider the role that DSM can play in reducing generation curtailment. Further, the methods devised in them compared with that in this paper are for different objectives with various constraints. The models and methodologies are demonstrated on different systems to test effectiveness and quantify benefits. Therefore, it is impossible to set a benchmark value to measure the benefits they can produce. The work in this chapter is an improvement over the previous congestion management to encourage DSM by considering the role of intelligent EV charging. Although there are no benchmark benefits, the results in this chapter show that the proposed strategy can achieve additional benefits over the techniques in [15].

3.7. Chapter Summary

This chapter integrates intelligent EV charging into the previous congestion management and assesses its additional cost-benefit. An important consideration in this optimisation analysis is the Time-Window Scale concept, which will be used to limit time domain for load shifting. Another important element is the alignment of demand shift with optimal generation curtailment, which requires reasonable selection rules to guide load shifting to minimise the annual generation curtailment.

A practical 33kV network is used as a test system. The simulation results indicate that intelligent EV charging can help previous congestion management reduce generation curtailment further by 7.9%, which means more renewable energy could be utilised in the network. Besides, larger time-window scale always results in larger operational benefits. Intelligent EV charging can save wind generation up to 141.6MWh in 24-hour time-window scale.

By analysing four different electricity price strategies, the best investment choice and the increased benefit from intelligent EV charging is found to be strongly dependent on the electricity price and its uncertainty, which is thus worth noting in the optimal network asset investment. Our results provide a viable and promising enhanced congestion management for distribution network operators, particularly for networks with high penetrations of renewable generation.

CHAPTER 4. IMPROVING THE INTELLIGENT EV CHARGING MODEL

This chapter improves the intelligent EV charging by applying bi-directional charging optimisation strategy and enhancing shifting principle with power flow constraint.

4.1. Introduction

Chapter 3 proposes the use of EVs as responsive demand to complement the previous congestion management that was purely based on generation curtailment to relieve network stresses. It is achieved by allowing EVs to absorb excessive renewable generation when they cause network pressure. The enhanced congestion management is proved to be capable of reducing the network stresses further without network reinforcement, resulting in more renewable generation being saved.

However, the charging model in Chapter 3 has two drawbacks. First, the excessive load /load shortage can only be shifted to/from latter hours. The strategy will be more beneficial if load shifting could be bi-directional. Second, the selection of timeslot for shifting only depends on EV flexibility. If the timeslot already suffers network congestion, it should not be chosen for load shifting even though it has large EV flexibility.

This chapter addresses these two drawbacks by proposing an enhanced charging strategy with two improvements:

1) Load shifting will be optimised to be bi-directional through 'trail and comparison' among several potential charging solutions. The operation objective is to minimise the total generation curtailment in individual time-window.
2) The selection of timeslot for load shifting depends on both EV flexibility and network power flow condition.

The rest of this chapter is organised as follows: Section 4.2 introduces the bi-directional intelligent EV charging algorithm; Section 4.3 enhances the load shifting principle by adding network power flow constraint; Section 4.4 provides a case study of a 33kV network; and the conclusions are drawn in Section 4.5.

4.2. Bi-directional Intelligent EV Charging

Like EV charging model in Chapter 3 (model 1), the proposed EV charging model (model 2) also detects network stress based on time-series power flow simulation. The

concept of time-window scale is still utilised to constrain the time horizon for EV load shifting. The differences between these two models are explained below.

In model 1, M-Time-Window means that when the congestion checking moves to the time-window which starts with timeslot t, if there exists network congestion at t, load shifting will be undertaken in the following hours from t+1 to t+M-1. Otherwise, the checking system will move on to the next time-window which starts with timeslot t+1 and the dispatch of EV load demand at timeslot t stays the same with the original dispatch.

In model 2, bi-directional operation means that in M-Time-Window Scale, when congestion checking moves to the time-window which starts with timeslot t, it will check the network condition of all timeslots in the time-window. As long as there exist line overloading, no matter which timeslot, the load shifting will be implemented within time period from t to t+M-1. Only if no network congestion is detected in any timeslots in the time-window, the checking system will move on to the next time-window which starts with timeslot t+1 and the dispatch of EV load demand at timeslot t stays the same with the original dispatch.

Model 2 allows load shifting to be more flexible. However, there may be several timeslots with network stresses in the time-window, and the potential of load shifting is limited. In that case, the most efficient timeslot will be selected for load shifting in prior. The procedure of selection will be explained in the next paragraph. Fig. 4-1 gives a 6-hour time-window example of model 2. The grids in grey stand for an individual 6-hour time-window, where both timeslot t+1 and t+4 (in bold) have the network congestion. Thus, there are two shifting solutions: shifting overloading on timeslot t+1 or shifting overloading on timeslot t+4. By comparing the performance of these two solutions, t+4 is selected as the more efficient timeslot. Then t+4 can shift its excessive EV load to either earlier hours or latter hours.

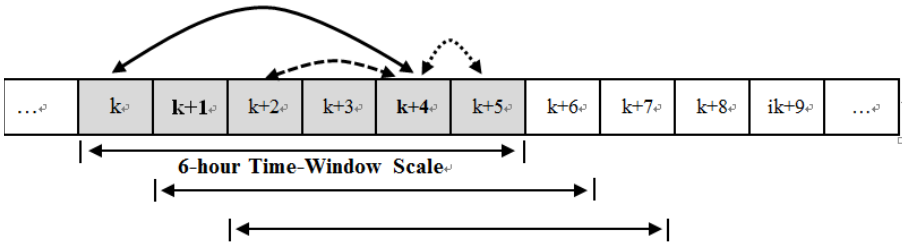

Figure 4-1 6-hour Time-window Example

The optimisation of EV charging is processed by "trial and comparison" from several charging solutions. The number of trials is determined by the number of timeslots that have network congestion. The original state of the network without load shifting is set as reference, in which each timeslot k in the time-window has original generation curtailment $GC_{0,t}$. Trial T means that the target for load shifting is to alleviate the overloading at timeslot T, i.e. EV charging demand at timeslot T should be swapped with other timeslots to relieve the congestion.

In trial T, after load shifting, the network generation curtailment at each timeslot t $GC_{T,t}$ in the time-window will be recalculated. The difference between $GC_{T,t}$ and $GC_{0,t}$ is the individual benefit at timeslot t due to load shifting in trial T. By summing all individual benefit in the time-window, the benefits of trial T can be obtained, shown in (4-1). By comparing GCR_T, the trial execution timeslot with largest GCR_T will be selected as the real execution timeslot for load shifting.

$$GCR_T = \sum_{t=1}^{TWS} (GC_{0,t} - GC_{T,t}) \quad (4\text{-}1)$$

where ,TWS indicates the Time-Window Scale.

4.3. Enhancing Load Shifting with Power Flow Constraint

The second improvement is in the process of shifting the excessive load from one timeslot to another. In the model in Chapter 3 (model 1), choosing proper timeslot to swap load only depends on EV flexibility. If the timeslot is already suffering network congestion, increasing or reducing its load demand may aggravate network congestion, resulting in more generation curtailment. The proposed model in this chapter (model 2) addresses this problem by considering both EV flexibility and network power flow

condition at each timeslot.

There are three main steps in detailed operation of load shifting:

1) In trial T, the most overloaded line l is first found. Then LTDF is introduced as reference matrix to select the most sensitive busbar to eliminate network stress, which is same with Chapter 3.

2) Find the most proper timeslot to swap EV load with timeslot T. The best timeslot is chosen by considering its EV flexibility and power flow condition. The timeslot with the maximum EV flexibility and the lowest power flow is chosen to conduct load shifting. Method of weighting is used to incorporate the two objectives as shown in (4-2).

$$Priority_t = w_{EV} \cdot EV_{i,t} - w_{OL} \cdot OL_{l,t} \quad (4\text{-}2)$$

where, $Priority_t$ is the shifting priority of timeslot t, $OL_{l,t}$ is the line overloading of line l at timeslot t, w_{EV} and w_{OL} are the weights of EV flexibility and line overloading, respectively.

3) For trial T, after load shifting, GCR_T is then calculated.

The detailed flowchart of enhanced intelligent EV charging is shown in Fig. 4-2.

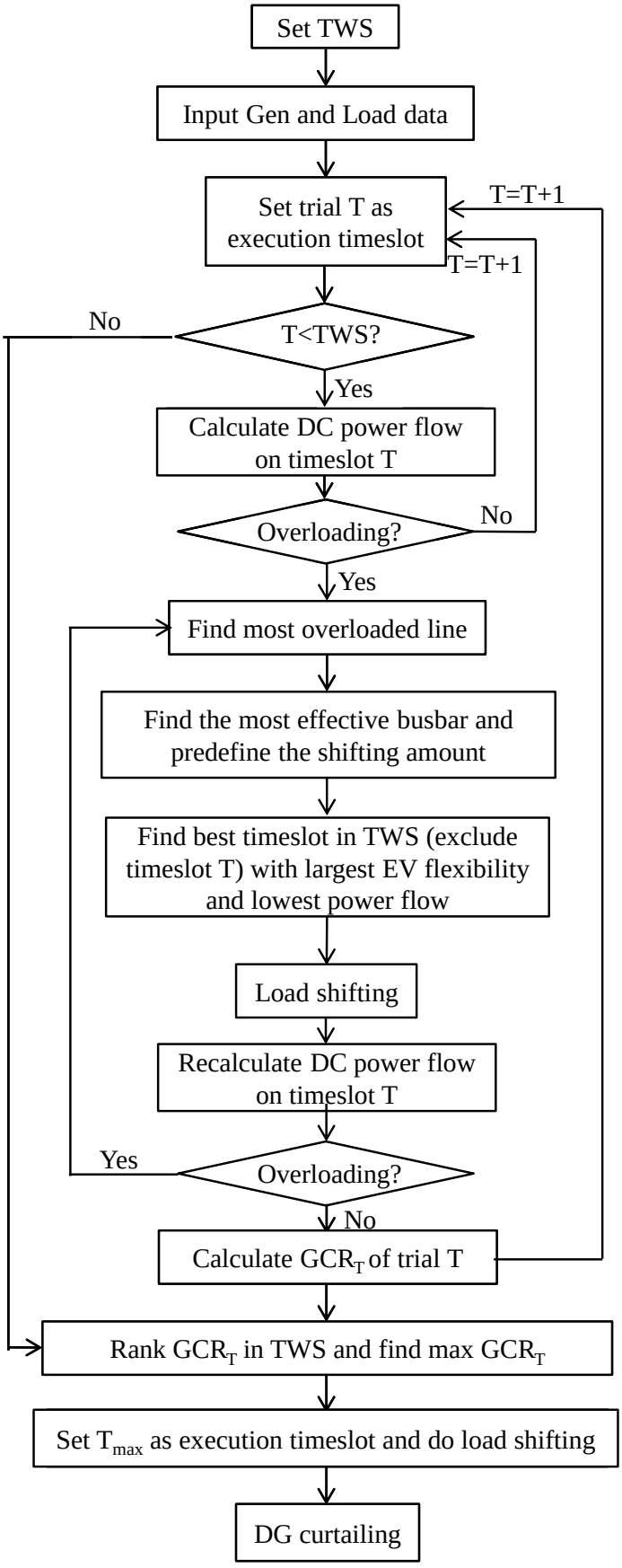

Figure 4-2 Flowchart of Enhanced Intelligent EV Charging

4.4. Case Study

4.4.1. General Case Study Results

In order to compare the operation of the model in Chapter 3 (model 1) and the enhanced model in this chapter (model 2), the Aberystwyth network described in Chapter 3 is used again for case study. Time-Window Scale is set to be 12-hour. The load and generation profiles of one day (24 hours) are chosen as the input data to do the simulation.

Simulation results of the 24 hours indicate that only line 5010-5012 has line overloading. Fig. 4-3 shows the power flow of line 5010-5012 in the 24 hours. The red line stands for the power flow at each timeslot, and the green dotted line is the line rating of line 5010-5012. According to Fig. 4-3, only timeslot 4 and 14 suffer the line overloading. Both these two timeslots require additional load demand to absorb excessive wind generation.

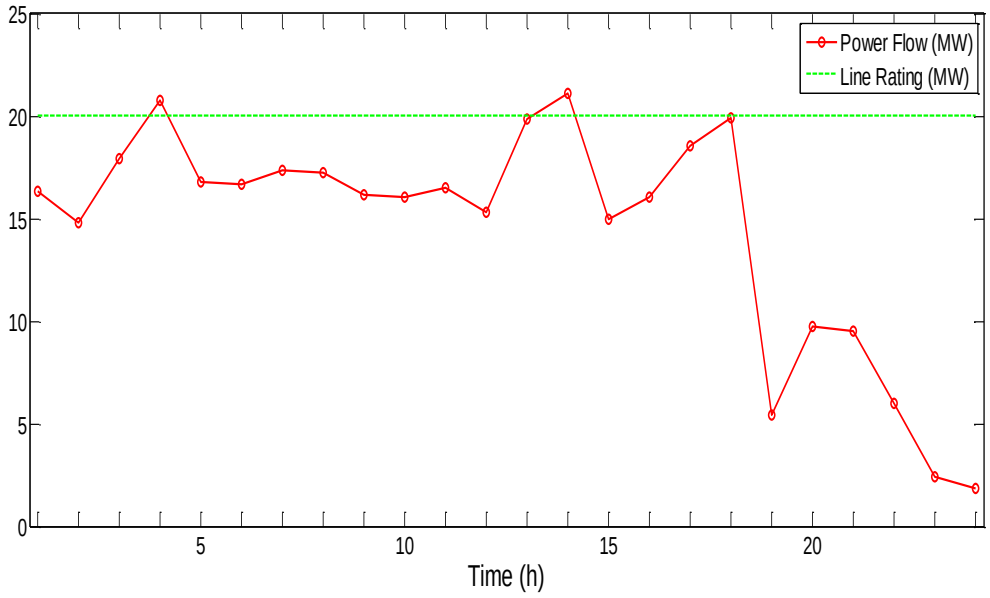

Figure 4-3 Power Flow on Line 5010-5012 in 24 Hours

4.4.1.1. Benefit from Improvement 1

Table 4-1 gives the particular load demand information after applying bi-directional operation in intelligent EV charging. The second column is the original load profile of

the day. The third and fourth columns are the hourly load profiles after EV recharging under model 1 and model 2, respectively. The numbers in bold indicate that there exist load demand change at those timeslots. It is obvious that the bi-direction optimisation in model 2 gives more times of load shifting.

Table 4-1 Comparison of the Change in Load Demand under Model 1 and Model 2

Time	Original Load Demand (MWh)	Load Demand in Model 1 (MWh)	Load Demand in Model 2 (MWh)
0:00	29.557	29.557	29.557
1:00	41.843	41.843	41.843
2:00	40.943	40.943	40.943
3:00	**43.326**	**43.408**	**43.503**
4:00	43.801	43.801	43.801
5:00	37.478	37.478	37.478
6:00	33.242	33.242	33.242
7:00	28.759	28.759	28.759
8:00	23.177	23.177	23.177
9:00	24.628	24.628	24.628
10:00	27.291	27.291	27.291
11:00	**29.743**	29.743	**29.703**
12:00	**34.680**	34.680	**34.592**
13:00	**37.957**	37.957	**39.133**
14:00	**46.029**	**45.947**	**45.947**
15:00	**42.015**	42.015	**41.920**
16:00	**37.228**	37.228	**37.119**
17:00	**35.615**	35.615	**35.475**
18:00	**37.488**	37.488	**37.304**
19:00	**38.660**	38.660	**38.475**
20:00	**33.982**	33.982	**33.827**
21:00	**34.396**	34.396	**34.281**
22:00	**33.980**	33.980	**33.890**
23:00	**29.014**	29.014	**28.944**

Fig. 4-4 shows the change of load demand after implementing intelligent EV charging in model 1. 0.082MWh load demand is shifted from timeslot 15 to timeslot 4. However, for timeslot 14, there is no load demand difference, which means there is no load shifting implemented. This is because in model 1, whether load shifting will be operated or not is determined by the power flow at the first timeslot in the time-window. If the first hour has no network congestion, no load shifting will be done and system will move to the next time-window directly.

In this case study, the Time-Window Scale is set as 12 hour, which means the last load shifting in the 24 hours is implemented within time period from timeslot 13 to 24. As there is no load overloading occurred at timeslot 13, no load shifting is done and the intelligent EV charging for this case study is finished. Thus, timeslot 14 has no opportunity to do load shifting to relieve its line overloading.

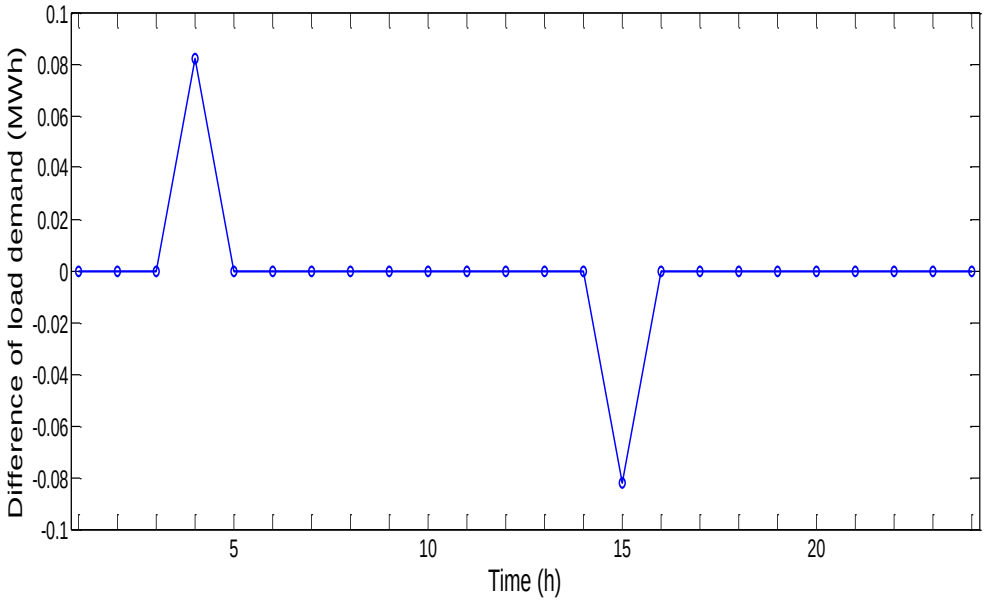

Figure 4-4 Change of Load Demand under Model 1

Fig. 4-5 shows the change of load demand after implementing intelligent EV charging in model 2. Like the situation in model 1, only line 5010-5012 has overloading at timeslot 4 and 14. However, since model 2 has optimised the shifting operation process. The load is allowed to be shifted to either earlier hours or latter hours. The timeslots with line overloading get more opportunities to be relieved through load shifting as there always exist timeslot overlapping between the adjacent time-windows. Furthermore, the network congestion happened in the latter hours is possible to be relieved in the earlier time-windows. In one word, the intelligent EV charging becomes more beneficial.

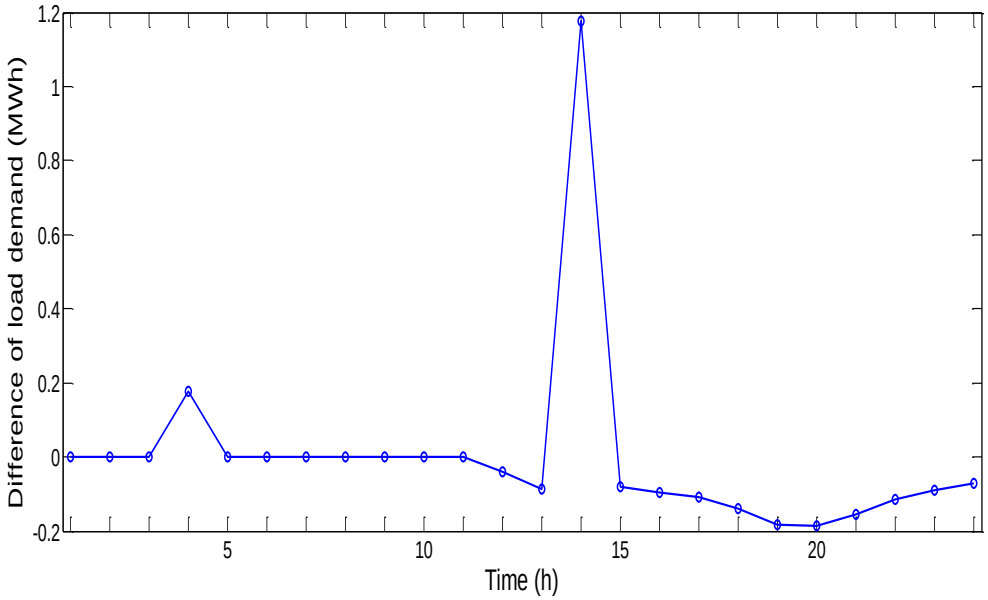

Figure 4-5 Change of Load Demand under Model 2

As shown in Fig. 4-5, the load demand at both timeslot 4 and 14 are increased. The increasing at timeslot 4 is 0.177MWh, which is nearly doubled, as against the increment in Fig. 4-4. Timeslot 14 also gets the opportunity to relive its line overloading in the earlier Time-Window. The load demand increment at timeslot 14 is 1.176MWh. The increment of load demand at these two timeslots comes from other hours that have no network congestion.

Table 4-2 gives generation curtailment comparison between these two models. According to the network condition, only timeslot 4 and 14 have the line overloading. The intelligent EV charging can partially release the overloading, thus it still requires generation curtailment to completely relieve the remaining line overloading. The total generation curtailment of the 24 hours in model 2 is about 45% less than that in model 1. Due to the multiple load-shifting in model 2, the generation curtailment in individual timeslots also reduced significantly. These results prove the efficiency of the improvement 1.

Table 4-2 Generation Curtailment of Model 1 and Model 2

	Model 1 (MWh)	**Model 2 (MWh)**
Timeslot 4	1.131	1.019
Timeslot 14	1.694	0.539
Total	2.825	1.558

4.4.1.2. Benefit from Improvement 2

Last section analyses the benefits coming from bi-directional optimisation. This section enhances model 2 further by adding improvement 2, i.e. power flow constraint, and analyses the benefits coming from improvement 2. As mentioned in (4-2), w_{EV} and w_{OL} are the weights of EV flexibility and power flow condition, respectively. The sum of the two weights should be one. However, since the values of line overloading are normally 100 times larger than the values of EV flexibility. Thus, w_{OL} should be divided by 100 to ensure the two factors comparable. The relationship of w_{EV} and w_{OL} is described below.

$$w_{OL} = \frac{1 - w_{EV}}{100} \tag{4-3}$$

Table 4-3 shows the model performance with and without improvement 2 (power flow constraint). Scenario 1 is the case without improvement 2. Scenario 2 involves improvement 2, where two factors are considered equally important. In 24-hour case, the values of generation curtailment in two scenarios are same, which indicate that the effect of improvement 2 is not as significant as that of improvement 1. In small rang of time horizon, like 24-hour, it does not show any benefits. However, if we extend the time horizon to the whole calendar year, improvement 2 exhibits its benefits. In Scenario 1, the annual generation curtailment amount is 1998.97MWh. When model 2 is enhanced with improvement 2, the annual generation curtailment can be reduced by 0.05%.

Table 4-3 Comparison of Model with and without Improvement 2

Time Horizon	**Scenario 1** (w_{EV}=0.1, w_{OL}=0)	**Scenario 2** (w_{EV}=0.5, w_{OL}=0.005)
24-hour case	1.5585 MWh	1.5585 MWh
Whole-year case	1998.97 MWh	1998.06 MWh

4.4.2. Sensitivity Analysis of Time-Window Scale

The benefits of the two improvements in model 2 have been proved in 4.4.1. This section analyses the annual generation curtailment under different time-window scales.

For each time-window scale, power flow calculations are carried out for 8760 operating states in sequence. The duration of each curtailment is one hour. The total curtailments are identified in the whole year. Overloading mainly occurs on line 5015-5017, 5010-5012, and 5018-5017, which is same with that in Chapter 3.

Fig. 4-6 shows the annual generation curtailment of the enhanced intelligent EV charging model when time-window scale increases. It indicates that, the annual generation curtailment decreases as the time-window scale increases, which is consistent with model 1. In model 2, 3-hour Time-Window requires the largest generation curtailment (2115.26MWh), while 24-hour Time-Window only curtails 1998.06MWh generation.

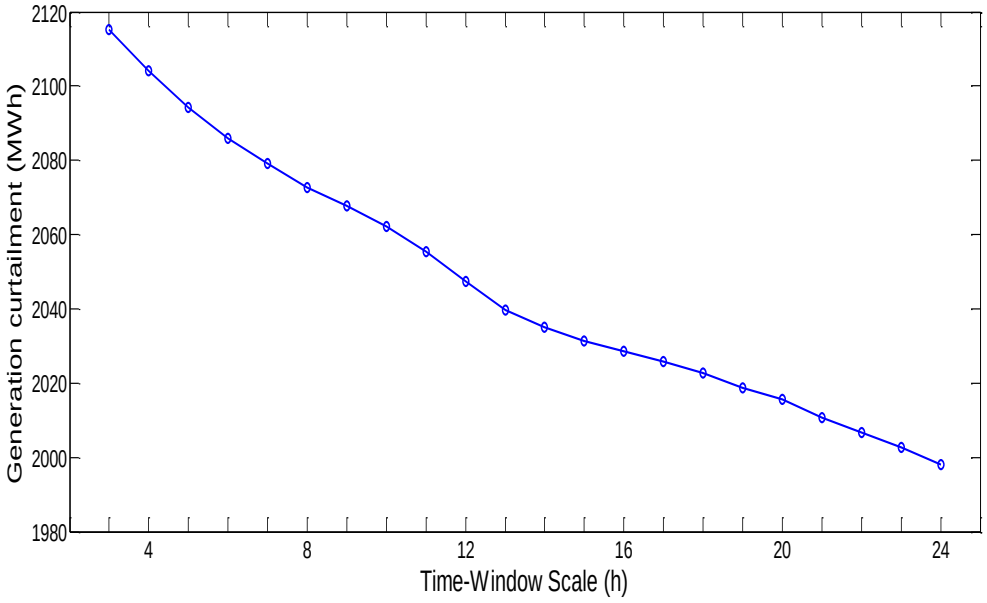

Figure 4-6 Annual Generation Curtailment of Enhanced Intelligent EV Charging Model under Different Time-Window Scales

As mentioned in 3.3.2, there is small fluctuations appearing in model 1 (Fig.3-5), which is due to the operation drawbacks of model 1. In model 1, load shifting depends on the line overloading of the first timeslot and the EV flexibility of the other timeslots. The operation in earlier hours may increase the power flow in later hours. Sometimes, the increased generation curtailment in later hours may be bigger than the saved generation curtailment in earlier hours, which makes the total annual generation curtailment more in the end and leads to the curve fluctuation. Model 2 sets the minimisation of total generation curtailment in time-window as the objective, and shifting process considers

both the EV flexibility and the power flow. Thus, there is no fluctuation in Fig. 4-6. The curve of model 2 is monotonically decreasing.

Table 4-4 lists the generation curtailment reduced by model 2 in different time-window scales. Model 2 can save more renewable generation by 3.93% in average, based on the curtailment level in model 1. The best condition reaches up to 5.67%, which is in 24-hour time-window scale. Table 4-4 clearly indicates that, compared with model 1, the operational benefit of model 2 also increases as time-window scale increases.

Table 4-4 Generation Curtailment Reduction in Different Time-Window Scales

Time-Window Scale (h)	**Model 1 (MWh)**	**Model 2 (MWh)**	**Generation Curtailment Reduction**
3	2152.45	2115.26	1.73%
4	2148.80	2104.03	2.08%
5	2144.99	2094.19	2.37%
6	2141.19	2085.92	2.58%
7	2137.01	2079.04	2.71%
8	2134.48	2072.76	2.89%
9	2132.03	2067.72	3.02%
10	2131.06	2062.26	3.23%
11	2130.27	2055.34	3.52%
12	2128.77	2047.49	3.82%
13	2128.52	2039.64	4.18%
14	2127.02	2035.03	4.33%
15	2126.07	2031.44	4.45%
16	2124.87	2028.53	4.53%
17	2124.36	2025.88	4.64%
18	2123.66	2022.56	4.76%
19	2121.67	2018.66	4.86%
20	2120.68	2015.57	4.96%
21	2120.63	2010.64	5.19%
22	2119.66	2006.64	5.33%
23	2119.87	2002.75	5.53%
24	2118.19	1998.06	5.67%

4.5. Chapter Summary

This chapter proposes an enhanced intelligent EV charging model to complement congestion management, where two significant improvements are proposed. Firstly, the

load shifting is optimised to be bi-directional, i.e. the excessive EV load demand can be shifted to either earlier hours or latter hours. Secondly, in the enhanced model, the selection of timeslot for shifting is improved with network power flow constraint.

Simulation results in the case study prove that the proposed enhance EV charging model can increase the utilisation level of renewable generation further based on the performance of intelligent EV charging model in Chapter 3. In a small range of time horizon (24 hours), bi-directional optimisation operation can further reduce the generation curtailment by 45%. The benefit from adding power flow constraint in load shifting is not as significant as the first improvement, but it still can reduce the annual generation curtailment by 0.05%. In terms of annual benefits, the enhanced intelligent EV charging can averagely save renewable energy by 3.93%.

CHAPTER 5. UNCERTAINTY MANAGEMENT WITH SR METHOD

This chapter proposes an uncertainty management strategy called SR method to allow the impact of risks that arise from network stress prediction on the expected operational benefits to be properly assessed, thus extending the traditional deterministic cost-benefit assessment to cost-benefit-risk assessment.

5.1. Introduction

Chapter 4 has proposed an enhanced congestion management with intelligent EV charging which refers to shifting flexible EV load over time to absorb excessive local wind generation. It acts as an efficient alternative to releasing network stresses and reducing wind generation curtailment. The charging optimisation is selected from several charging solutions which are determined by the overloaded timeslots and their corresponding network stresses. Due to the lack of real-time data, the model in Chapter 4 regards forecasted network data as real-time deterministic data for the simulation and analyses.

However, in practice, there are significant uncertainties in predicting network stresses introduced from wind forecasting error. Further, wind forecasting error increases as the lead time rises. Due to these two factors, the prediction of network stresses under different lead time are under different uncertainty levels. The operational benefits of EV charging solutions determined by network stresses will be under different uncertainty levels as well. It becomes difficult to compare the benefit of one EV charging solution to another when their benefits are under different uncertainty levels. EV charging optimisation should be improved from the traditional deterministic approach to a stochastic one by integrating uncertainty management.

This chapter addresses this critical challenge by applying SR concept, which is widely used by the financial sector for risk management. SR can help convert network operational benefits under different uncertainty levels into an equivalent benefit value under per unit uncertainty level, i.e. ‘mitigate’ the effects of uncertainty in the performance assessment.

The rest of this chapter is organized as follows: Section 5.2 gives an overview of uncertainty management; Section 5.3 introduces the basic SR theory in financial risk management and wind forecast error; Section 5.4 proposes the application of SR method to the enhanced congestion management; Section 5.5 provides a case study of a 33kV network; and the conclusions are drawn in Section 5.6.

5.2. Literature Review about Uncertainty Management

5.2.1. Concept of Uncertainty

Uncertainty means that it is impossible to exactly describe the existing state or a future outcome because of the limited knowledge about the state. In power system, uncertainty sources include generation availability, load requirements, unplanned outages, market rules, fuel price, energy price, market forces, weather and other interruptions, etc. [65]. They will affect power systems planning and operation in the following aspects:

1) Entry of new energy producing/trading participants,
2) Increases in regional and intraregional power transactions,
3) Increases in sensitive loads,
4) New types and numbers of generation resources.

Uncertainty analysis is a part of risk assessment that focuses on the uncertainties in the assessment. Important components of analysis include qualitative analysis that identifies the uncertainties, quantitative analysis of the effects of the uncertainties on the decision process, and communication of the uncertainty.

In power system, generation and load demand are important inputs for power flow analysis. In some operation situations, we have to forecast generation and load based on historical data to arrange the network operation in advance. However, it is impossible to accurately forecast load and generation even one hour ahead. Therefore, some degree of forecasting errors always exists. The uncertainties analysed in this thesis only refer to forecasting errors.

Many researches have been done to investigate the effect of forecasting errors in power system [66-76]. Most of the work is related with network reliability evaluation. Papers [66-68] use analytical methods on reliability evaluation of power system including wind generation. Paper [69] introduces a Monte Carlo based production cost simulation model to valuate reliability of a power system integrated with wind generation, where reliability indices Loss of Load Expectation and Expect Energy Not Served are analysed. The effects of load forecast uncertainty in bulk system reliability assessment are examined in paper [70-72], incorporating changes in system composition, topology,

load curtailment policies and bus load correlation levels. Papers [75] and [76] analyse System Average Interruption Duration Index and System Average Interruption Frequency Index to indicate the effects of load uncertainty in network reliability. Paper [73] and [74] show the calculation of optimal amount of spinning reserve to respond not only to generation outages but also to errors in the forecast for load and wind power output.

By now, however, little work has been done to investigate how forecasting errors would affect network operation, especially in ANM. In the enhanced congestion management proposed in this thesis, the wind and load forecasting errors will cause errors in the perdition of network stress, which will further introduce errors in the expected generation curtailment. Thus, this thesis will analyse the impacts of forecasting errors on the enhanced congestion management through evaluating the uncertain power flows.

5.2.2. Methods for Uncertain Power Flow Calculation

Some methods that incorporate uncertainty in system variables have been proposed to deal with the uncertain power flow analysis problem. According to applied mathematical techniques, these works can be classified into three categories: Monte Carlo Simulation, probability power flow method and fuzzy power flow method.

5.2.2.1. Monte Carlo Simulation Method

Monte Carlo Simulation [77] is the most straightforward method to solve uncertainty problem, which involves repeated simulation with values obtained from probability density function of the input variables. Firstly, each input variable with probabilistic distribution produces thousands of input scenarios. Secondly, the corresponding thousands of output scenarios are calculated with the deterministic load flow. Finally, the probabilistic distributions of output variables are obtained through evaluating the output scenarios. Due to the use of DC flow, the accuracy of solution is sensitive to a prior knowledge of input variables. If appropriate input information is available, the obtained results become more accurate.

Monte Carlo Simulation with simple random sampling is direct and, theoretically, it has no utilization limitation. For example, it can use accurate non-linear function of inputs to calculate the uncertain outputs. But it needs large quantity of computational efforts and memory to obtain significant results, which makes it normally be used to validate the accuracy of other methods.

5.2.2.2. Probabilistic Power Flow Method

Analytical probabilistic power flow method is one of suitable tools to analyse the uncertain impact of load/wind forecasting errors on the grid. By evaluating the uncertainties of output variables, the potential risky and weak points of the network can be found. Analytical method of probabilistic power flow was first proposed in 1974 by Borkowska. A simplified model with two assumptions was proposed: 1) The electric power system is introduced with a DC power network， therefore, reactive power is not considered and 2) the nodal active power demands are treated as random independent variables [78].

Later, Allan extended the method to AC power flow and widely applied it to network management, short-term and long-term electrical network planning etc.[79-85]. The original probabilistic power flow method utilized convolution method to calculate the probability distributions of power flows. Although it reduces the computational burden, it is still costly to obtain the probability density function of a single line when the network model is extended. Moreover, the convolution method requires that the input variables are independent or linearly related.

Fast Fourier transform techniques were proposed to reduce the computational burden [81], but this method is linked to the convolution technique, and does not solve the problem efficiently. Paper [86] proposed a method using cumulants of the probability density function and the Gram Charlier expansion. It requires low computational burden. However, for non-Gaussian probability density function, Gram Charlier expansion has serious convergence problems. Paper [87] proposed a method based on cumulants of the probability density function and the Cornish-Fisher expansion. The author demonstrated that Cornish Fisher expansion performed better than Gram Charlier expansion for non-Gaussian distribution. A recent proposal is the point

estimate method [88, 89]. It approximates the moments of the system variables of interest to calculate the moments of the output variables. Then the probability distribution of the output variables can be derived from their moments.

The core of probabilistic power flow method is to obtain network power flows in terms of probability distributions or cumulative distributions through the probability distribution functions or cumulative distribution functions of nodal inputs. Thus, the uncertainties in nodal inputs can be reflected in the probability distributions. In paper [79], the expected values and standard deviation of each power flow are calculated and overall balance of power in the system is determined in terms of a density function. This allows quantitative assessment of network reliability and security. Papers [90, 91] use probabilistic power flow method to investigate distribution network's voltage security caused by wind power integration.

5.2.2.3. Fuzzy Power Flow

Another family of algorithms for load flow calculation under uncertainty is based on the fuzzy set theory [92-94]. The concept of fuzzy set theory was introduced by Zadeh in 1965 and it was first introduced in 1979 for solving power system problems [93]. Unlike the probabilistic power flow models highly related to the statistical behaviour of a phenomenon, the uncertainty from system variables in fuzzy models is usually given in fuzzy numbers with known possibility distributions which is a vague or inaccurate concept. The corresponding power flow results are therefore in fuzzy numbers with possibility distribution [92]. Although the computation burden of fuzzy power flow is smaller than probabilistic power flow, there is high imprecision involved in fuzzy method. Furthermore, fuzzy method requires to build up membership functions for input variables, which will heavily rely on historical data.

Basically a fuzzy logic system consists of the following 5 steps [95]:

1) Fuzzification: Converting the crisp inputs to membership functions which comply with intuitive perception of system status.
2) Rules Processing: Calculating the response from system status inputs according to the pre-defined rules matrix (control algorithm implementation).

3) Inference: Evaluating each case for all fuzzy rules
4) Composition: Combining information from rules
5) Defuzzification: Converting the result to crisp values.

5.3. SR Theory and Wind Forecast Error

5.3.1. SR Theory in Financial Risk Management

Financial risk management is the process to identify, assess, measure, and manage financial risk in order to create economic value [96]. For a general portfolio, its return and initial investment value has a relationship as in (5-1):

$$R = \frac{\Delta R}{IC} \tag{5-1}$$

where, ΔR is the profit/loss of a portfolio over a fixed horizon, IC is the initial investment, and R is the future rate of return.

When we confront with several portfolios to invest, a risk-adjusted performance measurement is needed to help make the decision. The simplest method is Sharpe Ratio [97], which is the ratio of the average rate of return μ_R in excess of the risk-free rate R_F divided by the volatility σ_R:

$$SR = \frac{\mu_R - R_F}{\sigma_R} \tag{5-2}$$

where, the mean rate of return is defined as μ_R. The standard deviation is often called volatility, defined as σ_R.

In order to assist understanding, a simple example is provided here. Suppose we have certain amount of money to invest, for example, two options: stocks and bonds. They have different average rate of return and volatility. Stocks has higher average rate of return but also higher volatility. Therefore, SR is used to determine their value to invest. Keeping the cash in pocket is set as the reference investment case because it is risk-free. The reference case has a return of 3%. The slope of the line from cash to each investment option as shown in Fig. 5-1 is the SR value of corresponding options. SR transfers the rate of return under different risk levels to equivalent rate of return under

unity risk, making the profits of different investment options comparable. In this case, stocks have a higher SR than bonds, indicating that under the same volatility bonds have higher rate of returns than bonds. Thus, stocks will be chosen to invest the money.

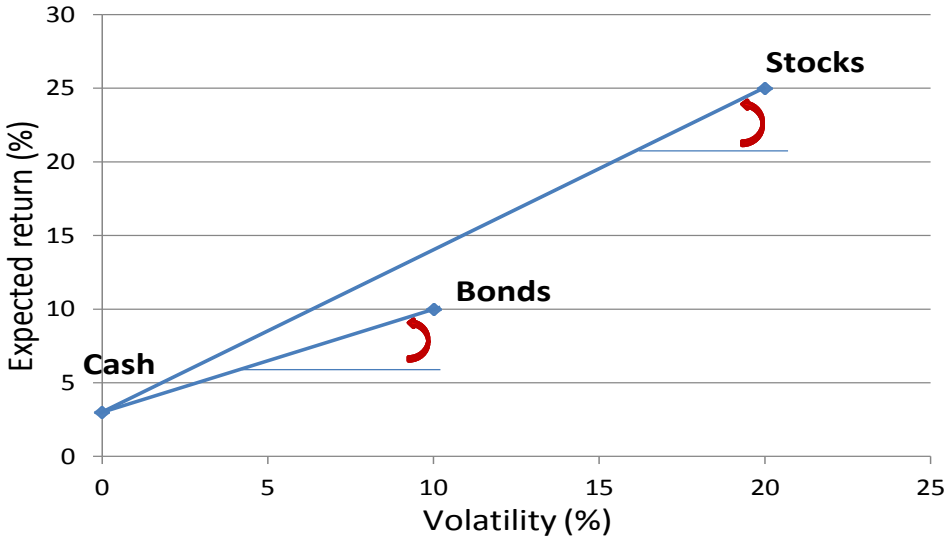

Figure 5-1 Illustration of SR Operation in Financial Sector

5.3.2. Wind Forecasting Error

In order to simplify the analyses of applying SR method to intelligent EV charging, the uncertainties in this chapter only refer to wind forecasting errors. Wind power is clean but also contains high intermittency. Exponential smoothing method is applied to forecast wind generation.

The concept exponential smoothing was first suggested by Robert Goodell Brown in 1956 [98]. The simplest form of exponential smoothing is given by the formula (5-3) [99].

$$s_t = \alpha \cdot x_{t-1} + (1-\alpha) \cdot s_{t-1} \quad (5\text{-}3)$$

where, $\{x_t\}$ is the raw data sequence of observations, the smoothed statistics $\{s_t\}$ is the output, α is the smoothing factor, and $0 < \alpha < 1$. In other words, the smoothed statistic $\{s_t\}$ is a simple weighted average of the previous observation $\{x_{t-1}\}$ and the previous smoothed statistic $\{s_{t-1}\}$.

The drawback of simple exponential smoothing is that it does not consider the trend in the data [100]. The basic idea to improve the exponential smoothing is to introduce a term to stand for the possible trend. This slope component is itself updated via exponential smoothing. Paper [101] shows a model to explain the double exponential smoothing method. The in-depth equations are listed in (5-4)-(5-8).

$$s_t^{(1)}=\alpha\cdot x_{t-1}+(1-\alpha)s_{t-1}^{(1)} \tag{5-4}$$

$$s_t^{(2)}=\alpha\cdot s_t^{(1)}+(1-\alpha)s_{t-1}^{(2)} \tag{5-5}$$

$$a_t = 2s_t^{(1)} - s_t^{(2)} \tag{5-6}$$

$$b_t = \frac{\alpha}{1-\alpha}\left(s_t^{(1)}-s_t^{(2)}\right) \tag{5-7}$$

$$X_{t+m}=a_t+m\cdot b_t \tag{5-8}$$

where, the output of the algorithm is now written as $\{X_{t+m}\}$. m is the lead time of forecasting. a_t is the estimated level at timeslot t, and b_t is the estimated trend at timeslot t.

The double exponential smoothing is suitable for time-series forecasting with linear trend. Due to the intermittency of wind, the trend of its forecasting is non-linear. Thus, triple exponential smoothing method is adopted in this chapter to forecast wind generation. Paper [102] has explained the operation of triple exponential smoothing as shown in (5-9)-(5-15).

$$s_t^{(1)}=\alpha\cdot x_{w,t-1}+ (1-\alpha)s_{t-1}^{(1)} \tag{5-9}$$

$$s_t^{(2)}=\alpha\cdot s_t^{(1)}+(1-\alpha)s_{t-1}^{(2)} \tag{5-10}$$

$$s_t^{(3)}=\alpha\cdot s_t^{(2)}+(1-\alpha)s_{t-1}^{(3)} \tag{5-11}$$

$$a_t=3s_t^{(1)}-3s_t^{(2)}+s_t^{(3)} \tag{5-12}$$

$$b_t=\frac{\alpha}{2(1-\alpha)^2}\left((6-5\alpha)s_t^{(1)}-(10-8\alpha)s_t^{(2)}+(4-3\alpha)s_t^{(3)}\right) \tag{5-13}$$

$$c_t = \frac{\alpha^2}{2(1-\alpha)^2}\left(s_t^{(1)}-2s_t^{(2)}+s_t^{(3)}\right) \tag{5-14}$$

$$X_{W,t+m}=a_t+m\cdot b_t+m^2\cdot c_t \tag{5-15}$$

where, $\{x_{w,t}\}$ represents the sequential actual real-time data of wind generation, $\{X_{W,\,t+m}\}$ is the forecasted sequential wind data in m-hour ahead, and α is normally set as 0.4.

Fig. 5-2 shows the statistical distributions of wind forecasting errors on busbar 5019 at the 1st, 12th and 24th hour. No matter which type it is fit, the accuracy of wind forecasting is decreasing as the time horizon increases. Shorter time horizon probably has more concentrated error distribution around zero, indicating that the forecasting results are more accurate and reliable. Larger time horizon has more flat distribution, implying that the prediction results are more scattered and less accurate.

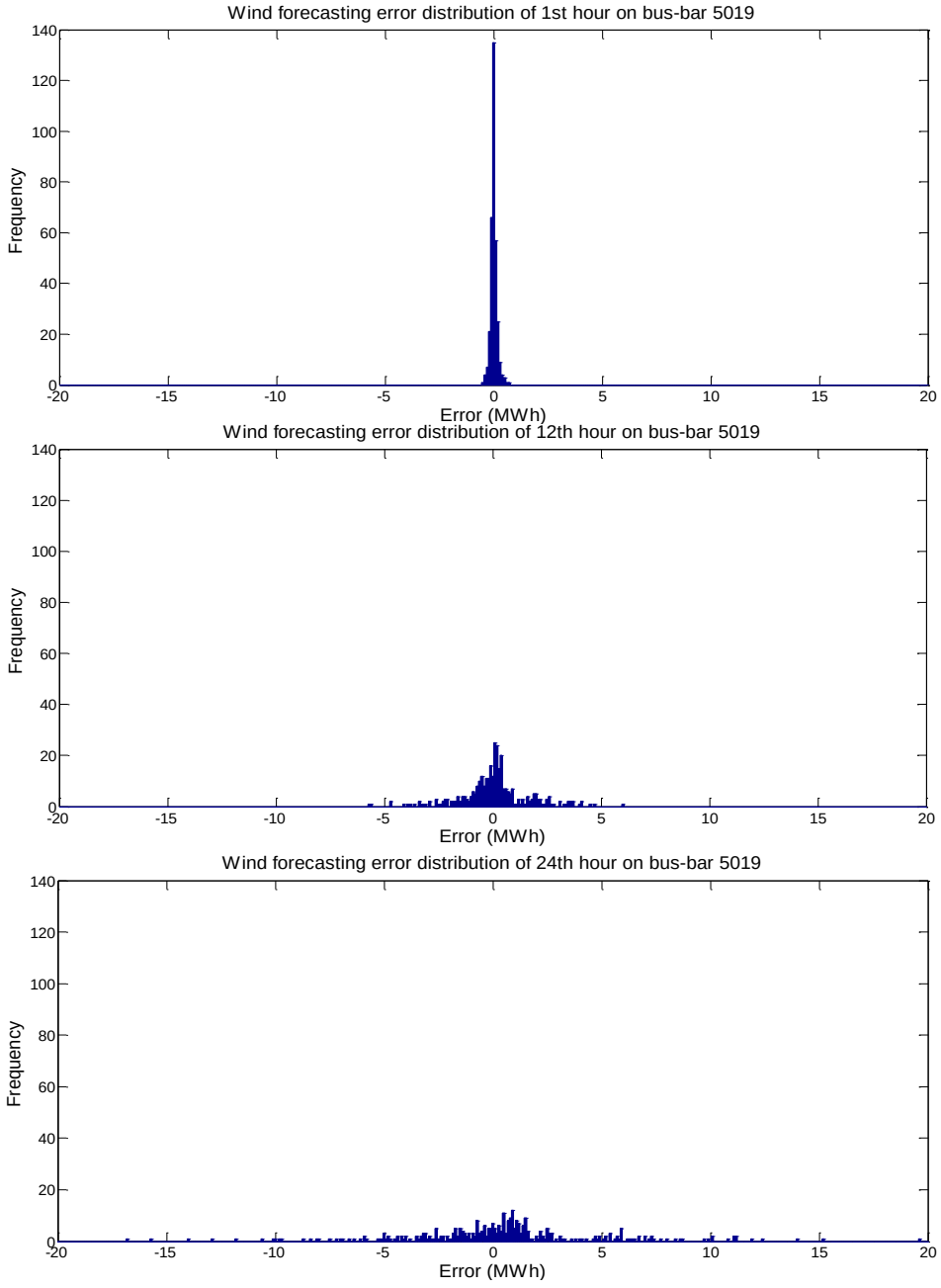

Figure 5-2 Distribution of Wind Forecast Error on Busbar 5019

Fig. 5-3 gives the in-depth information about the wind forecasting errors on busbar 5019. Both the mean value and standard deviation of forecasting error increase as the forecasting time horizon increases, which is consistent with Fig. 5-2. The increasing speed of standard deviation is much higher than the mean values.

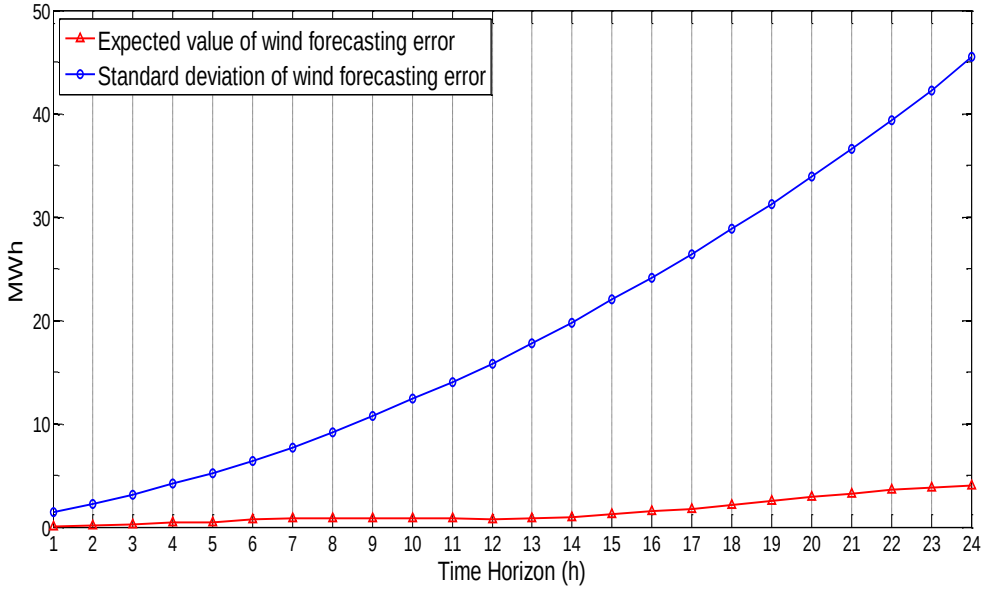

Figure 5-3 Mean Value and Standard Deviation of Wind Forecasting Error on Busbar 5019

5.4. Uncertainty Management with SR Method

The proposed uncertainty management in intelligent EV charging has two steps. Firstly, the uncertain network power flows with wind forecasting errors involved are calculated. Since the statistical distribution of wind forecasting error has already been obtained and the analytical probabilistic power flow method is easily understood, this chapter adopts the convolution method to calculate the uncertain power flow. Secondly, SR method is adopted to 'mitigate' the effects of uncertainties in decision-making stage of congestion management.

5.4.1. Basic Analytical Probabilistic Power Flow

The basic analytical probabilistic power flow method is convolution method which is applied with two assumptions:

1) The distribution of wind forecasting errors are in normal distribution, which will be validated by Monte Carlo Simulation in the case study;
2) The power injections on busbars are regarded as independent variables.

As explained in Appendix B, in DC power flow, the relationship between nodal injected power and branch power flow is linear. Element PTDF(l, i) in the matrix indicates the change of active power flow on line l when one unit of power injection is added on busbar i. According to PTDF matrix and the convolution techniques, the probability density function of power flow on line l at timeslot t ($f(PF_{T,t,l})$) can be derived below in (5-16).

$$f(PF_{T,t,l})=(PTDF(l,1)\times f(P_{T,t,1}))\otimes\ldots\otimes(PTDF(l,NB)\times f(P_{T,t,NB})) \quad (5\text{-}16)$$

where, $f(P_{T,t,1})$ is the probability density function of nodal injected power on busbar 1 at timeslot t. And $\otimes$ is the convolution symbol.

According to the probability theory and mathematical statistics, if we have two independent random variables x_1 and x_2 which follow normal distribution:

$$x_1 \sim N(\mu_1, {\sigma_1}^2),\ x_2 \sim N(\mu_2, {\sigma_2}^2) \quad (5\text{-}17)$$

and $y= x_1+ x_2$, through the convolution calculation, the probability density function of y is also in normal distribution:

$$y \sim N(\mu_1 + \mu_2, {\sigma_1}^2 + {\sigma_2}^2) \quad (5\text{-}18)$$

This rule works even there are several independent variables. Therefore, if the probability density functions of forecasted wind generation are normal distributions and the busbars are assumed to be independent to each other, the useful conclusions can be used directly:

1) The mean value of the power flow on line l $\mu_{PF_{T,t,l}}$ can be directly calculated based on (5-19).

$$\mu_{PF_{T,t,l}}=\sum_{i=1}^{NB} PTDF(l,i)\times\mu_{P_{T,t,i}} \quad (5\text{-}19)$$

2) The standard deviation of power flow on line l $\sigma_{PF_{T,t,l}}$ can be directly calculated based on (5-20).

$$\sigma_{PF_{T,t,l}}{}^2 = \sum_{i=1}^{NB} (PTDF(l,i) \times \sigma_{P_{T,t,i}})^2 \quad (5\text{-}20)$$

5.4.2. SR Method in Intelligent EV Charging

When wind forecasting error is considered, original deterministic $GC_{0,t}$ will be replaced by the mean value $\mu_{GC_{0,t}}$, with standard deviation $\sigma_{GC_{0,t}}$. The original deterministic $GC_{T,t}$ at each timeslot t in trial T will be replaced by the mean value $\mu_{GC_{T,t}}$, with standard deviation $\sigma_{GC_{T,t}}$. The detailed deviation is listed below.

Probabilistic power flow has given the mean values $\mu_{PF_{T,t,l}}$ and standard deviation $\sigma_{PF_{T,t,l}}$ of branch power flow according to mean value and standard deviation of nodal power injections. The mean value $\mu_{OL_{T,t,l}}$ and standard deviation $\sigma_{OL_{T,t,l}}$ of line overloading is derived in (5-21) and (5-22).

$$\mu_{OL_{T,t,l}} = \mu_{PF_{T,t,l}} - P_l^{max} \quad (5\text{-}21)$$

$$\sigma_{OL_{T,t,l}} = \sigma_{PF_{T,t,l}} \quad (5\text{-}22)$$

The mean value $\mu_{GC_{T,t,l,i}}$ and standard deviation $\sigma_{GC_{T,t,l,i}}$ of generation curtailment caused by a specific line l is determined in (5-23) and (5-24), respectively.

$$\mu_{GC_{T,t,l,i}} = \frac{\mu_{OL_{T,t,l}}}{PTDF(l,i)} \quad (5\text{-}23)$$

$$\sigma_{GC_{T,t,l,i}} = \frac{\sigma_{OL_{T,t,l}}}{PTDF(l,i)} \quad (5\text{-}24)$$

However, one overloaded line may require one or more nodes to curtail their wind generation to completely release congestion. Assume the generation curtailments on these nodes are uncorrelated with each other. Thus, the expected value and standard deviation of total generation curtailment amount caused by overloaded line l at timeslot t are defined in (5-25) and (5-26):

$$\mu_{GC_{T,t,l}} = \sum_{CN} \mu_{GC_{T,t,l,i}} \quad (5\text{-}25)$$

$$\sigma_{GC_{T,t,l}} = \sqrt{\sum_{CN} \sigma_{GC_{T,t,l,i}}^2} \quad (5\text{-}26)$$

Where, CN stands for nodes need to curtail wind generation curtailed in order to relieve the overloading on line l.

At a specific timeslot t, there may be several overloaded lines, which are assumed to be uncorrelated with each other. Thus, the mean value $\mu_{GC_{T,t}}$ and standard deviation $\sigma_{GC_{T,t}}$ of total generation curtailment in the network at timeslot t in trial T is shown in (5-27) and (5-28):

$$\mu_{GC_{T,t}} = \sum_{M} \mu_{GC_{T,t,l}} \quad (5\text{-}27)$$

$$\sigma_{GC_{T,t}} = \sqrt{\sum_{M} \sigma_{GC_{T,t,l}}^2} \quad (5\text{-}28)$$

where, M stands for all the lines with congestion at timeslot t.

When uncertainty is considered, the selection principle of execution timeslots changes from "largest generation curtailment reduction" to "larger generation curtailment reduction - less uncertainty". The mean values $\mu_{GC_{T,t}}$ from probabilistic power flow are not sufficient for choosing the "largest generation curtailment reduction - least uncertainty" trial. For example, it is possible that two trials have exactly same mean values. However, one has very flat distribution, i.e. large error, whereas the other one is more sharply distributed, i.e. less error. The latter timeslot could be easily selected as the execution timeslot. Thus, the selection guide is redefined in (5-29).

$$GCR'_T = \sum_{t=1}^{TWS} \frac{\mu_{GC_{0,t}} - \mu_{GC_{T,t}}}{\sigma_{GC_{T,t}}} \quad (5\text{-}29)$$

The generation curtailment reduction at each timeslot k is a sub-benefit of trial T. The sub-benefits are under different uncertainty levels since the network stress prediction at each timeslot are under different lead time forecasting. As in (5-29), the sub-benefits are converted into equivalent sub-benefit value under unity uncertainty level first. Then, summing up all equivalent sub-benefits in the time-window can get the performance assessment GCR'_T of trial T. There is no unit for GCR'_T because the units of

numerator and denominator in (5-29) are all MWh. By comparing $GCR_T^{'}$, the trial execution timeslot with the largest $GCR_T^{'}$ is selected as the real execution timeslot to conduct load shifting. The detailed flowchart is shown in Fig. 5-4.

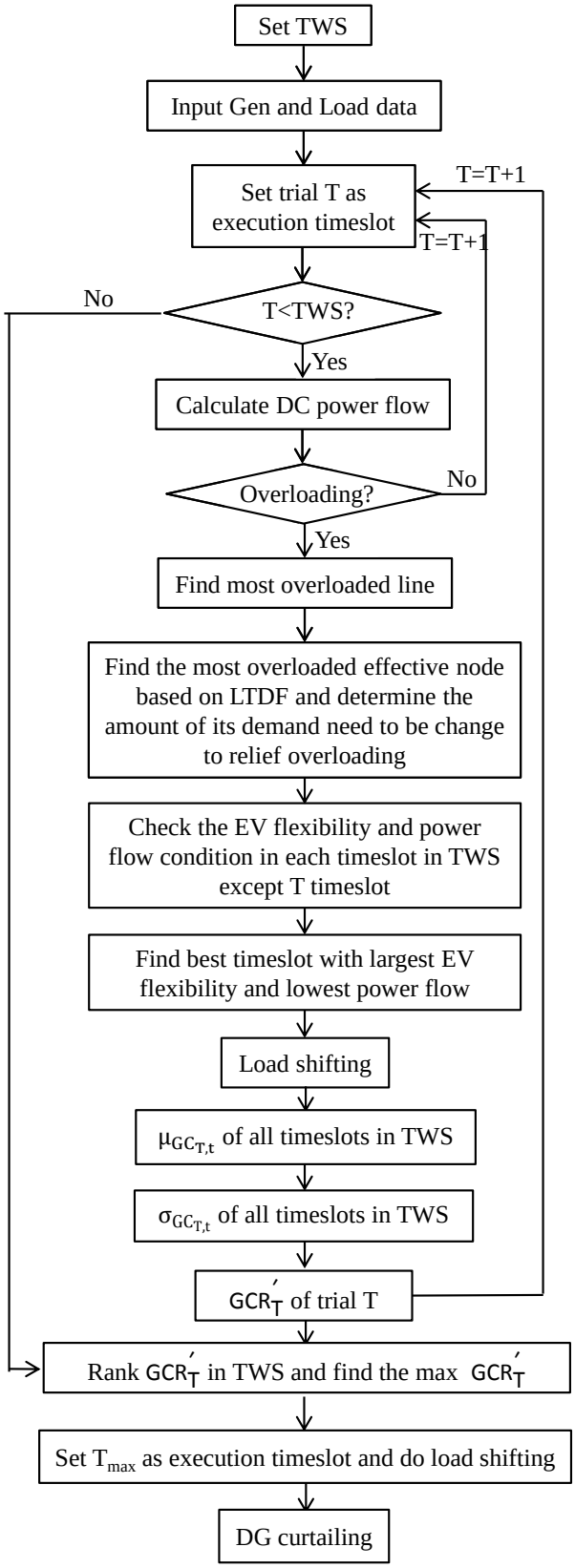

Figure 5-4 Flowchart of Intelligent EV Charging with SR Method

5.5. Case Study

Aberystwyth 33kV network is still the test system to analyse the effects of wind forecasting error on the enhanced congestion management. The load and generation profiles of one day (24h) are used to do the simulations and the time-window scale is set to be 24 hours. The analyses consist of two parts: 1) validate the assumptions made in the SR method; 2) evaluate the effects brought by wind forecasting error on system operation.

Chapter 3 and Chapter 4 regard forecasted data of load and wind generation in year 2030 as real-time data to do the simulation, i.e. the short-term forecasting errors (within 24 hours) were assumed as zero. In this chapter, however, the forecasted hourly generation data in year 2030 are regarded as the base value for short-term forecasting. The mean value and standard deviation of wind forecasting error have been obtained in Section 5.3.2. The hourly load data are still utilised as deterministic data.

5.5.1. Validation of Assumption

Monte Carlo Simulation is utilised in this section to validate the assumption that the wind forecasting errors follow normal distribution. The number of Monte Carlo Simulation sampling is 50000. In each sampling, the procedure is as follows:

1) According to the real distributions of wind forecasting errors as shown in Section 5.3.2, Matlab is used to generate a random value of power output for each wind farm.
2) Input the wind generation samples and other network variables to calculate the DC network power flow.
3) Record the power flows and go back to step 1).

Fig. 5-5 shows the distribution of power flow on line 5010-5012 at 24th hour calculated by Monte Carlo Simulation.

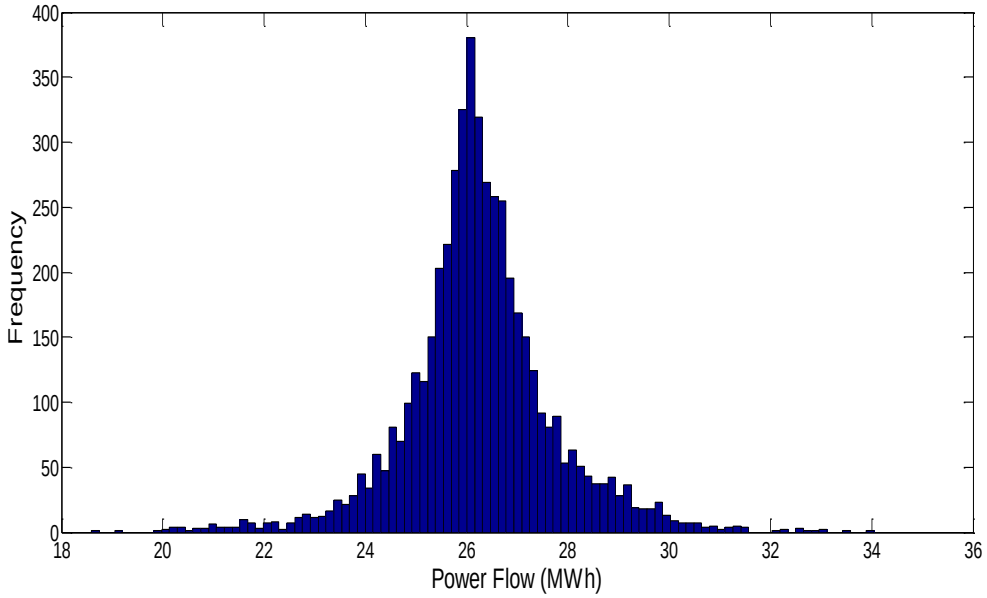

Figure 5-5 Distribution of Power Flow on Line 5010-5012 at 24th Hour under Monte Carlo Simulation

Fig. 5-6 gives the entire 24-hour uncertain power flow on line 5010-5012 under Monte Carlo Simulation. The blue curve is the mean value of power flow. The red dotted line is the line rating of line 5010-5012. The filling areas with orange colour show the distribution of uncertain power flow. The darkness of the colour indicates the probability of power flow in this area. Darker area indicates higher probability of power flow value locating in this area. The 24-hour data is forecasted at 0:00 a.m. of the chosen day. Fig. 5-6 shows that the distribution of power flow in latter hours is much scatter than those in early hours, which is consistent with the characteristics of wind forecast error.

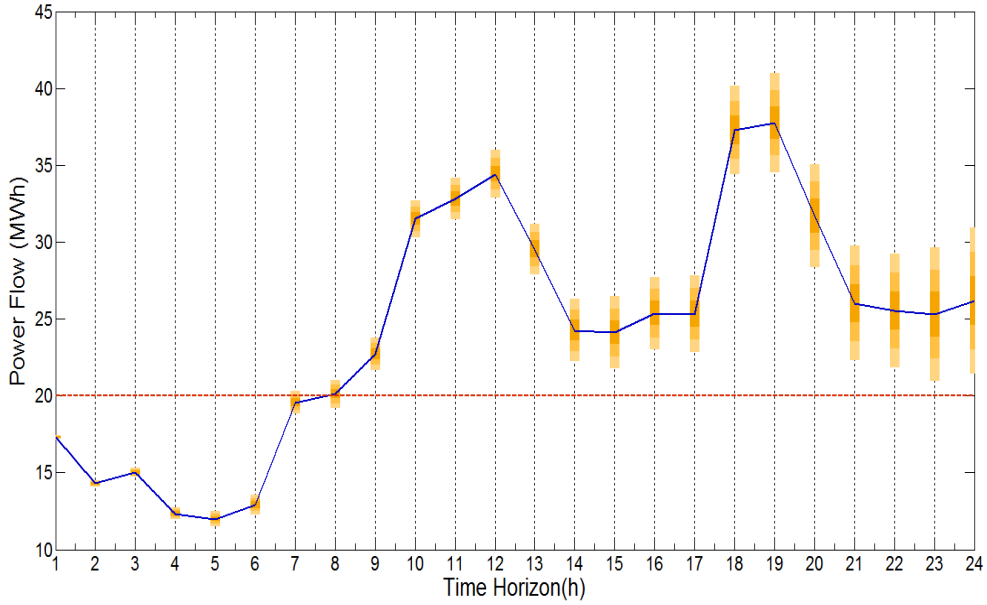

Figure 5-6 Uncertain Power Flow on Line 5010-5012 in 24 Hours Based on Monte Carlo Simulation

Fig. 5-7 shows the uncertain power flow on line 5010-5012 derived by the simplified convolution method with assumptions. The uncertain levels of power flow in Fig. 5-6 and Fig. 5-7 are very similar, which indicates that the assumptions made about wind forecasting error will not influence the system operation too much. The in-depth differences in probabilistic power flow results between Monte Carlo Simulation and simplified convolution method are listed in Table 5-1.

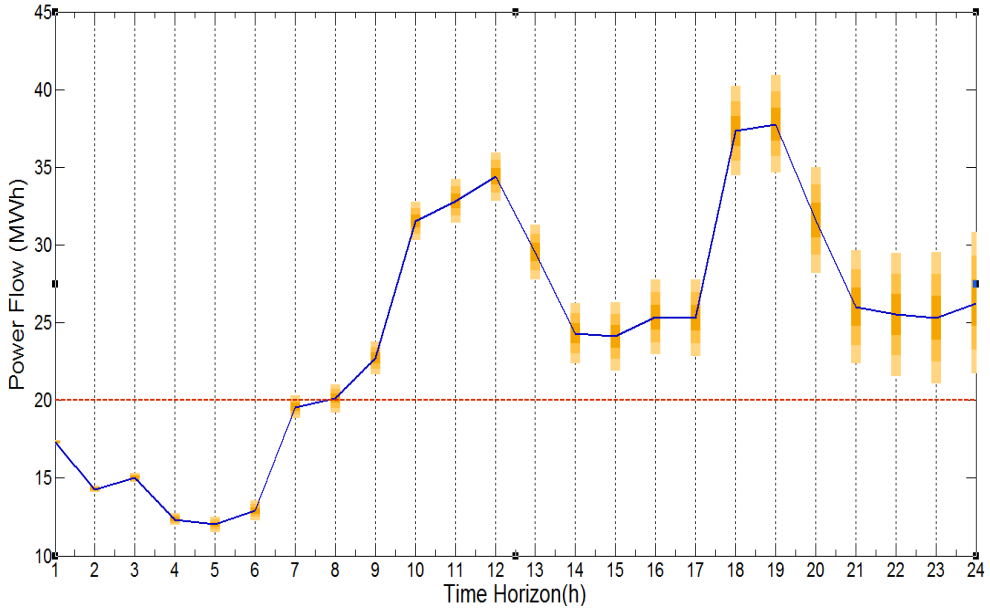

Figure 5-7 Uncertain Power Flow on Line 5010-5012 Based on Simplified Convolution Method

Table 5-1 compares the mean value and standard deviation of power flow on line 5010-5012 in 24 hours. The results from Monte Carlo Simulation are the reference data. The maximum difference brought by the assumptions in expected value and standard deviation are 0.31% and 6.64%, respectively. The difference level in standard deviation is higher than that in mean value, which however still can be tolerated.

Table 5-1 Comparison of Monte Carlo Simulation and Simplified Convolution Method

Time (h)	Mean Value of Power Flow			Standard Deviation of Power Flow		
	Monte Carlo Simulation	Simplified Convolution Method	Difference	Monte Carlo Simulation	Simplified Convolution Method	Difference
1	17.301	17.300	-0.01%	0.043	0.044	1.43%
2	14.292	14.286	-0.04%	0.076	0.073	-4.38%
3	15.015	15.014	-0.01%	0.104	0.102	-1.58%
4	12.347	12.347	0.00%	0.129	0.135	5.06%
5	11.993	11.998	0.04%	0.170	0.172	0.94%
6	12.900	12.898	-0.02%	0.214	0.214	0.24%
7	19.567	19.570	0.01%	0.251	0.253	0.66%
8	20.107	20.116	0.05%	0.300	0.302	0.68%
9	22.731	22.719	-0.05%	0.350	0.351	0.45%
10	31.499	31.520	0.07%	0.408	0.410	0.50%
11	32.814	32.824	0.03%	0.451	0.464	3.01%
12	34.418	34.388	-0.09%	0.515	0.523	1.43%
13	29.540	29.530	-0.03%	0.552	0.585	6.01%
14	24.244	24.275	0.13%	0.676	0.645	-4.59%
15	24.111	24.104	-0.03%	0.778	0.728	-6.52%
16	25.365	25.340	-0.10%	0.788	0.800	1.56%
17	25.320	25.302	-0.07%	0.831	0.814	-1.99%
18	37.277	37.313	0.10%	0.950	0.959	0.91%
19	37.748	37.762	0.04%	1.069	1.046	-2.12%
20	31.683	31.592	-0.29%	1.119	1.133	1.21%
21	26.018	25.994	-0.09%	1.239	1.220	-1.54%
22	25.537	25.504	-0.13%	1.234	1.316	6.64%
23	25.303	25.283	-0.08%	1.450	1.413	-2.56%
24	26.179	26.261	0.31%	1.586	1.517	-4.31%

5.5.2. Results of SR method

This section analyses the necessity of considering both mean value and standard deviation in uncertainty management, which in turn proves the rationality of SR method. If the uncertainty management only be represented by mean values, the selection rule will be same with that in Chapter 4, i.e. the timeslot with largest

generation curtailment reduction will be selected as real execution timeslot. The only difference is that the deterministic power flow in Chapter 4 is replaced by the mean value of power flow in this section. We call this case "EX case" for convenience. The case with selection rule based on SR method is called "SR case".

Fig. 5-8 shows the performance assessment of every trial execution timeslot in both EX case and SR case. Red line stands for the performance assessment in EX case (quantified by GCR) and blue line represents the SR case (quantified by GCR'). In the first 7 trials, both the GCR and GCR' values are zero since there is no network congestion from 1:00 a.m. to 7:00 a.m. According to charging rule, no intelligent EV charging will be done. Therefore, there is no generation curtailment reduction.

For SR case, trial 10 gives the largest GCR' (0.351), making it as the real execution timeslot. In EX case, trial 10 also gives the largest GCR (0.580), which guides the same selection result as in SR case. In this 24-hour case, the final decision does not reflect the importance of standard deviation. However, the in-depth performance information of trials as listed in Table 5-2 indicates the necessity of considering both mean value and standard deviation in uncertainty analysis.

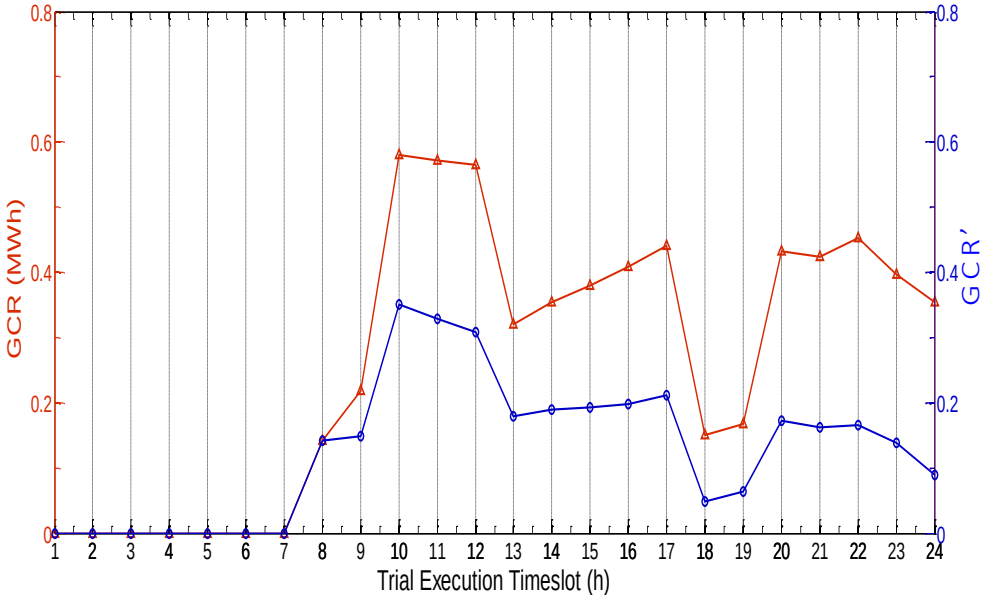

Figure 5-8 Selection of Execution Timeslot in EX Case and SR Case

Table 5-2 gives the performance ranking of the trial execution timeslots in both EX case and SR case. Except the top three timeslots, the ranking order of the remaining timeslots

changes dramatically, which indicates the decision-making will be affected by standard deviation.

Table 5-2 Performance Ranking of Trial Execution Timeslot

Trial Execution Timeslot	EX Case		SR Case	
	GCR	Ranking	GCR'	Ranking
1	0	18	0	18
2	0	18	0	18
3	0	18	0	18
4	0	18	0	18
5	0	18	0	18
6	0	18	0	18
7	0	18	0	18
8	0.141	17	0.141	13
9	0.217	14	0.148	12
10	0.580	1	0.351	1
11	0.572	2	0.328	2
12	0.565	3	0.308	3
13	0.321	13	0.180	8
14	0.353	11	0.190	7
15	0.380	10	0.193	6
16	0.408	8	0.198	5
17	0.441	5	0.212	4
18	0.150	16	0.049	17
19	0.167	15	0.063	16
20	0.432	6	0.173	9
21	0.424	7	0.162	11
22	0.452	4	0.165	10
23	0.397	9	0.138	14
24	0.353	11	0.089	15

According to EX case, trail 22 has larger GCR than trail 17. However, trail 22 also contains larger standard deviation. This is because intelligent EV charging in trail 22 is done based on values 22-hour ahead forecasted, while the operation in trial 17 depends on data from 17-hour ahead forecasting. Thus, trial 17 has higher priority than trial 22 in SR case, which proves that mean value of power flow is not sufficient to completely reflect the characteristics of forecasting errors in wind power. SR method introduces a new way to evaluate the effect of uncertainty involving both mean value and standard deviation. The generation curtailment of SR method should be not smaller than that in PPF case. It is because that EX case chooses the largest generation curtailment reduction trial, while SR case chooses the trial considering both benefit and volatility, which may be the one with less generation curtailment reduction.

5.6. Chapter Summary

This chapter proposes an uncertainty management for the enhanced congestion management. Uncertainty management is a complicated task associated with many factors. To get started in analysing uncertainties, this chapter makes several assumptions to simplify the problem. Only wind forecasting error is considered in this chapter and the distribution of wind forecasting error is assumed to be normal distribution. The validation of the assumption is proved by Monte Carlo Simulation. The uncertain power flow are generated by simplified convolution method. The most valuable innovation of this chapter is to borrow SR concept which is widely used in financial risk management to help make a trade-off between operational benefits and its associated risks.

SR method normalizes the benefits of EV charging solutions under different uncertainty levels to an equivalent benefit value under per unit uncertainty level to help make system operation decision. In order to simplify the strategy, only wind forecasting error is considered in SR model. Although many research have investigated the effects of uncertainties, most of the work focuses on reliability analysis and uncertain power flow calculation. Little work has been done in ANM. This thesis states a specific problem in active network operation which has never been investigated, and provides a completely new way to treat uncertainty. Therefore, it is difficult to validate SR method with other methods. The only way to verify SR method is to prove the rationality of its definition, which is detailedly demonstrated in case study.

Applying the financial concept to power system gives a new perspective to analyse the uncertainty in ANM. SR method allows the impact of risks that arise from network stress prediction on the expected operational benefits to be properly assessed, thus extending the traditional deterministic cost-benefit assessment to cost-benefit-risk assessment. The principle of SR method is very straight forward and can easily accommodate uncertainty without any big change in the operation structure of ANM. It has low calculation burden, which implies that it can be easily applied to other power system areas with uncertainty problems. This is the major contribution of this thesis.

CHAPTER 6. ENHANCING UNCERTAINTY MANAGEMENT WITH RAROC METHOD

This chapter proposes an enhanced uncertainty management method called RAROC method to address the limitations in SR method. Both wind and load forecasting errors are considered and they are allowed to be in any distribution.

6.1. Introduction

Chapter 5 proposes a SR method to integrate wind forecasting error into the enhanced congestion management. However, SR method utilises the standard deviation to describe the risk level of benefit. It can only be implemented with the condition that the probability distribution of variables follows normal distributions. If the probability distributions of variables are not symmetrical with the mean value points, i.e. they are non-normal distributed, the standard deviation is no long the proper parameter to describe the risk level of benefit.

This chapter extends the uncertainty analysis by considering both wind and load forecasting errors. In practice, the distribution type of load and wind forecasting errors are actually unknown. Although many researches have been done to mimic their distribution types, there always exists inaccuracy. Thus, the probability distribution type of nodal power injection is difficult to derive. So do the network power flows.

This chapter introduces an enhanced risk measurement method called Risk Adjusted Return on Capital (RAROC) to address the distribution type limitation. Based on the error data of both wind and load forecasting, sequence operation theory is adopted to derive uncertain network power flow. It is a mathematical approach specially designed to handle the difficulty and complexity of the operations of random variables.

The rest of the chapter is organized as follows: Section 6.2 explains the load demand forecasting models and the corresponding results; Section 6.3 explains the application of sequence operation theory in probabilistic power flow; Section 6.4 introduces the basic RAROC theory in financial risk management; Section 6.5 proposes the application of RAROC method in intelligent EV charging; Section 6.6 provides a case study of a 33kV network; and the conclusions are drawn in Section 6.7.

6.2. Data Forecasting

6.2.1. Load Demand Forecasting

The wind forecasting has been investigated in Chapter 5. In this section, the method for load forecasting is briefly introduced and some results about forecasting error are given. The key point of node load forecasting is appropriate identification of load patterns. The load forecasting method in this chapter is based on pattern recognition.

The detailed procedure of this forecasting algorithm can be described as follows:

1) Using hierarchy clustering method to cluster the historical daily load patterns, and generate the typical load pattern set LP={1,2,…,i,…,N} where 1~N represent different patterns.
2) According to load pattern set LP and the pattern recognitions of historical days, transfer matrix M_{ij} which records the transfer probability from load pattern i in the reference day to load pattern j (j=1~N) in the forecasted day is established by using Markov chain method.
3) Based on the transfer matrix, the load pattern with highest probability M_{ik} ($M_{ik}=\max(M_{i1},M_{i2},\ldots, M_{iN})$) is selected as the load pattern of the forecasted day.
4) Record the historical days that are in load pattern k, using exponential smoothing method to forecast the load profile of the forecasted day.

Fig. 6-1 shows the statistical distributions of load forecasting errors on busbar 5021 at 1st, 12th and 24th hour. Unlike the wind forecasting, the accuracy of load forecasting does not always decrease as the lead time increases. Because the short-term load forecasting is always implemented as one day ahead forecasting.

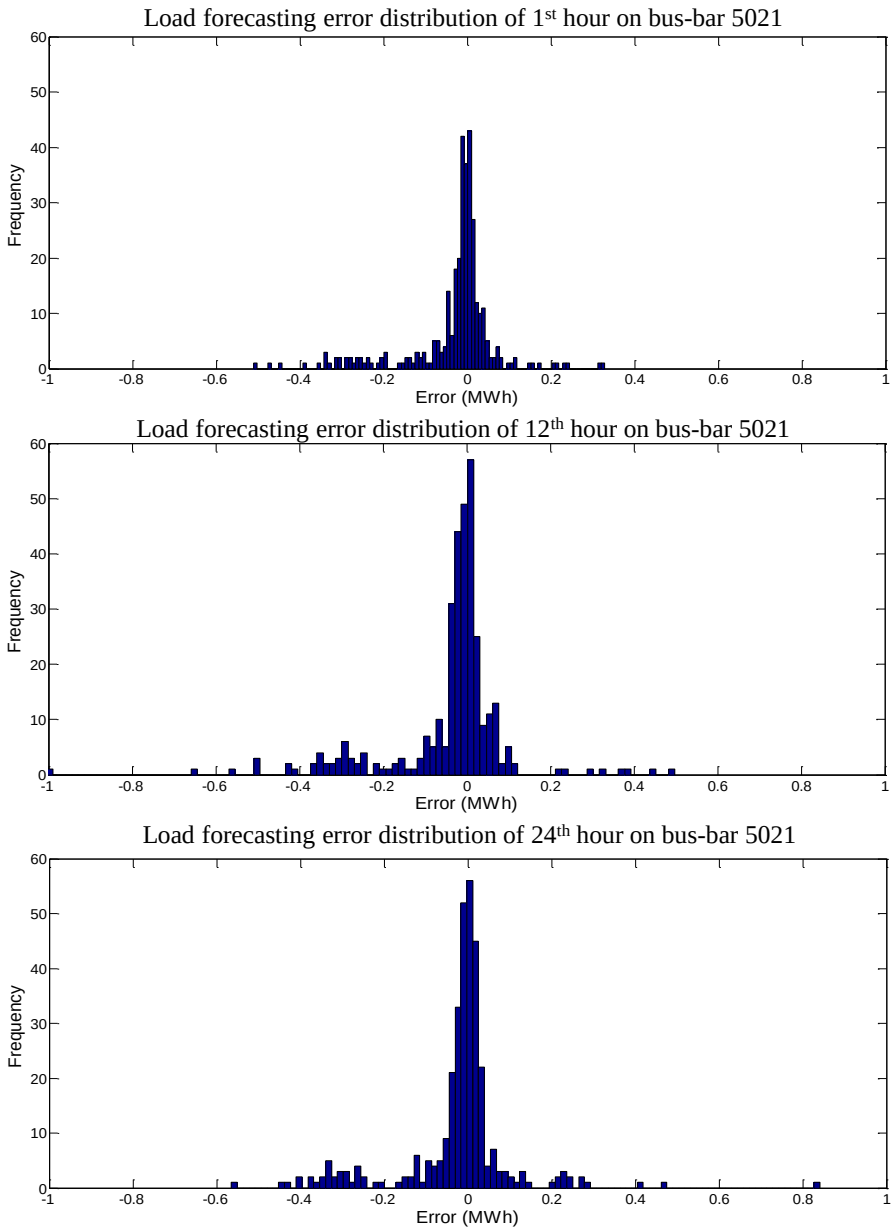

Figure 6-1 Distribution of Load Forecast Error on Busbar 5021

Fig. 6-2 gives the in-depth information about the load forecasting errors on busbar 5021. Both the mean value and standard deviation of forecasting errors just fluctuate slightly around a certain level. The characteristics of errors in wind and load forecasting are significantly different. Thus, it becomes difficult to analytically describe the probability distribution of injected power on network busbars.

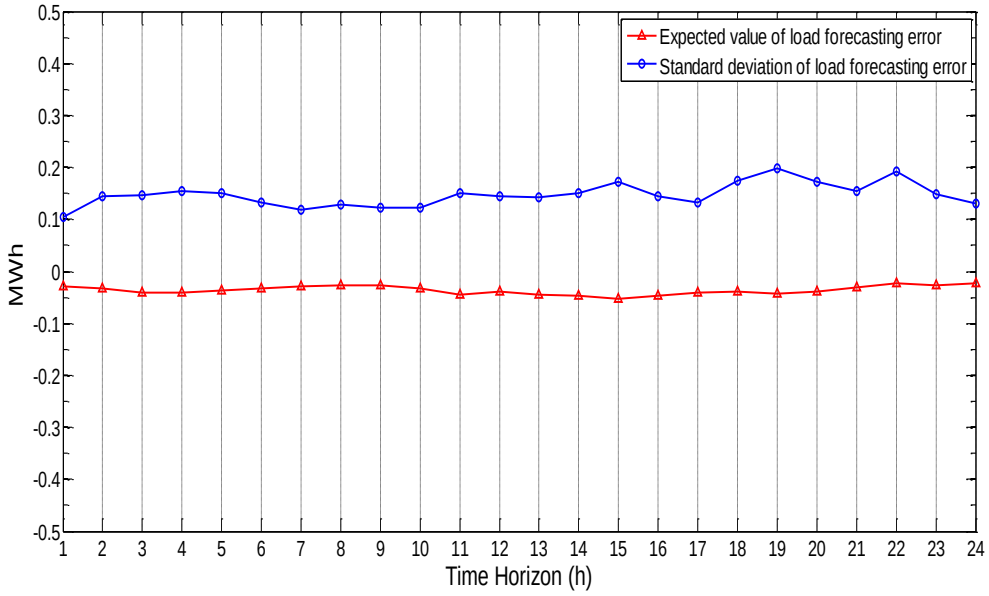

Figure 6-2 Expected Value and Standard Deviation of Load Forecasting Error in 24 hour on Busbar 5021

6.2.2. Forecasting Errors for Nodal Power Injections

After the forecasting data of load demand $\{X_{L,t+m}\}$ and wind generation $\{X_{W,t+m}\}$ have been obtained, the sequential forecasting errors of nodal power injections $\{E_{P,t+m}\}$ can be generated as in (6-1). The lengths of $\{X_{L,t+m}\}$ and $\{X_{W,t+m}\}$ should be the same and their time sequences should be in alignment.

$$\{E_{P,t+m}\}=(\{X_{W,t+m}\}-\{X_{L,t+m}\})-(\{x_{W,t+m}\}-\{x_{L,t+m}\}) \quad (6\text{-}1)$$

6.3. Sequence Operation Theory

When both load and wind forecasting errors are considered, it is difficult to analytically derive probability distributions of nodal power injections. Moreover, the probability distribution of nodal power injections will be non-normal in practice. Sequence operation theory, which was proposed by Prof. Kang, can address these challenges through discretising the probability distribution of each variable and generating probabilistic sequences in order [103]. It has been successfully applied in reliability evaluation [103] and clustered wind power output analysis [104].

The theory is mainly composed of two parts, which are independent sequence operation theory and dependent sequence operation theory. The only difference is whether correlation between input variables is considered or not. This chapter only addresses the problem that input variables are non-normal distributed. So independent sequence operation theory is applied in this chapter. The effects of correlation will be further analysed in Chapter 7 with dependent sequence operation theory.

For sequence operation theory [105], random variables are modelled as probabilistic sequences (PS) in their arithmetic operation process, hence it is named sequence operation theory. Here are some basic concepts of PS.

Definition 1 (Length of PS). Assume the probability density function of variable a is $f_a(a)$ and the discretisation interval is Δd. The corresponding discrete probability sequences A(i) is derived as in (6-2):

$$A(i)= \int_{i\Delta d-\frac{\Delta d}{2}}^{i\Delta d+\frac{\Delta d}{2}} f_a(a)da, \quad a\in[0, a_{max}], \ i=1,2,\ldots,N_a \tag{6-2}$$

where, N_a is the maximum integer less than $a_{max}/\Delta d$. A(i) is called a PS if following conditions are met:

$$A(i)\geq 0, \ i=0,1,2,\ldots,N_a \tag{6-3}$$

$$\sum_{i=0}^{N_a} A(i) = 1 \tag{6-4}$$

Definition 2 (Equality of two PSs). Given two PSs A(i) and B(i), with length N_a and N_b, respectively. It is said that sequence A(i) is equal to B(i) if and only if:

$$N_a=N_b \tag{6-5}$$

$$A(i)=B(i), \ i=0,1,2,\ldots,N_a \tag{6-6}$$

There are four types of discrete sequence operations called addition-type-convolution, subtraction-type-convolution, AND-type-product and OR-type-product. Four derived sequences x(i), y(i), u(i) and v(i) with length N_x, N_y, N_u and N_v are named addition-type-convolution, subtraction-type-convolution, AND-type-product and OR-type-product sequence, respectively. They are called generated sequences. If two independent variables a and b have two PSs A(i) and B(i) with length N_a and N_b,

respectively, four operation types between A(i) and B(i) are defined as follows:

$$x(i)=\sum_{i_a+i_b=i} A(i_a)\cdot B(i_b),\quad i=0,1,2,\ldots, N_x \tag{6-7}$$

$$y(i)=\begin{cases}\sum_{i_a-i_b=i} A(i_a)\cdot B(i_b),\ i=1,2,\ldots, N_y \\ \sum_{i_a\le i_b} A(i_a)\cdot B(i_b),\quad i=0\end{cases} \tag{6-8}$$

$$u(i)=\sum_{\min(i_a,i_b)=i} A(i_a)\cdot B(i_b),\ i=0,1,2,\ldots, N_u \tag{6-9}$$

$$v(i)=\sum_{\max(i_a,i_b)=i} A(i_a)\cdot B(i_b),\ i=0,1,2,\ldots, N_v \tag{6-10}$$

where,

$$N_x=N_a+N_b \tag{6-11}$$

$$N_y=N_a \tag{6-12}$$

$$N_u=\min(N_a,N_b) \tag{6-13}$$

$$N_v=\max(N_a,N_b) \tag{6-14}$$

It should be noted that (6-7)-(6-10) are in simplified form. For example, full expression of '$\sum$' in (6-7) for addition-type-convolution should be $\{0\le i_a\le N_a;\ 0\le i_b\le N_b; i_a+i_b=i\}$. The equations $0\le i_a\le N_a$ and $0\le i_b\le N_b$ are the constraint condition upon their definition domain. Assume any two subscripts i_a and i_b for sequence $A(i_a)$ and $B(i_b)$, their contribution to sequence x(i) should be only at subscript $i_x=i_a+i_b$. In other words, there are totally $(N_a+1)(N_b+1)$ composite states (i_a,i_b). Each product $A(i_a)\cdot B(i_b)$ makes contribution to only one of $\{x(0),x(1),\ldots,x(N_x)\}$. So do equations (6-8)-(6-10).

In power system, the busbars can be regarded as several independent variables. Since the probability distributions of power injection on each busbar have been obtained, sequence operation theory can be easily applied to calculate the discrete distribution of uncertain power flows. The accuracy of calculation is determined by the size of discretization interval Δd.

6.4. Basic RAROC Concept

The concept Risk Adjusted Return On Capital was developed by Bankers Trust and principal designer Dan Borge in the late 1970s [106]. It is a risk-based profitability measurement framework for analysing risk-adjusted financial performance and providing a consistent view of profitability across businesses [107]. RAROC is defined as in (6-15).

$$\text{RAROC}=\frac{\mu_R-R_F}{\text{VAR}} \tag{6-15}$$

where, the numerator is the average rate of return $\mu(R)$ in excess of the risk-free rate R_F, which is the same as that in SR definition (5-2). The denominator is the Value-At-Risk (VAR) of investment.

In economics and finance, VAR is a widely used risk measure of the risk of loss on a specific portfolio of financial assets [108-110]. It has four main uses in finance: risk management, financial control, financial reporting and computing regulatory capital [109]. The concept is defined as the maximum loss not exceeded with a given probability defined as the confidence level, over a given period of time.

Fig. 6-3 shows a simple example of VAR [110]. It is a frequency distribution of a company's daily returns. The red bars compose the "left tail" of the distribution, which are the worst profit cases. They take up 5% of the distribution, running from daily loss of 4% to 8%. Thus, we can say with 95% confidence that the worst daily loss will not exceed 4%. If the investment amount is £100, we are 95% confident that our worst daily loss will not exceed £4. VAR does not express absolute certainty but instead makes a probabilistic estimate. If the confidence level is increased to 99%, the VAR will move to the left further to the point where the "left tail" only takes up 1%.

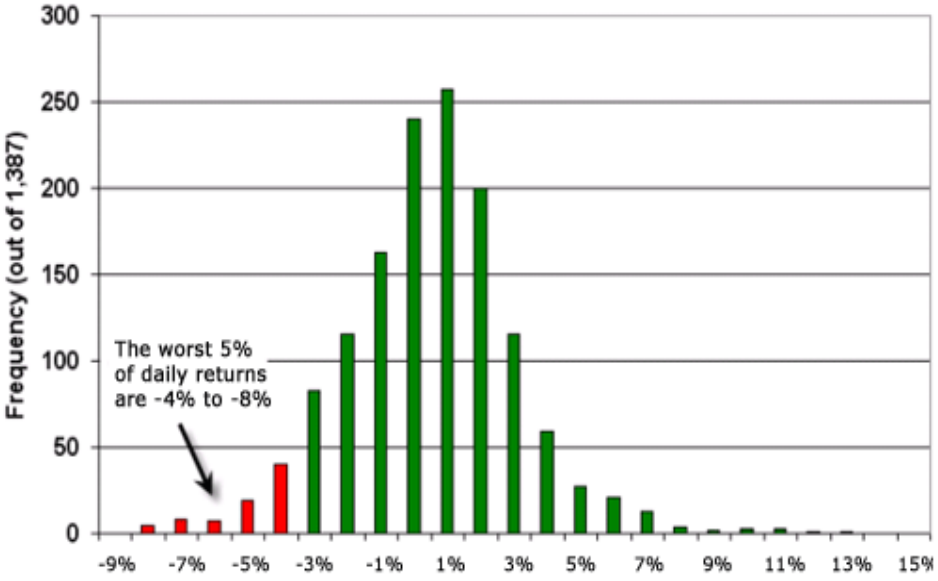

Figure 6-3 Distribution of a Companies' Daily Returns [110]

6.5. RAROC Method in Intelligent EV Charging

RAROC method utilizes the VAR to represent the risk levels. The confidence level c ($c \in (0,1)$) should be set first. The charging optimization in RAROC model also follows 'trial and comparison' rule. The number of trials is determined by the number of timeslots that have network congestion. Trial T means that according to the mean value of power flow, there exists line overloading at timeslot T. The EV charging demand at timeslot T should be swapped with other timeslots to relieve the congestion. The location and level of EV load shifting are determined in the same way as in SR method. RAROC method has main three steps as follows.

6.5.1. Determine the Reference Situation

The original state of the network without load shifting is set as reference, in which each timeslot t in the time-window has original generation curtailment. Since the reference should reflect risk-free situation, $VAR_{GC_{0,t}}$ is determined by the VAR of network power flows with preset confidence level. In RAROC model, before load shifting, the mean value and in-depth probability distribution of original power flow $f(PF_{0,t,l})$ on line l is calculated through the probabilistic power flow with sequential operation theory.

According to $f(PF_{0,t,l})$ and the confidence level c, VAR of power flow $VAR_{PF_{0,t,l}}$ can be calculated from in (6-16). In financial sector, the worst case happens in the "left tail". However, in power system, the worst situation happens in the "right tail". Because when the value of power flow is increasing, it may exceed the line rating, resulting in network congestion.

$$Prob(PF_{0,t,l}>VAR_{PF_{0,t,l}})=\int_{VAR_{PF_{0,t,l}}}^{+\infty} f(PF_{0,t,l})\cdot dPF_{0,t,l}=1-c \tag{6-16}$$

Based on $VAR_{PF_{0,t,l}}$, the VAR of generation curtailment $VAR_{GC_{0,t,l}}$ caused by a specific line l is determined in (6-17).

$$VAR_{GC_{0,t,l}}=\frac{VAR_{PF_{0,t,l}}-P_l^{max}}{PTDF(l,i)} \tag{6-17}$$

where, $VAR_{GC_{0,t,l}}$ means within the confidence level, the generation curtailment that needs to be curtailed to ensure the safety on line l will not exceed $VAR_{GC_{0,t,l}}$.

The VAR of total generation curtailment of the network $VAR_{GC_{0,t}}$ is determined by summing individual $VAR_{GC_{0,t,l}}$ up as in (6-18).

$$VAR_{GC_{0,t}}=\sum_{l=1}^{M} VAR_{GC_{0,t,l}} \tag{6-18}$$

6.5.2. Trial Charging Solutions

In trial T, after load shifting, the mean value $\mu_{PF_{T,t,l}}$ and in-depth distribution $f(PF_{T,t,l})$ of network power flows at timeslot t will be recalculated. The average generation curtailment $\mu_{GC_{T,t}}$ is determined by $\mu_{PF_{T,t,l}}$, and the VAR of generation curtailment at each timeslot $VAR_{GC_{T,t}}$ is recalculated according to $f(PF_{T,t,l})$. The RAROC method to measure the performance of trial T is shown in (6-19).

$$RAROC_T=\sum_{t=1}^{TWS}\frac{VAR_{GC_{0,t}}-\mu_{GC_{T,t}}}{VAR_{GC_{T,t}}} \tag{6-19}$$

The difference between $VAR_{GC_{0,t}}$ and $\mu_{GC_{T,t}}$ is the benefit at timeslot t due to load shifting in trial T. The denominator $VAR_{GC_{T,t}}$ indicates the maximum generation curtailment may occur to ensure the confidence level, which reflects the risk level of trial T.

6.5.3. Decision Making

As shown in (6-19), after trial T, the benefit (generation curtailment reduction) and the risk (VAR) at each timeslot t are converted to equivalent benefit under unity risk. $RAROC_T$ is the sum of generation curtailment reduction of trial T under unity risk. There is no unit for $RAROC_T$ because the units of numerator and denominator in (6-19) are all MWh. By comparing $RAROC_T$, the trial execution timeslot with the largest $RAROC_T$ is selected as the real execution timeslot to conduct load shifting. The detailed flowchart is shown in Fig. 6-4.

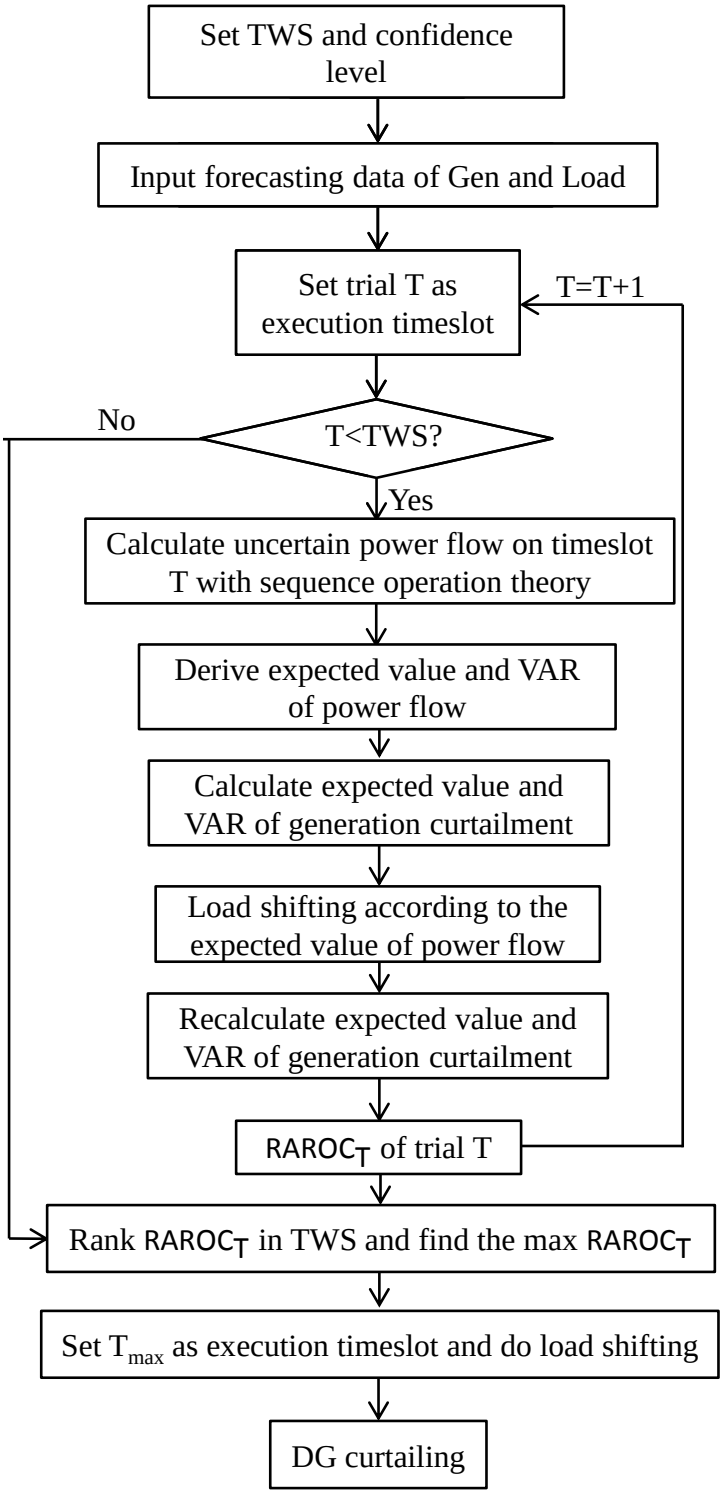

Figure 6-4 Flowchart of Intelligent EV Charging with RAROC Method

6.6. Case Study

6.6.1. Case Study with 90% Confidence Level

The 33kV Aberystwyth network is utilised as case study. One day (24 hours) are chosen to do the simulation. Time-Window Scale is set to be 24 hours. Fig. 6-5 shows the power flow conditions of line 5010-5012. The red line is the line rating. The green line is the deterministic power flow, which is consistent with Fig. 5-5. The blue line is the mean values of uncertain power flow calculated through sequence operation theory, which is significantly different with the green line. Fig. 6-5 also shows the VAR of power flow, which is indicated in yellow dotted line.

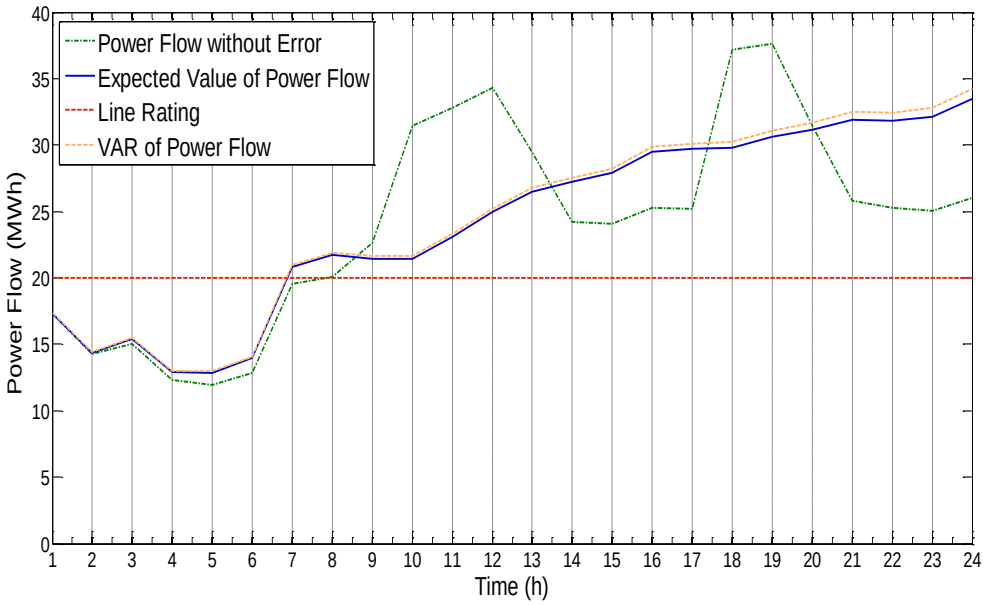

Figure 6-5 Power Flow on Line 5010-5012

Fig. 6-6, 6-7 and 6-8 show the process of determining the VARs of power flow. The blue lines in these figures are the cumulative distribution function (CDF) of the power flow on line 5010-5012 at 1st, 12th and 24th hour. The red lines are the preset confidence level, which is 90%. The crossing points in these figures are the VARs, which are 17.36MWh in Fig. 6-6, 25.24MWh in Fig. 6-7 and 34.23MWh in Fig. 6-8.

Among the three figures, the cumulative probability in Fig. 6-6 increases fastest. 80% (from 10% to 90%) of forecasting samples are within the power flow interval [17.29, 17.36], while those in Fig. 6-7 and Fig. 6-8 are [24.74, 25.24] and [32.85, 34.23],

respectively. Under same confidence level, smaller interval stands for higher accuracy. This phenomenon indicates that, although the accuracy of load demand forecasting is not decreasing as time horizon increases, the accuracy of power flow still decreases as time horizon increases, which is consistent with the characteristics of wind forecasting error.

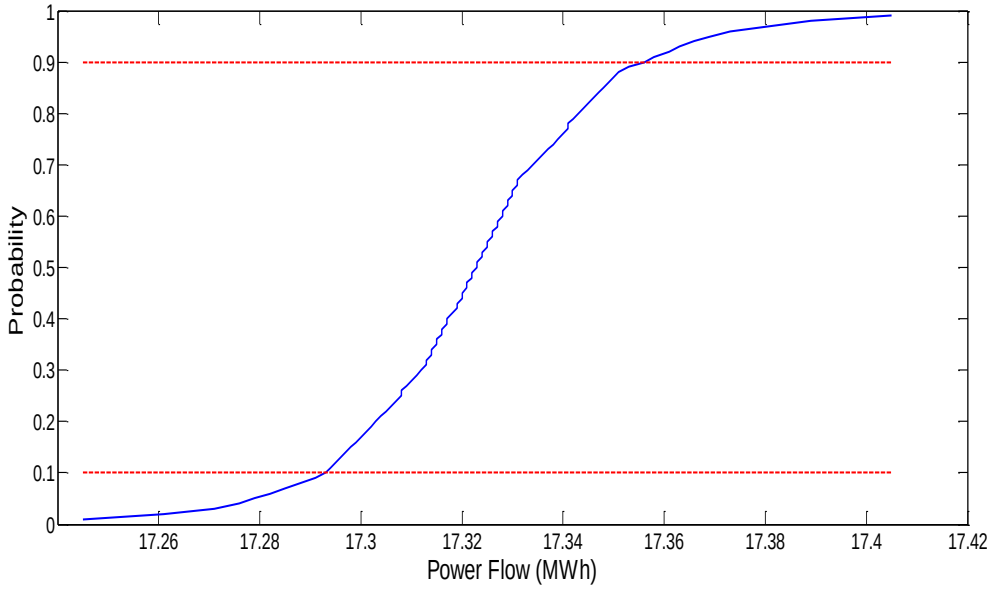

Figure 6-6 CDF of Line 5010-5012 at 1st Hour

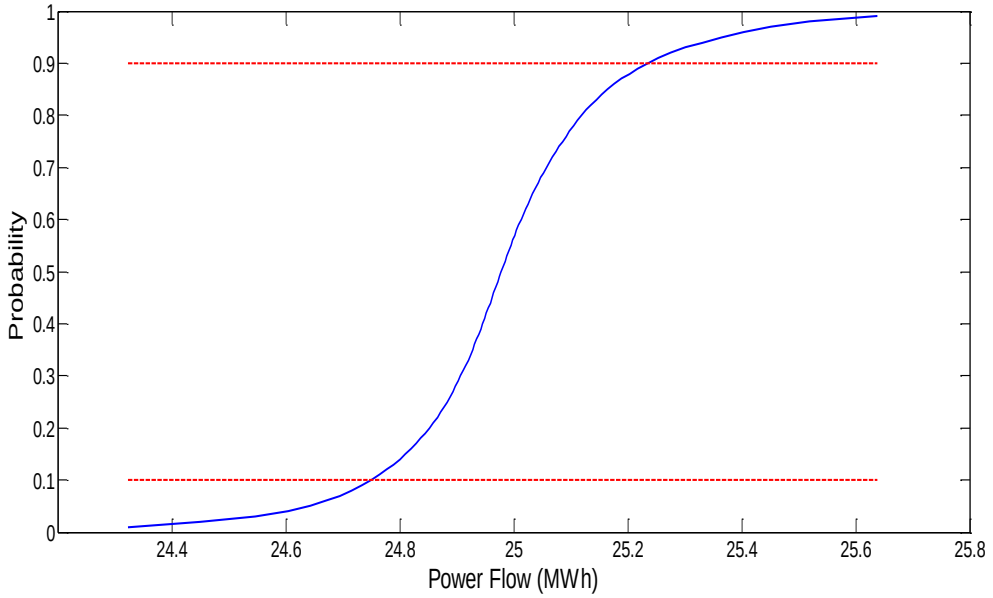

Figure 6-7 CDF of Line 5010-5012 at 12th Hour

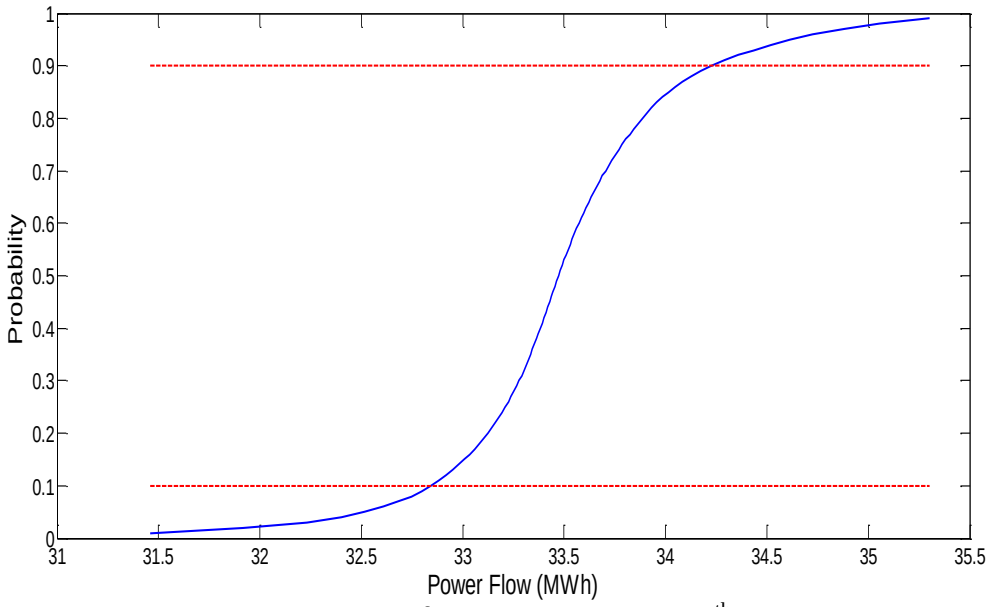

Figure 6-8 CDF of Line 5010-5012 at 24th Hour

Since the VARs of power flow are always larger than mean values of power flow, they should require larger generation curtailment. Fig. 6-9 shows the original generation curtailment before load shifting according to Fig. 6-5. The blue line is the mean value of generation curtailment (GC0_EX) which is calculated by mean values of power flow. The yellow line indicates the VAR of generation curtailment (GC0_VAR) which is calculated by VARs of power flow. Table 6-1 lists the detail information. In all timeslots, GC0_VAR is larger than GC0_EX. The total GC0_VAR is 21.448MWh larger than the total GC0_EX.

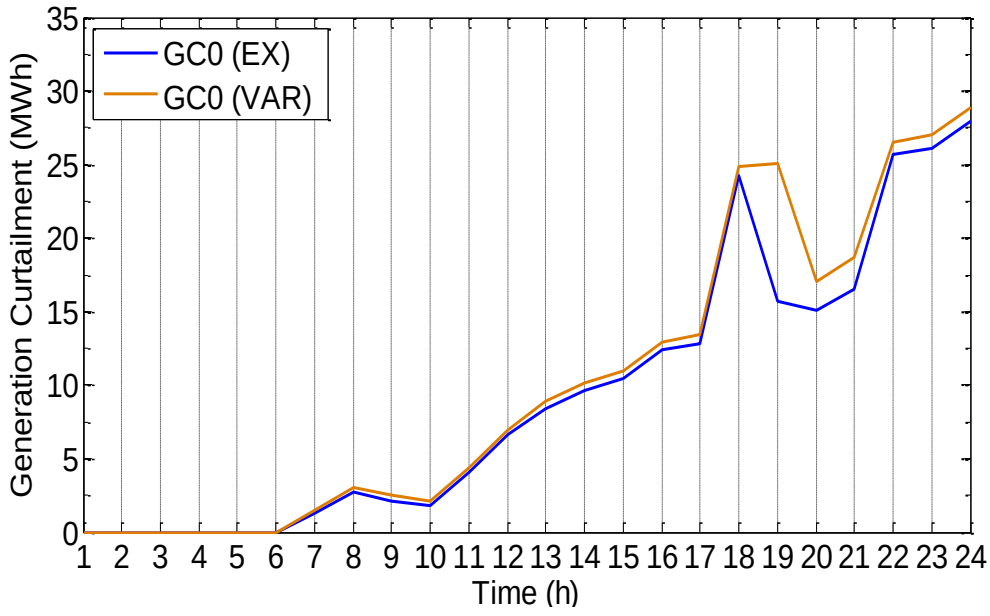

Figure 6-9 Mean Value and VAR of Generation Curtailment before Load Shifting

Table 6-1 Generation Curtailment of 24 Hours before Load Shifting

Time (h)	GC0_EX (MWh)	GC0_VAR (MWh)
1	0.000	0.000
2	0.000	0.000
3	0.000	0.000
4	0.000	0.000
5	0.000	0.000
6	0.000	0.000
7	1.253	1.501
8	2.703	3.011
9	2.154	2.517
10	1.833	2.106
11	4.038	4.389
12	6.598	6.966
13	8.416	8.853
14	9.672	10.109
15	10.429	10.960
16	12.415	12.958
17	12.826	13.446
18	24.223	24.874
19	15.689	25.109
20	15.114	17.084
21	16.570	18.679
22	25.636	26.526
23	26.061	26.996
24	27.905	28.899
Total	223.535	244.983

Fig.6-10 shows the RAROCs of the 24 trials. The RAROCs of trial 1-6 are zero. It is because both the mean values and VARs of power flows in these timeslots are not overloaded, resulting no execution of intelligent EV charging. According to Fig. 6-10, trial 18 has largest RAROC value which is 1.987. Therefore, it is chosen as the real execution timeslot.

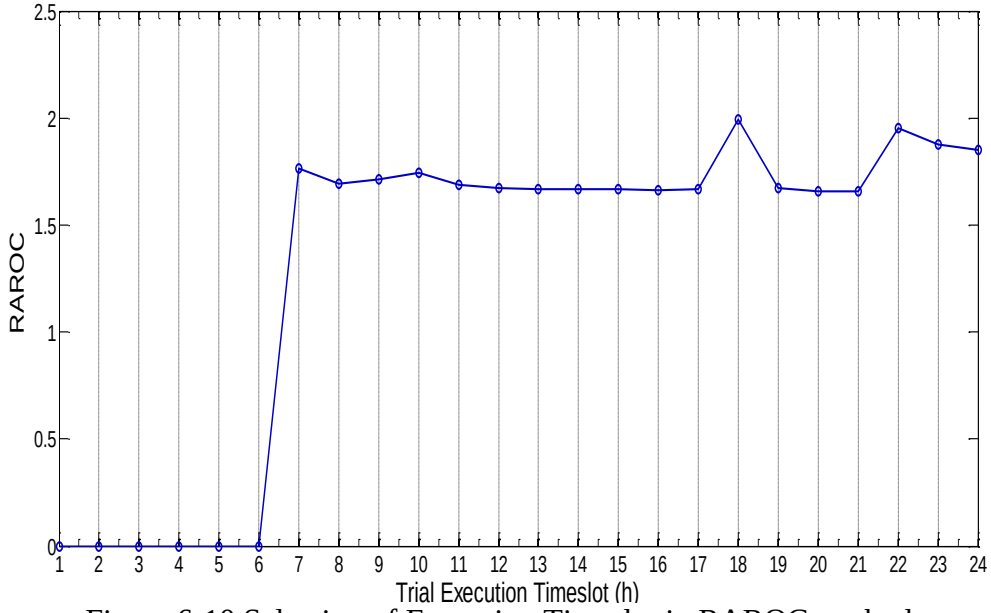

Figure 6-10 Selection of Execution Timeslot in RAROC method

Table 6-2 explains how RAROC works. The second column GC_EX is mean value of total generation curtailment in the network after each EV charging solution. The third column ΔGC_EX is mean value of total generation curtailment reduction generated by trial load shifting, where trial 18 has the largest reduction 9.252MWh. The fourth column GC_VAR is the VARs of total generation curtailment in the network after each trial load shifting. Trial 19 has the smallest GC_VAR which is only 244.552MWh. However, the benefit ΔGC_EX on trial 19 is only 0.997MWh, which is far lower than trial 18. Thus, by balancing the benefit and risk, RAROC value helps to make a final decision. Execution timeslot 18 is more profit than timeslot 19.

Table 6-2 Benefit Comparison of 24 Trials

Trial	GC_EX (MWh)	ΔGC_EX(MWh)	GC_VAR (MWh)	RAROC
1	–	–	–	–
2	–	–	–	–
3	–	–	–	–
4	–	–	–	–
5	–	–	–	–
6	–	–	–	–
7	223.386	0.147	244.837	1.762
8	223.390	0.144	244.840	1.691
9	223.374	0.159	244.825	1.713
10	223.348	0.185	244.799	1.745
11	223.324	0.209	244.775	1.690
12	223.304	0.229	244.755	1.671
13	223.271	0.262	244.722	1.668
14	223.238	0.295	244.689	1.667
15	223.212	0.321	244.663	1.667
16	223.184	0.350	244.634	1.664
17	223.151	0.383	244.601	1.666
18	214.281	**9.252**	245.139	**1.987**
19	222.536	0.997	**244.552**	**1.673**
20	223.194	0.339	244.645	1.658
21	223.194	0.339	244.645	1.656
22	215.038	8.495	244.590	1.951
23	216.065	7.469	246.028	1.875
24	216.422	7.112	245.791	1.849

6.6.2. Case Study with 80% and 99% Confidence Levels

Last section has analysed the performance of RAROC method under 90% confidence level. This section analyses the performance of RAROC method under varying confidence levels, i.e. 99% and 80% levels. The same 24 hours' data as in 6.6.1 are used to do the simulation and the Time-Window Scale is still 24 hours.

Fig. 6-11 shows the power flow conditions of line 5010-5012 under 99% confidence level. Differing confidence levels only changes the VARs of power flow. The blue line and red line are the VARs of power flow under 90% and 99% confidence levels, respectively, which conform to the rule: higher confidence level requests larger VAR to ensure the security. Fig. 6-12 shows the corresponding VARs of generation curtailment

under 90% and 99% confidence levels.

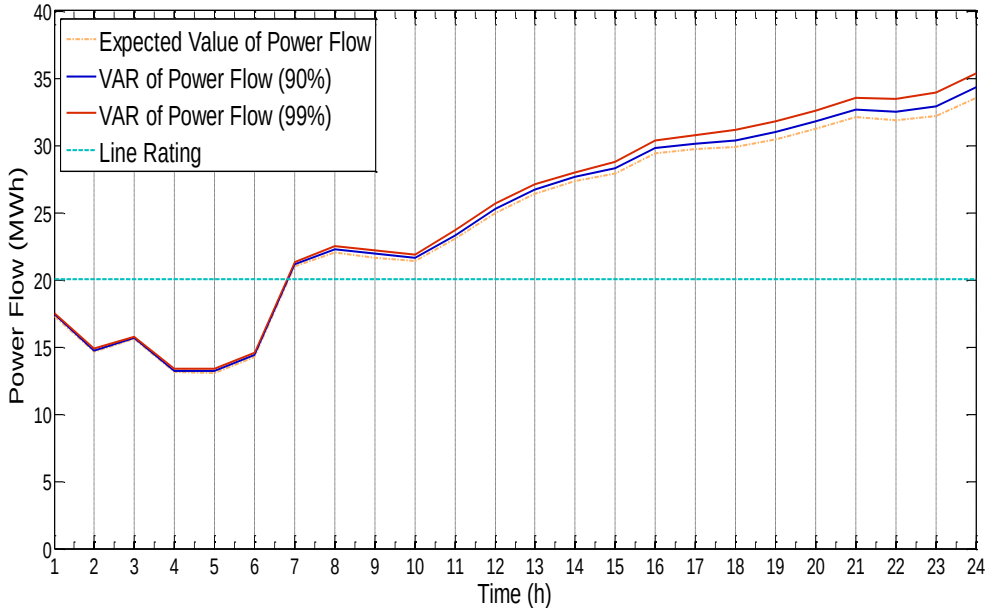

Figure 6-11 Power Flow on Line 5010-5012 under 99% and 90% Confidence Levels

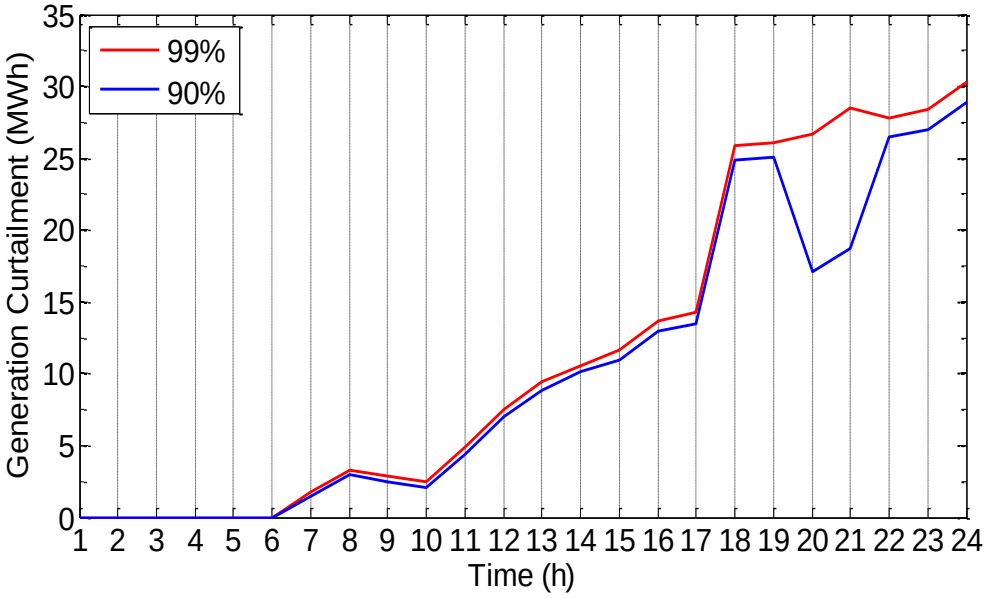

Figure 6-12 VAR of Generation Curtailment under 99% and 90% Confidence Levels

Fig. 6-13 shows the RAROC values of trial execution timeslot under 99% and 90% confidence levels. The RAROCs under 99% confidence level are much higher than those under 90% confidence level, which indicates the RAROC method performs better in higher confidence level. Under 99% confidence level, trial 18 is chosen as the real execution timeslot with the largest VAR value (3.653), which is the same with the result under 90% confidence level. The phenomenon that the trends of the two lines are similar indicates that within the confidence level interval [90%, 99%], the chosen of

real execution timeslot will always be the same.

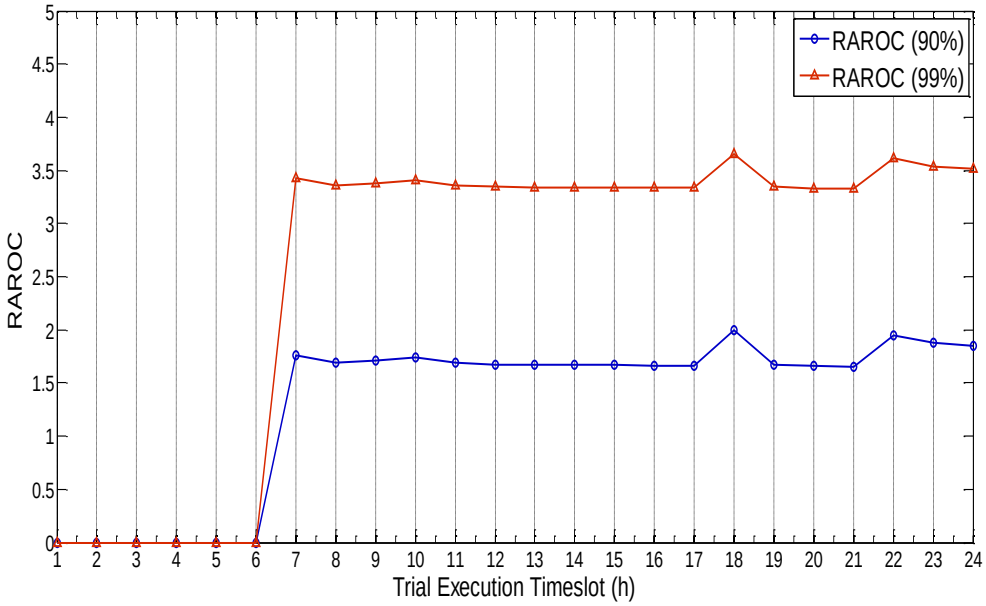

Figure 6-13 Selection of Execution Timeslot under 99% and 90% Confidence Levels

Fig. 6-14 shows the power flow conditions of line 5010-5012 under 80% confidence level. The blue line and red line are the VARs of power flow under 90% and 80% confidence levels, respectively, which meet the rule: lower confidence level requests smaller VAR to ensure the security. Fig. 6-15 shows the corresponding VARs of generation curtailment under 90% and 80% confidence levels.

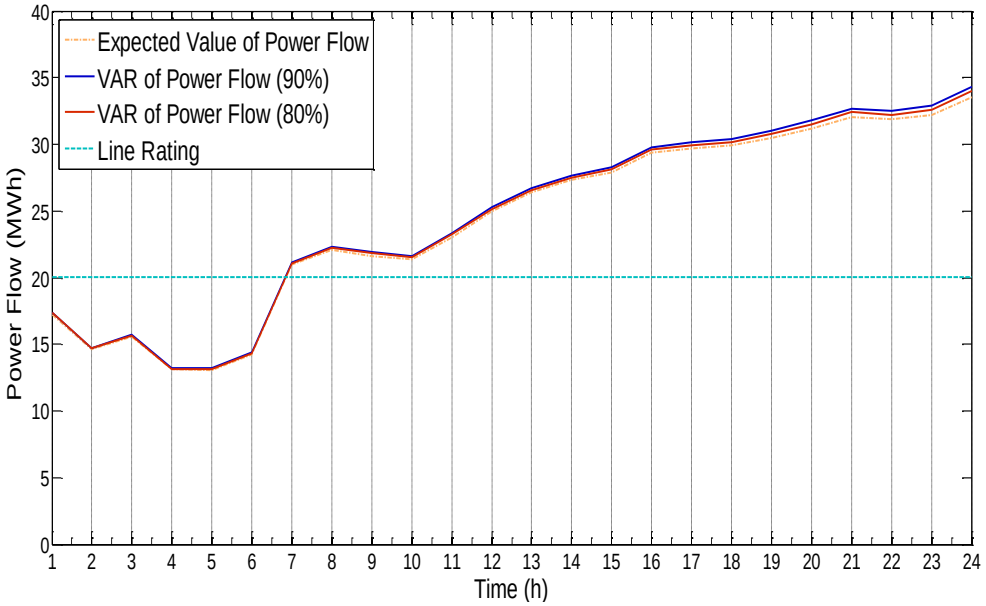

Figure 6-14 Power Flow on Line 5010-5012 under 80% and 90% Confidence Levels

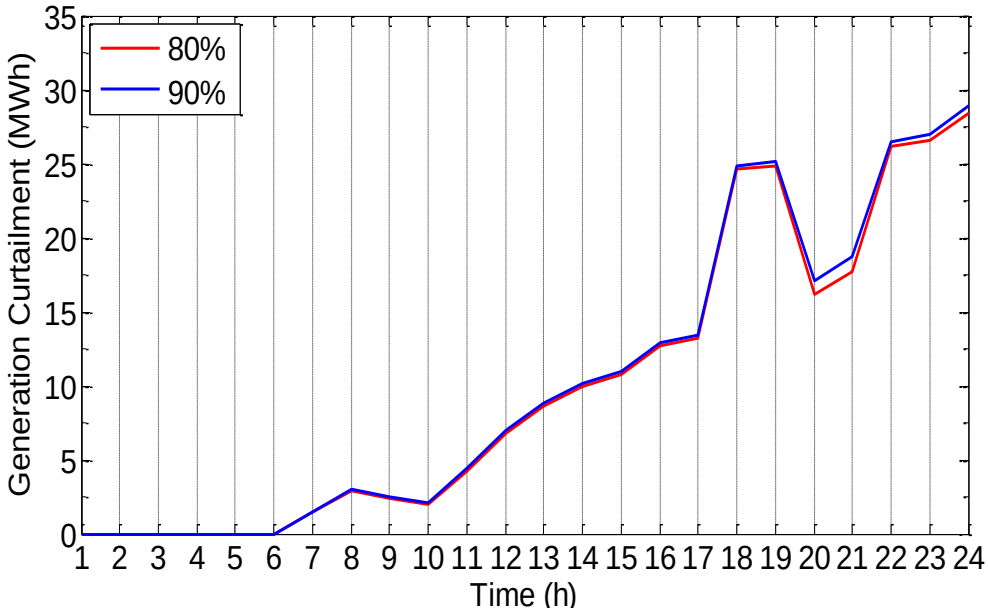

Figure 6-15 VAR of Generation Curtailment under 80% and 90% Confidence Levels

Fig. 6-16 shows the RAROC values of trial execution timeslot under 80% and 90% confidence levels. Again, higher confidence level (90%) gives larger RAROC values. However, by comparing with the blue line (90% confidence level), the trend of red line (80% confidence level) is dramatically changed, resulting in different decision-making. Under 80% confidence level, although trial 18 is still chosen as the real execution timeslot with the largest VAR value (1.549), the ranking of other trials has changed a lot. The profit of trial 23 increases from No. 3 to No. 2. Trial 19 becomes comparable with trial 18 and trial 23. This phenomenon indicates that when the confidence level decreases, the chosen of real execution timeslot will be changed with differing confidence levels.

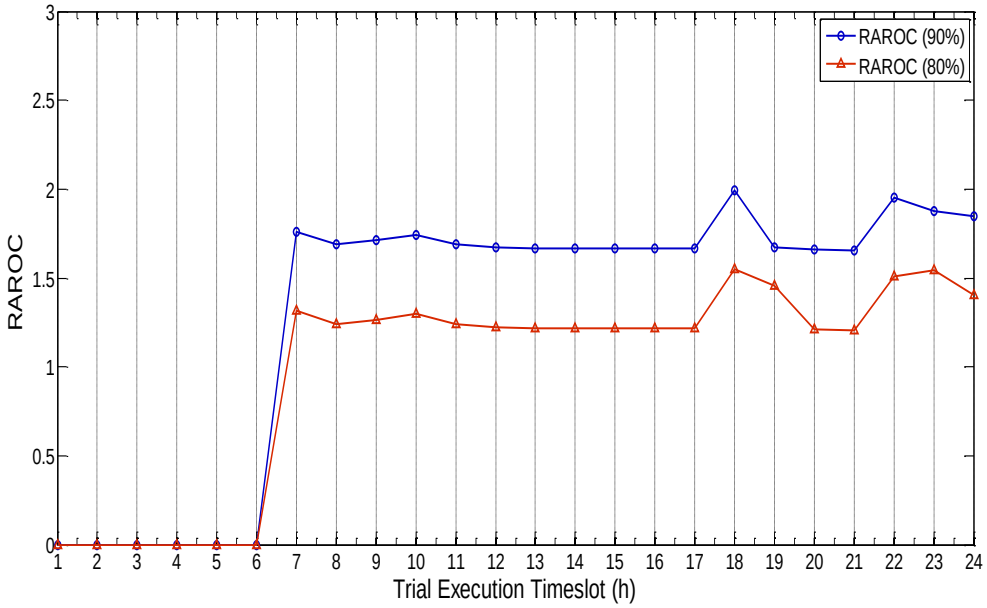

Figure 6-16 Selection of Execution Timeslot under 80% and 90% Confidence Levels

6.7. Chapter Summary

After analysing the limitations in SR method, this chapter proposes an enhanced uncertainty management by borrowing RAROC concept from financial risk management. RAROC method uses VAR concept to represent the uncertainty levels based on their nature distributions. Independent sequence operation theory is applied to calculate the uncertain power flow considering both wind and load forecasting error.

The simulation results indicate that with RAROC method, more network uncertainties can be integrated, even when they are in different distribution patterns. The VARs of power flows can be easily determined based on the statistics of uncertain power flow and can represent the risk levels appropriately. The results also indicate that the decision-making will change when the confidence level changes. To put it briefly, the proposed RAROC method extends the feasibility of uncertainty management by allowing the forecasting errors to be in any distribution.

CHAPTER 7. UNCERTAINTY MANAGEMENT WITH CORRELATION CONSIDERED

This chapter applies Copula theory to integrate the correlations of forecasting errors between nodal power injections into uncertainty management, giving more accurate network stress prediction and a more convincing stochastic congestion management strategy.

7.1. Introduction

Chapter 6 introduced an uncertainty management with RAROC method, considering both load and wind forecasting errors. However, it does not consider the influence from correlations of forecasting errors between nodal power injections. Since wind forecasting is strongly dependent on weather condition in an area, the wind forecasting errors on different busbars in the area have strong correlations. Besides, the load forecasting errors on different busbars somehow also have correlations since weather influences the electricity consumption pattern. Thus, forecasting error of power injection on one busbar is correlated with other busbars.

This chapter applies Copula theory to integrate the correlations of forecasting errors between nodal power injections into uncertainty management, so that the network stress prediction will be more accurate and the congestion management will be more convincing.

The rest of the chapter is organized as follows: Section 7.2 explains the basic Copula theory and its application in dependence sequence operation theory; Section 7.3 provides a case study of the proposed model; and the conclusions are drawn in Section 7.4.

7.2. Dependent Sequence Operation Theory with Copula

7.2.1. Literature about Correlation Analysis

Some methods have been presented to consider the correlation of forecasting errors between input variables in power system [84, 85, 111, 112]. Paper [84] introduces the correlations in probabilistic power flow problem. However, it did not evaluate the correlation of input variables, just assume the right probability density function for the correlated input variables and use convolution method to analyse the branch flow, where the input variables are assumed to be normal distributed.

Later, paper [85] utilised linear relation to model the statistical dependence between load uncertainties in the probabilistic power flow solution. Due to the use of linearized power flow equations about an expected operating point, the method would be less accurate when there is high level of uncertainty. Because the input data in tail region is much inaccurate as they are furthest from the point of linearization. To increase the accuracy of calculation, paper [111] added the multi-linearization based on the previous method. Although the enhanced method reduced the inaccuracy, it increased the complexity and computation burden.

Paper [113] introduces a new method based on Monte Carlo Simulation to reflect the non-Gaussianity and the nonlinear correlations of probability density functions of input variables in AC probabilistic power flow calculation. The main contribution of the work is to improve the sampling method. Markov Chain Monte Carlo is used to generate the samples from arbitrary distribution.

7.2.2. Stochastic Dependence and Copulas Theory

Stochastic dependence refers to the behaviour of a random variable that is affected by others. If one random variable has no impact on the probability distribution of the other, these two variables are regarded as independent variables. Otherwise, they are regarded stochastically dependent.

As stated in [104]: "Some mathematical tools, like covariance and joint probability distribution, have been widely used in probabilistic relationship studies. However, covariance can only provide a way of measuring the stochastic dependence level between two or more variables. It cannot reflect the in-depth dependence between them. Joint probability distribution can perfectly reflect the dependence among variables. But it is difficult to find a multivariate analytical formula for variables with complex marginal distributions." For instance, if one variable has a Weibull distribution and the other has a Gaussian distribution, their stochastic dependence can hardly be modelled by an analytical bivariate function. Thus, the application of joint probability distribution in practice is very complex.

7.2.2.1. Basic Concepts for Copula Theory

Copula theory inspires a new way to model stochastic dependence. It was first mentioned by Abe Sklar in 1959. As defined in [114], copulas are functions that join or "couple" multivariate distribution functions to their one-dimensional marginal distribution functions.

A two-dimensional example is used here to further explain Copula theory. Suppose a and b are two random variables with probability density functions $f_a(a)$ and $f_b(b)$, respectively. Their invertible CDFs are $F_a(a)$ and $F_b(b)$. Their joint probability density function is $f_{ab}(a,b)$ and joint probability function is $F_{ab}(a,b)$. If $F_a(a)$ and $F_b(b)$ are regarded as random variables, both of them will follow the uniform distributions as below:

$$F_a(a)\sim u(0,1), \quad F_b(b)\sim u(0,1) \tag{7-1}$$

In other words, $F_a(a)$ and $F_b(b)$ transform a and b into uniform distributions, respectively.

In copula theory, there only exists one Copula function C to derive $F_{ab}(a,b)$ as in (7-2). Another way to say is that if the individual probability functions of variables (a and b) and the copula function between them are obtained, their joint probability function can be easily derived.

$$F_{ab}(a,b)=C\left(F_a(a),F_b(b)\right) \tag{7-2}$$

Copula theory transforms the modelling of $F_{ab}(a,b)$ into the modelling of $F_a(a)$, $F_b(b)$ and $C(\cdot)$ separately. It takes the advantage of the fact that stochastic dependence is more easily recognized for uniform variables ($F_a(a)$ and $F_b(b)$) than for other arbitrarily distributed variables (a and b).

Copula function $C(\cdot)$ is a special kind of multivariate CDF that has uniform margins. If we set $u=F_a(a)$ and $v=F_b(b)$, $C(\cdot)$ can be expressed as:

$$C(u,v)= F_{ab}\left(F_a^{-1}(u),F_b^{-1}(v)\right) \tag{7-3}$$

According to copula theory, the joint probabilistic density function $f_{ab}(a,b)$ can be derived as:

$$
\begin{aligned}
f_{ab}(a,b) &= \frac{\partial^2 F_{ab}(a,b)}{\partial a \partial b} = \frac{\partial^2 C\left(F_a(a),F_b(b)\right)}{\partial a \partial b} \\
&= \frac{\partial^2 C\left(F_a(a),F_b(b)\right)}{\partial F_a(a) \partial F_b(b)} \cdot \frac{\partial F_a(a)}{\partial a} \cdot \frac{\partial F_b(b)}{\partial b} \\
&= c\left(F_a(a),F_b(b)\right) \cdot f_a(a) \cdot f_b(b) \\
&= c(u,v) \cdot f_a(a) \cdot f_b(b)
\end{aligned}
\tag{7-4}
$$

where, $c(u,v)$ is the probabilistic density function of $C(u,v)$ and it can be constructed according to copula theory for dependent variables.

7.2.2.2. Addition-type-convolution with Copula

As explained in [104], if a and b are independent, the addition-type-convolution PS x(i) of $f_a(a)$ and $f_b(b)$ can be written as:

$$
x(i) = \sum_{i_a+i_b=i} A(i_a) \cdot B(i_b), \quad i=0,1,2,\ldots, N_x \tag{7-5}
$$

If a and b are dependent, the addition-type-convolution PS x(i) of $f_a(a)$ and $f_b(b)$ cannot be written as the product of $A(i_a)$ and $B(i_b)$. x(i) should be calculated from the joint probability function $f_{ab}(a,b)$ as in (7-6).

$$
\begin{aligned}
x(i) &= \sum_{i_a+i_b=i} \int_{i_a\Delta d-\Delta d/2}^{i_a\Delta d+\Delta d/2} \int_{i_b\Delta d-\Delta d/2}^{i_b\Delta d+\Delta d/2} f_{ab}(a,b)\, da\, db \\
&= \sum_{i_a+i_b=i} \int_{i_a\Delta d-\Delta d/2}^{i_a\Delta d+\Delta d/2} \int_{i_b\Delta d-\Delta d/2}^{i_b\Delta d+\Delta d/2} c(u,v) \cdot f_a(a) \cdot f_b(b)\, da\, db, \quad i=0,1,2,\ldots,N_x
\end{aligned}
\tag{7-6}
$$

In (7-6), the integral is constrained in the region $[\, i_a\Delta d-\Delta d/2, i_a\Delta d+\Delta d/2\,] \times [i_b\Delta d-\Delta d/2, i_b\Delta d+\Delta d/2]$. If the discretization interval Δd is very small, $c(u,v)$ can be regarded as a constant. Thus, (7-6) can be simplified as in (7-7).

$$
\begin{aligned}
x(i) &\approx \sum_{i_a+i_b=i} c(u,v) \cdot \int_{i_a\Delta d-\Delta d/2}^{i_a\Delta d+\Delta d/2} \int_{i_b\Delta d-\Delta d/2}^{i_b\Delta d+\Delta d/2} f_a(a) \cdot f_b(b)\, da\, db \\
&= \sum_{i_a+i_b=i} c(u,v) \int_{i_a\Delta d-\Delta d/2}^{i_a\Delta d+\Delta d/2} f_a(a)\, da \int_{i_b\Delta d-\Delta d/2}^{i_b\Delta d+\Delta d/2} f_b(b)\, db
\end{aligned}
$$

$$= \sum_{i_a+i_b=i} c(u,v)\cdot A(i_a)\cdot B(i_b) \tag{7-7}$$

The further expression of c(u,v) can be obtained in (7-8).

$$c(u,v)= c\big(F_a(a),F_b(b)\big)=c\left(\sum_{m=0}^{i_a} A(m), \sum_{n=0}^{i_b} B(n)\right) \tag{7-8}$$

Hence the Copula sequence for A(i) and B(i) can be expressed in (7-9).

$$c_s(i_a, i_b)=c\left(\sum_{m=0}^{i_a} A(m), \sum_{n=0}^{i_b} B(n)\right),\ i_a=0,1,\ldots,N_a,\ i_b=0,1,\ldots,N_b \tag{7-9}$$

x(i) thus can be further expressed with $c_s(i_a, i_b)$ in (7-10).

$$x(i)= \sum_{i_a+i_b=i} c_s(i_a, i_b)\cdot A(i_a)\cdot B(i_b),\ i=0,1,2,\ldots, N_x \tag{7-10}$$

7.2.2.3. Typical Copula Functions

There are four typical Copula functions mainly include Gaussian copula, t copula, Clayton copula, Gumbel copula and Frank copula [104, 115, 116]. Fig. 7-1 shows density functions of four typical functions (Gaussian copula, t copula, Clayton copula and Gumbel copula). Their linear correlation factors are all set as 0.7 [104].

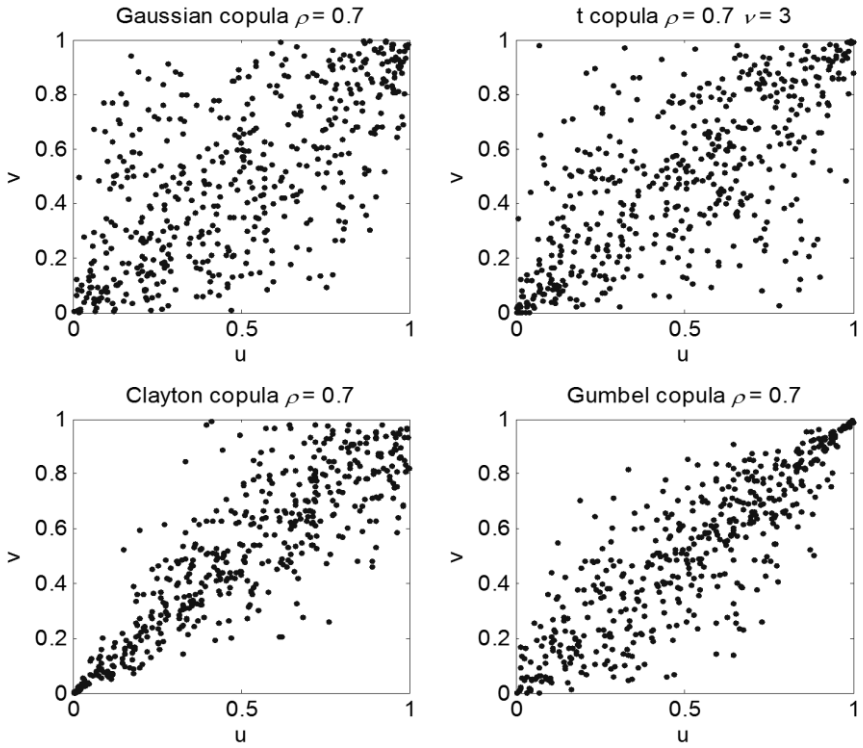

Figure 7-1 Four typical distribution of copula function [104]

As stated in [104]: "Different kinds of copula show different dependence structures. Gaussian copula and t copula focus on the correlation on both maximum and minimum values. Clayton copula focuses on the correlation on minimum value, while Gumbel copula pays more attention on the maximum point." Thesis [104] proves that the correlation between wind farms follows Gaussian copula properly.

More descriptions of copula theory can be found in [117]. Copula theory has been applied to power system analysis, especially wind power [118-121]. Papers [118] and [119] use it in modelling the special dependence of wind power output from multiple wind farms. Papers [120] and [121] use it to model the relationship between wind speed and wind farm output in a probabilistic forecasting model.

7.2.3. Dependent Sequence Operation Theory with Copula

Since Chapter 6 utilises sequence operation theory to calculate uncertain power flow, for comparison convenience, this chapter adopts dependent sequence operation theory with Copula, which was proposed by Dr. Ning Zhang in [104], to analyse the effects of correlations. The basic sequence theory is same in independent and dependent sequence

operation theories. The only difference is to integrate Copula in dependent sequence operation theory.

The flowchart of dependent sequence operation theory is shown in Fig. 7-2 [104]. Nodal injected power on each busbar is regarded as one variable. There are two main steps in the process: 1) build the PS of each variable, 2) build the Copula sequence of all variables. The PS of each variable in dependent sequence operation theory is same with that in independent case as in (6-2).

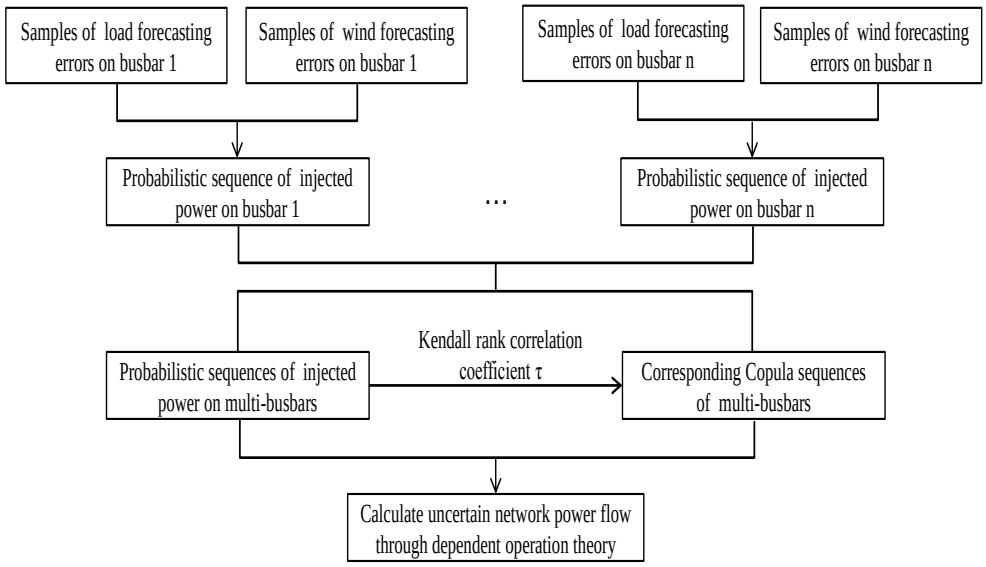

Figure 7-2 Model of Dependent Operation Theory

(7-11) gives the density function of two-dimensional Gaussian copula:

$$c(u,v)=\frac{\exp\{-\frac{1}{2(1-\rho)^2}[\rho^2\emptyset^{-1}(u)^2-2\rho^2\emptyset^{-1}(u)\emptyset^{-1}(v)+\rho^2\emptyset^{-1}(v)^2]\}}{\sqrt{1-\rho^2}} \quad (7\text{-}11)$$

where, $\emptyset^{-1}(\cdot)$ is the inverse function of standard normal distribution and ρ is the correlation parameter which is estimated through Kendall rank correlation coefficient τ.

According to [122] and [123], the definition of Kendall rank correlation coefficient τ is as follows. Let (x_1, y_1), (x_2, y_2),…, (x_n, y_n) be a set of observations of the joint random variables X and Y. Randomly select two observations (x_i, y_i) and (x_j, y_j) to make a pair. If both $x_i > x_j$ and $y_i > y_j$ or if both $x_i < x_j$ and $y_i < y_j$, the pair is said to be concordant. If $x_i > x_j$ and $y_i < y_j$ or if $x_i < x_j$ and $y_i > y_j$, the pair is said to be discordant. If $x_i = x_j$ or $y_i = y_j$, the pair is neither concordant nor discordant. The Kendall τ coefficient is defined

as in (7-12). The denominator is the total number pair combinations, so the coefficient must be in the range $-1 \leqslant \tau \leq 1$.

$$\tau = \frac{\text{number of concordant pairs-number of discordant pairs}}{n(n-1)/2} \tag{7-12}$$

If the rankings in X and Y are the same, the coefficient has value 1. If one ranking is the reverse of the other, the coefficient has value −1. If X and Y are independent, then we would expect the coefficient to be approximately zero.

There exists direct relationship between Kendall τ coefficient and the parameter ρ in copula function which is defined in (7-13).

$$\rho = \sin\left(\frac{\pi\tau}{2}\right) \tag{7-13}$$

7.3. Case Study

Again, the Aberystwyth 33 KV network is used for case study. After we get the forecasting error sequence of power injection on each node $\{E_{P,t+m}\}$ based on the methods introduced in 6.2.2, the correlation τ between busbars can be calculated according to (7-13).

Table 7-1 shows the Kendall τ coefficients between 16 nodes that have wind generation/ load demand in 20-hour ahead forecasting. The correlation matrix will change as lead time changes. That is because the error sequence of power injection forecasting on each busbar changes dramatically when the lead time changes.

Table 7-1 Kendall τ Coefficients between 16 Nodes in 20-hour Ahead Forecasting

	5023	**5022**	**5021**	**5020**	**5019**	**5018**	**5017**	**5016**	**5014**	**5013**	**5012**	**5010**	**5008**	**5005**	**2005**	**2004**
5023	1.000	0.229	0.338	0.157	0.031	0.031	0.348	0.153	0.149	0.089	0.102	0.006	0.122	0.017	0.006	0.034
5022	-	1.000	0.284	0.225	-0.023	-0.023	0.244	0.312	0.282	0.261	0.158	0.029	0.092	0.020	0.030	0.008
5021	-	-	1.000	0.137	0.059	0.059	0.295	0.035	0.116	0.046	0.044	0.043	0.041	-0.003	0.043	0.055
5020	-	-	-	1.000	-0.027	-0.027	0.196	0.319	0.302	0.330	0.166	0.015	0.049	-0.032	0.016	-0.028
5019	-	-	-	-	1.000	1.000	0.042	0.016	0.012	-0.010	0.064	0.311	0.051	0.039	0.310	0.398
5018	-	-	-	-	-	1.000	0.042	0.016	0.012	-0.010	0.064	0.311	0.051	0.039	0.310	0.398
5017	-	-	-	-	-	-	1.000	0.178	0.191	0.136	0.089	0.003	0.150	0.004	0.004	0.062
5016	-	-	-	-	-	-	-	1.000	0.458	0.525	0.181	0.048	0.051	-0.066	0.049	0.019
5014	-	-	-	-	-	-	-	-	1.000	0.403	0.260	0.022	0.068	0.031	0.024	-0.027
5013	-	-	-	-	-	-	-	-	-	1.000	0.177	0.019	0.053	-0.061	0.020	-0.018
5012	-	-	-	-	-	-	-	-	-	-	1.000	0.044	0.055	0.210	0.044	0.038
5010	-	-	-	-	-	-	-	-	-	-	-	1.000	0.035	0.036	0.998	0.334
5008	-	-	-	-	-	-	-	-	-	-	-	-	1.000	0.039	0.035	0.085
5005	-	-	-	-	-	-	-	-	-	-	-	-	-	1.000	0.036	-0.022
2005	-	-	-	-	-	-	-	-	-	-	-	-	-	-	1.000	0.334
2004	-	-	-	-	-	-	-	-	-	-	-	-	-	-	-	1.000

Fig. 7-3 compares the mean values and VARs of power flows on line 5010-5012 with and without considering correlations. Confidence level is set as 90%. The red lines are the power flow condition without correlations. The blue lines stand for the power flow condition with correlations. It is clearly shown that both the mean values and VARs of power flow on line 5010-5012 change significantly when correlation is considered. For line 5010-5012, under same confidence level, the difference between mean value and VAR becomes much larger when the correlation is considered.

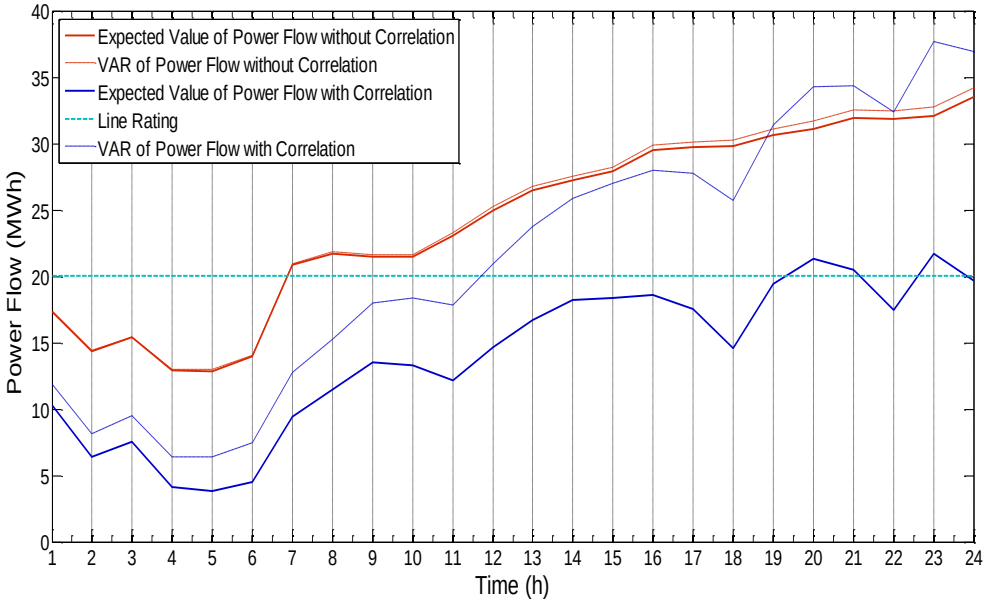

Figure 7-3 Comparison of Power Flow on Line 5010-5012

For line 5010-5012, the mean values of power flow are generally decreased. The number of timeslots with line overloading reduces from 18 (from 7:00 to 24:00) to 3 (20:00, 21:00 and 23:00). However, it does not mean the power flows on all lines are reduced when correlation is integrated. Table 7-2 gives the changes of power flows in several lines. The power flows on some lines are reduced while those on the others are increased.

Table 7-2 lists the effects of correlations on network power flows. The first and second columns list the lines connected between node A and node B. The third and fourth columns are the mean values of power flows without and with correlation, respectively. Since the node directly connected to the line has the largest influence on the line. Table 7-2 lists the correlations between node A and node B, which are in the fifth column.

Table 7-2 Change in Power Flows due to Correlation

Node A	Node B	PPF without correlation	PPF with correlation	Correlation
5023	5022	-2.088	-39.400	0.229
5013	5017	-27.051	-34.732	0.136
5013	5021	-9.710	9.493	0.046
5021	5022	5.497	17.799	0.284
5013	5016	4.396	-115.410	0.525
5008	5010	-4.094	-9.325	0.035
5018	5020	20.172	21.088	-0.027
5018	5017	29.978	20.169	0.042
5020	5021	17.135	18.715	0.137
5013	5014	4.773	-94.383	0.403
5013	5012	-27.901	-78.747	0.177
5010	5012	31.197	21.336	0.044
5008	5013	11.987	5.976	0.053
5008	5005	0.001	0.0005	0.039
5017	5008	-0.578	-6.866	0.15
5023	5022	-2.088	-39.400	0.229

Fig. 7-4 indicates the impact of correlations on the calculation of uncertain power flow more clearly. Red line is the difference in power flow for the lines listed in Table 7-2, and blue line is correlation values for these lines. Generally speaking, the trends of these two curves are concordant. It is reasonable since the system without considering correlation is a special case of the system with correlation, where the coefficient of correlation is zero.

Larger correlation always results in larger difference in power flow. There are some fluctuations in the consistency between correlation and difference in power flow. It is because Fig. 7-4 only lists the correlation which has largest impact on the line, while the power flow on the line is determined by all the busbars in the network.

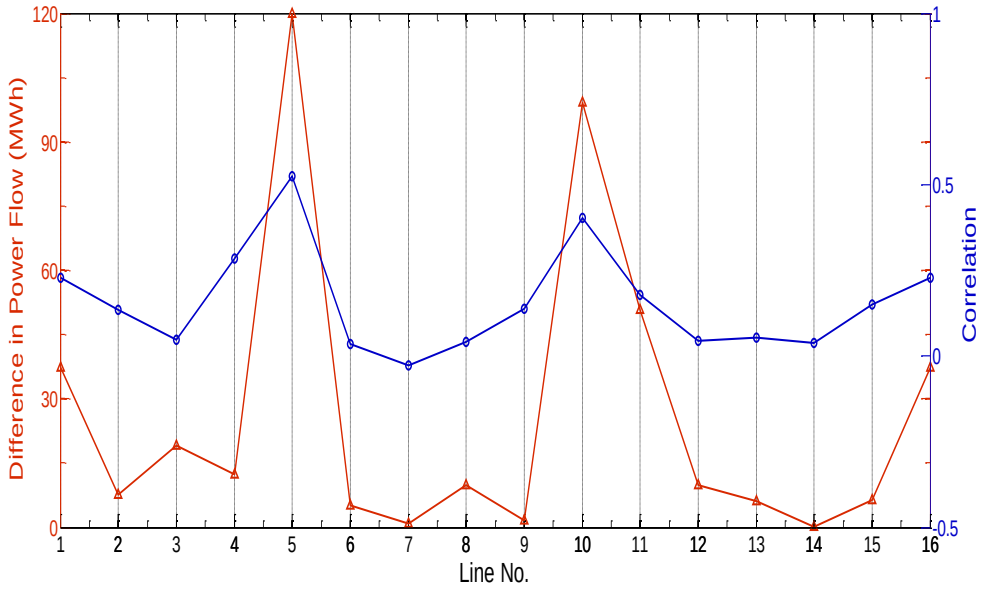

Figure 7-4 Comparison of Power Flows and Correlations

Fig. 7-5 gives the result of EV charging optimisation with RAROC method when the correlations are considered, which is represented by the blue line. The red line is the RAROC results when the busbars are assumed to be independent, which is consistent with Fig.6-9. The effect of correlation on RAROC value is significant. The average value scale of RAROC increases from 2 to 14 when correlation is considered. Trial 5 gets the largest RAROC (14.853) when correlation is involved, while trial 18 has largest RAROC (1.995) if the busbars are independent. The reason that causes the significant increases in the value scale of RAROC is explained later in Table 7-4.

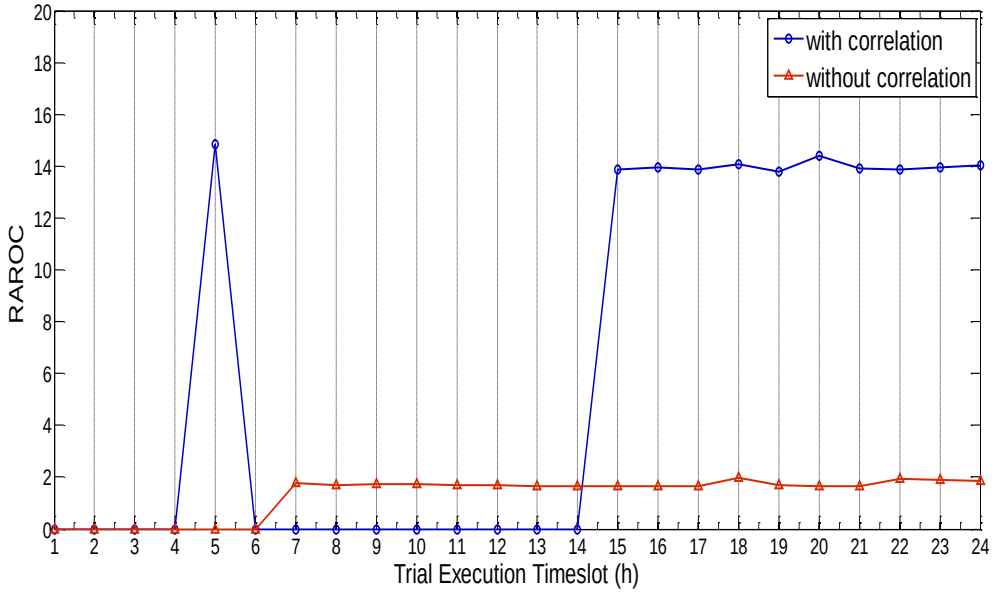

Figure 7-5 Selection of Execution Timeslot in RAROC method

For timeslot 5, when no correlation is considered, the mean value of power flow on line 5020-5021 is 9.608 MWh. This value climbs to 17.916MWh when correlation is considered. The line rating of 5020-5021 is 17.06MWh. Thus, there is overloading occurs in timeslot 5 when correlation is involved. The busbars that have high PTDF to line 5020-5021are listed in Table 7-3. According to Table 7-1, most of the sensitive busbars have correlations with each other, and the values of many correlation coefficients are quite high. Thus, the power flow on 5020-5021 is changed a lot when correlation is involved.

Table 7-3 PTDFs for Line 5020-5021

Busbar	**PTDF (5020-5021)**
5023	-0.197
5022	-0.197
5021	-0.197
5020	0.550
5019	0.340
5018	0.340
5017	0.061
5012	0.001
5010	0.008
5009	0.025
5008	0.025
2005	0.008
2004	0.025

Table 7-4 uses the performance of trial 18 in the system with and without correlation as an example to further explain the effects of correlation on generation curtailment and RAROC. According to the data in Table 7-4, when correlation is considered, the difference between mean values and VARs of generation curtailment is increased by a large quantity, which is consistent with the situation of power flow in Fig. 7-3. Quote the definition of RAROC in Chapter 6 to (7-15). The increasing difference between mean value and VAR of generation curtailment will increase the operational benefit, which is the numerator in (7-15). The increasing range in numerator is much higher than that in denominator, resulting in significant increase in the value of RAROC.

$$RAROC_T = \sum_{k=1}^{k=TWS} \frac{VAR_{GC_{0,k}} - \mu_{GC_{T,k}}}{VAR_{GC_{T,k}}} \tag{7-15}$$

Table 7-4 Performance for Trial 18 with and without Correlation

Time (h)	With correlation			Without correlation		
	GC_EX (MWh)	GC_VAR (MWh)	RAROC of each timeslot	GC_EX (MWh)	GC_VAR (MWh)	RAROC of each timeslot
1	0.000	0.000	–	0.000	0.000	–
2	0.000	0.000	–	0.000	0.000	–
3	0.000	0.000	–	0.000	0.000	–
4	0.000	0.000	–	0.000	0.000	–
5	1.947	5.131	0.731	0.000	0.000	–
6	0.000	0.699	1.000	0.000	0.000	–
7	0.000	0.000	–	1.253	1.501	0.165
8	0.000	1.228	1.000	2.703	3.011	0.102
9	0.000	0.000	–	2.154	2.517	0.144
10	0.000	0.000	–	1.833	2.106	0.130
11	0.000	0.000	–	4.102	4.453	0.064
12	0.000	1.245	1.000	6.663	7.032	0.043
13	0.000	5.648	1.000	8.416	8.853	0.049
14	0.000	16.768	1.000	9.672	10.109	0.043
15	1.680	21.766	0.923	10.429	10.960	0.049
16	8.632	30.984	0.721	12.415	12.958	0.042
17	0.940	24.143	0.965	12.826	13.446	0.046
18	1.829	27.612	0.813	14.841	24.900	0.403
19	2.837	23.956	0.882	15.689	25.109	0.375
20	6.270	39.958	0.843	15.114	17.084	0.115
21	8.688	45.032	0.807	16.570	18.679	0.113
22	8.106	42.532	0.809	25.636	26.526	0.034
23	13.047	53.729	0.757	26.061	26.996	0.035
24	8.810	52.086	0.831	27.905	28.899	0.034
Total	62.785	392.515	14.083	214.281	245.139	1.987

7.4. Chapter Summary

This chapter analyses the effects of correlation of forecasting errors between nodal power injections on the enhanced congestion management. Firstly, Copula theory is applied to integrate the correlations in the calculation of uncertain power flow. Then, according to the distribution of uncertain power flow, RAROC method is used to guide the congestion management.

Simulation results in the case study show that the network power flows are dramatically changed when correlations are considered, which will significantly influence the corresponding generation curtailment and the decision-making in congestion management. Copula theory helps to visualise the correlations in the calculation of uncertain power flow, which provides the DNOs with a more accurate network stress prediction and a more convincing congestion management strategy.

CHAPTER 8. THESIS SUMMARY AND FUTURE WORK

This chapter draws the conclusion to the thesis by outlining the key findings. Future work that can improve the investigations of ANM and uncertainty analysis are also presented.

8.1. Thesis Summary

Two contributions are made in this thesis to the area of ANM. First, it enhances the previous congestion management by integrating intelligent EV charging. The intelligent EV charging strategy refers to economically shifting flexible EV load demand over time to absorb excessive wind generation when they cannot be exported to the supply network. The enhanced congestion management can further improve network efficiency of the existing distribution networks to accommodate increasing DGs. The cost-benefit assessment informs DNOs of the trade-off between investment in ANM strategy and in the primary network assets, thus helping them to make cost-effective investment decisions.

Second, it enhances the congestion management further by integrating uncertainty management. The uncertainty management strategies refer to SR and RAROC methods which can help the enhanced congestion management make operational decisions when both operational benefit and its associated risk are considered. Through converting the operational benefits under different uncertainty levels to an equivalent benefit value under per unit uncertainty level, the impacts of uncertainty on the performance assessment can be 'mitigated'. Thus the traditional deterministic cost-benefit assessment can be extended to cost-benefit-risk assessment. Besides, the proposed uncertainty management strategy requires low calculation burden and is scalable to any systems, which is the major contribution of this thesis.

The design of the strategy focuses on the following five steps.

8.1.1. Designing an Intelligent EV Charging Model

An intelligent EV charging model is designed and integrated into the previous congestion management to help release the network stresses and reduce generation curtailment. A concept called Time-Window Scale is used to set up a time horizon to restrain coordinated EV charging. When and how much the charging demand should be shifted is determined by network power flows. Where to shift the demand is optimised to align with the wind generation, thus minimise the year round generation curtailment.

Furthermore, the intelligent EV charging is constrained by the number of EVs, battery characteristics and road travel behaviour in an area.

A practical 33kV network is exemplified as a test system for enhanced congestion management with intelligent EV charging. Based on the historical load profile in year 2006, the load demand of the network from 2030 to 2050 is forecasted, including the EV electricity consumption. Through the cost-benefit assessment, it is found that with intelligent EV charging, congestion management can further reduce generation curtailment up to 7.9%, i.e. 7.9% more renewable energy could be absorbed in the network. It is also found that larger time-window scale always produces better performance, resulting in more generation curtailment reduction. The annual generation curtailment amount decreases from 1672.9 MWh in 2-hour time-window scale to 1649.2 MWh in 24-hour time-window scale.

The increased benefits from integrating intelligent EV charging are also found to be highly dependent on electricity price and its uncertainty, which is thus worth noting in optimal network asset investment. The highest net investment profit is increased by £566k. In general, intelligent EV charging provides a viable and promising enhancement to previous congestion management, particularly for networks with high penetrations of renewable generation.

8.1.2. Enhancing Intelligent EV Charging Model

An enhanced intelligent EV charging model is established with two improvements. First, the shifting of EV charging demand is optimised to be bi-directional, i.e. the excessive load could be shifted to either earlier hours or later hours. Second, the shifting principle is enhanced with power flow constraint.

Aberystwyth 33kV network is used to test the enhanced charging model. Simulation results in the case study prove that the proposed enhance EV charging model can increase the utilisation level of renewable generation further compared with initial EV charging model. In a small range of time horizon (24 hours), the first improvement can reduce the generation curtailment further by 45%. The magnitude of the second improvement is not as significant as the first one, but it still can reduce the annual

generation curtailment by 0.05%. In terms of annual operational benefits, the enhanced intelligent EV charging can save renewable energy further by 3.93% in average.

8.1.3. Uncertainty Management with SR Method

Based on the enhanced intelligent EV charging, an uncertainty management model is designed to deal with the uncertainties introduced from wind forecasting error in the congestion management. Firstly, uncertain network power flow is calculated based on traditional convolution method. Then, SR concept from financial risk management is applied to assess the benefits of EV charging solutions when they are under differing risk levels. SR method compares the performance of the charging solutions by converting their operational benefits under different uncertainty levels into an equivalent benefit value under per unit uncertainty level, i.e. 'mitigating' the effect of uncertainties in the decision-making stage of EV charging optimization.

In order to simplify the strategy, the busbars are assumed to be independent. And the distribution of wind forecasting error is assumed to be normal distribution, which is validated by Monte Carlo Simulation. Although many research have investigated the effects of uncertainties, most of the work focuses on reliability analysis and uncertain power flow calculation. Little work has been done in ANM. This thesis states a specific problem in active network operation which has never been investigated, and provides a completely new way to treat uncertainty. Therefore, it is difficult to validate SR method with other methods. The only way to verify SR method is to prove the rationality of its definition, which is detailedly demonstrated in case study.

The principle of SR method is very straight forward and has low calculation burden, which implies that it can be easily applied to other power system areas with uncertainty problems. In general, SR method allows the impact of risks that arise from network stress prediction on the expected operational benefits to be properly assessed, thus extending the traditional deterministic cost-benefit assessment to cost-benefit-risk assessment.

8.1.4. Enhancing Uncertainty Management with RAROC method

SR method utilises standard deviation to describe the risk level of benefit. However, it is only suitable in the model where the variables follow normal distribution. If the probability density functions of variables are non-normal, the standard deviation is no longer the proper parameter to describe risk level of benefit. Thus, the enhanced uncertainty management model (RAROC method) is established based on SR method, but with higher applicability.

RAROC method utilises VAR to represent the risk level rather than standard deviation. Sequence operation theory is applied to calculate uncertain network power flow considering both wind and load forecasting errors.

The simulation results indicate that with RAROC method, more network uncertainties can be integrated in uncertainty management, even when they are in different distribution patterns. The VARs of power flows can be easily determined based on the statistics of uncertain power flow and can represent the risk levels appropriately. The results also indicate that the decision-making will change when the confidence level changes. In one word, the proposed RAROC method addresses the type limitation on the distribution of forecasting error in SR method, providing an enhanced uncertainty management in congestion management.

8.1.5. Enhancing Uncertainty Management with Correlations

The uncertainty management is further developed to integrate the correlations of forecasting errors between nodal power injections. Since wind forecasting is strongly dependent on weather condition in an area, the wind forecasting errors on different busbars in the area have strong correlations with each other. Besides, the load forecasting errors on different busbars somehow also have correlations since weather influences the electricity consumption pattern. Thus, forecasting error of power injections on one busbar is correlated with other busbars. The real-time deterministic control is not able to integrate the correlations.

Copula theory is applied to integrate the correlations into the calculation of uncertain power flows. Then, according to the distribution of uncertain power flow, RAROC method is used to guide the congestion management. Simulation results in the case study show that the power flows are dramatically changed when correlations of forecasting errors between nodal power injections are considered, which will significantly influence the corresponding generation curtailment and the decision-making in congestion management. Copula theory helps to visualise the correlations in the calculation of uncertain power flow, which provides the DNOs with a more accurate network stress prediction and a more convincing congestion management strategy.

8.2. Research Limitations and Future Work

8.2.1. Improve Intelligent EV Charging with EV Customer Types

The performance of the intelligent EV charging method is tested and proved to be profitable already. However, the customer type of EVs in this thesis is assumed to be domestic only. The behaviour of different customer types (domestic, commercial and industrial) will be significantly different. To generalise the application of intelligent EV charging, a study can be carried out in the future to study and compare the characteristics of different customer types. Therefore, the intelligent EV charging model should be modified accordingly to differentiate and identify common points between customer types.

8.2.2. Improve Intelligent EV Charging with Market Pricing

The objective of the intelligent EV charging model proposed in this thesis is to minimise generation curtailment. However, the market price is not considered in the model. In practice, the three constraints mentioned in the thesis: number of EVs, EV battery characteristics and road trip limitations are not sufficient to restrain the intelligent charging since the customers are normally who decide the charging time for their EVs according to the electricity price.

Accordingly, there may be a mismatch between the customer's will and the network's will in deciding the most appropriate shifting levels of the flexible EV charging demand. There should be incentives to guide customers to align the timeslots of their EV charging with the available renewable generation. The incentives will be reflected in the electricity price, which will be the cost of intelligent EV charging. Therefore, there will be two targets in intelligent EV charging: minimisation of both generation curtailment and incentive costs.

8.2.3. Intelligent EV Charging between Busbars

The intelligent EV charging in this thesis focuses on shifting load over time on the same busbar. If the flexible EV charging demand can be shifted between different busbars first when there is congestion, followed by load shifting over time, the network congestion and generation curtailment will be further reduced. In that case, the customer diversity in the network should be considered and analysed. The determination of EV flexibility on different busbars will be more complicated due to the uncertainties introduced form customers' trip routes and their willingness to charge their EVs in other area.

8.2.4. Extend Intelligent EV Charging by Considering Several Intermittent Renewable Energy Resources

This thesis has analysed the "EV-wind complementarity". In the near future, the UK government also emphasises the development of solar photovoltaic (PV) in distribution networks because of its versatility and scalability. The integration of PV will increase the network uncertainty. Although wind and PV are all intermittent resources, their power output characteristics are significantly different. The power output from PVs is focused on daytime while the output from wind farms will not be time-restrained. Generally speaking, the wind in the night is much stronger than that over the day. Thus, if PV generation is to be applied in intelligent EV charging, the relationship between wind and PV generation should be properly analysed under uncertainty management.

REFERENCE

[1] Department of Energy and Climate Change, "UK Renewable Energy Roadmap Update 2013," November 2013.

[2] Department of Energy and Climate Change, "UK Renewable Energy Roadmap," July 2011.

[3] Department of Energy and Climate Change, "Draft Report on capturing the full electricity efficiency potential of the U.K.," July 2012.

[4] S. Jupe and P. Taylor, "Strategies for the control of multiple distributed generation schemes," 20th International Conference and Exhibition on Electricity Distribution - Part 1, CIRED, pp. 1-4, 2009.

[5] R. Dunn, Z. Hu and F. Li, "Benefit Assessment of AuRA-NMS on Loss Reduction and Investment Deferral," Department of Electronic & Electrical Engineering, University of Bath, 2009.

[6] A. K. Gooding, R. A. F. Currie, G. W. Ault, D. F. MacLeman, and C. E. T. Foote, "Tackling smartgrid deployment challenges," 20th International Conference and Exhibition on Electricity Distribution - Part 1, CIRED, pp. 1-4, 2009.

[7] P. Djapic, C. Ramsay, D. Pudjianto, G. Strbac, J. Mutale, N. Jenkins, *et al.*, "Taking an active approach," IEEE Power and Energy Magazine, vol. 5, pp. 68-77, 2007.

[8] F. D. A. Collinson, A. Beddoes, and J. Crabtree, "Solutions for the connection and operation of distributed generation," U.K. Department of Trade and Industry (DTI) New & Renewable Energy Programme, 2003.

[9] R. A. F. Currie, G. W. Ault, C. E. T. Foote, G. M. Burt, and J. R. McDonald, "Fundamental research challenges for active management of distribution networks with high levels of renewable generation," 39th International Universities Power Engineering Conference (UPEC), vol.2, pp. 1024-1028, 2004.

[10] R. Hidalgo, C. Abbey, and G. Joos, "A review of active distribution networks enabling technologies," IEEE Power and Energy Society General Meeting, pp. 1-9, 2010.

[11] C. L. Masters, "Voltage rise: the big issue when connecting embedded

generation to long 11 kV overhead lines," Power Engineering Journal, vol. 16, pp. 5-12, 2002.

[12] D. A. Roberts, "Network management system for active distribution networks - a feasibility study," DTI, K/EL/00310/REP, 2004.

[13] R. Macdonald, G. Ault, and R. A. F. Currie, "Deployment of Active Network Management technologies in the UK and their impact on the planning and design of distribution networks," IET-CIRED Seminar ON SmartGrids for Distribution, pp. 1-4, 2008.

[14] R. A. F. Currie, G. W. Ault, C. E. T. Foote, and J. R. McDonald, "Active power-flow management utilising operating margins for the increased connection of distributed generation," IET Generation, Transmission & Distribution, vol. 1, pp. 197-202, 2007.

[15] Z. Hu and F. Li, "Cost-Benefit Analyses of Active Distribution Network Management, Part I: Annual Benefit Analysis," IEEE Transactions on Smart Grid, vol. 3, pp. 1067-1074, 2012.

[16] S. C. E. Jupe, P. C. Taylor, and A. Michiorri, "Coordinated output control of multiple distributed generation schemes," IET Renewable Power Generation, vol. 4, pp. 283-297, 2010.

[17] M. J. Dolan, E. M. Davidson, G. W. Ault, and J. R. McDonald, "Techniques for managing power flows in active distribution networks within thermal constraints," 20th International Conference and Exhibition on Electricity Distribution - Part 1, pp. 1-4, 2009.

[18] E. M. Davidson, M. J. Dolan, S. D. J. McArthur, and G. W. Ault, "The Use of Constraint Programming for the Autonomous Management of Power Flows," 15th International Conference on Intelligent System Applications to Power Systems, pp. 1-7, 2009.

[19] E. M. Davidson, S. D. J. McArthur, M. J. Dolan, and J. R. McDonald, "Exploiting intelligent systems techniques within an autonomous regional active network management system," IEEE Power & Energy Society General Meeting, pp. 1-8, 2009.

[20] M. J. Dolan, E. M. Davidson, G. W. Ault, K. R. W. Bell, and S. D. J. McArthur, "Distribution Power Flow Management Utilizing an Online Constraint Programming Method," IEEE Transactions on Smart Grid, vol. 4, pp. 798-805, 2013.

[21] L. F. Ochoa, A. Keane, C. Dent, and G. P. Harrison, "Applying active network management schemes to an Irish distribution network for wind power maximisation,"20th International Conference and Exhibition on Electricity Distribution - Part 1, CIRED, pp. 1-4, 2009.

[22] R. A. F. Currie, G. W. Ault, and J. R. McDonald, "Methodology for determination of economic connection capacity for renewable generator connections to distribution networks optimised by active power flow management," IEE Proceedings-Generation, Transmission and Distribution, vol. 153, pp. 456-462, 2006.

[23] Y. Wu and J. Hong, "A literature review of wind forecasting technology in the world," IEEE Lausanne Power Tech, pp. 504-509, 2007.

[24] N. Leemput, J. Van Roy, F. Geth, P. Tant, B. Claessens, and J. Driesen, "Comparative analysis of coordination strategies for electric vehicles," IEEE PES in Innovative Smart Grid Technologies (ISGT Europe), pp. 1-8, 2011.

[25] Department of Energy and Climate Change, "A Smart Grid Routemap," Feb. 2010.

[26] J. O. G. Tande and K. Uhlen, "Wind turbines in weak grids-constraints and solutions," 16th International Conference and Exhibition on Electricity Distribution, 2001. Part 1: Contributions. CIRED. vol. 4, p. 5, 2001.

[27] U. S. Department of Energy,"2009 wind technologies market report,"[Online] http://www.nrel.gov/docs/fy10osti/48666.pdf.

[28] J. Mutale, "Benefits of active management of distribution networks with distributed generation," IEEE Power Systems Conference and Exposition, pp. 601-606, 2006.

[29] P. Siano, P. Chen, Z. Chen, and A. Piccolo, "Evaluating maximum wind energy exploitation in active distribution networks," IET Generation, Transmission & Distribution, vol. 4, pp. 598-608, 2010.

[30] G. Strbac, N. Jenkins, T. Green, D. Pudjianto, "Review of innovative network concepts," Imperial College London and University of Manchester, Technical Report for DG-Grid2006.

[31] D. Porter, G. Strbac and J. Mutale, "Ancillary services market opportunities in active distribution networks," 2nd Int. Symp. on Distributed Generation: Power System and Market Aspects, Session 9: Active Networks, 2002.

[32] E. Technology, "A technical review and assessment of active network

management infrastructures and practices," Report to U.K. Department of Trade and Industry (DTI), Apr. 2006.

[33] G. Strbac, N. Jenkins, M. Hird, P. Dja and G. Nicholson,"Integration of operation of embedded generation and distribution networks," Department of Electrical Engineering &Electronics, University of Manchester, 2002.

[34] M. Fila, D. Reid, G. A. Taylor, P. Lang, and M. R. Irving, "Coordinated voltage control for active network management of distributed generation," IEEE Power & Energy Society General Meeting, pp. 1-8, 2009.

[35] V. Thornley, J. Hill, P. Lang, and D. Reid, "Active network management of voltage leading to increased generation and improved network utilisation," IET-CIRED Seminar in SmartGrids for Distribution, pp. 1-4, 2008.

[36] J. Hiscock, N. Hiscock, A. Kennedy, "Advanced Voltage Control for Network with Distributed Generation," CIRED, 2007.

[37] S. Grenard, D. Pudjianto, and G. Strbac, "Benefits of active management of distribution network in the UK," 18th International Conference and Exhibition on Electricity Distribution, CIRED, pp. 1-5, 2005.

[38] Electricity Association, "Guidelines for actively managing power flows associated with the connection of a single distributed generation plant," Engineering Technical Report 124 (ver-002)2003.

[39] Z. Hu and F. Li, "Distribution network reinforcement utilizing active management means," IEEE Power and Energy Society General Meeting, pp. 1-3, 2010,.

[40] T. Luo, G. Ault, and S. Galloway, "Demand Side Management in a highly decentralized energy future," 45th International Universities Power Engineering Conference (UPEC), pp. 1-6, 2010.

[41] V. Hamidi, F. Li, L. Yao, and M. Bazargan, "Domestic demand side management for increasing the value of wind," China International Conference on Electricity Distribution, pp. 1-10, 2008,.

[42] G. Strbac, " Demand-side management: benefits and challenges," Energy Policy Vol.36, pp. 4419–4426, 2008.

[43] C. W. Gellings, "The concept of demand-side management for electric utilities," Proceedings of the IEEE, vol. 73, pp. 1468-1470, 1985.

[44] P. Palensky and D. Dietrich, "Demand Side Management: Demand Response, Intelligent Energy Systems, and Smart Loads," IEEE Transactions on Industrial

Informatics, vol. 7, pp. 381-388, 2011.

[45] R. C. Green, L. Wang, and M. Alam, "The impact of plug-in hybrid electric vehicles on distribution networks: a review and outlook," IEEE Power and Energy Society General Meeting, pp. 1-8, 2010.

[46] Z. Li, H. Sun, Q. Guo, Y. Wang, B. Zhang, "Study on wind-EV complementation in transmission grid side," IEEE Power and Energy Society General Meeting, pp. 1-12, 2011,.

[47] J. Taylor, A. Maitra, M. Alexander, D. Brooks, and M. Duvall, "Evaluation of the impact of plug-in electric vehicle loading on distribution system operations," IEEE Power & Energy Society General Meeting, pp. 1-6, 2009,.

[48] S. Shao, M. Pipattanasomporn, and S. Rahman, "Grid Integration of Electric Vehicles and Demand Response With Customer Choice," IEEE Transactions on Smart Grid, vol. 3, pp. 543-550, 2012.

[49] G. Li. and X. Zhang, "Modeling of Plug-in Hybrid Electric Vehicle Charging Demand in Probabilistic Power Flow Calculations," IEEE Transactions on Smart Gri,, vol. 3, pp. 492-499, 2012.

[50] A. Lojowska, D. Kurowicka, G. Papaefthymiou, and L. van der Sluis, "Stochastic Modeling of Power Demand Due to EVs Using Copula," IEEE Transactions on Power Systems, vol. 27, pp. 1960-1968, 2012.

[51] S. S. Raghavan and A. Khaligh, "Impact of plug-in hybrid electric vehicle charging on a distribution network in a Smart Grid environment," IEEE PES Innovative Smart Grid Technologies (ISGT), pp. 1-7, 2012.

[52] O. Sundstrom and C. Binding, "Flexible Charging Optimization for Electric Vehicles Considering Distribution Grid Constraints," IEEE Transactions on Smart Grid, vol. 3, pp. 26-37, 2012.

[53] E. M. Davidson, M. J. Dolan, G. W. Ault, and S. D. J. McArthur, "AuRA-NMS: An autonomous regional active network management system for EDF energy and SP energy networks," IEEE Power and Energy Society General Meeting, pp. 1-6, 2010.

[54] T. Green, "AuRA-NMS: A substation automation project for a potential smart grid," IET Conference on Substation Technology 2009: Analysing the Strategic and Practical Issues of Modern Substation, pp. 1-30, 2009.

[55] E. M. Davidson, S. McArthur, C. Yuen, and M. Larsson, "AuRA-NMS: Towards the delivery of smarter distribution networks through the application of multi-

agent systems technology," IEEE Power and Energy Society General Meeting - Conversion and Delivery of Electrical Energy in the 21st Century, pp. 1-6, 2008.

[56] T. Ikegami, K. Ogimoto, H. Yano, K. Kudo, and H. Iguchi, "Balancing power supply-demand by controlled charging of numerous electric vehicles," IEEE International Electric Vehicle Conference (IEVC), pp. 1-8, 2012.

[57] K. Clement, E. Haesen, and J. Driesen, "Coordinated charging of multiple plug-in hybrid electric vehicles in residential distribution grids," IEEE/PES Power Systems Conference and Exposition, pp. 1-7, 2009.

[58] Q. Kejun, Z. Chengke, M. Allan and Y. Yue, "Load model for prediction of electric vehicle charging demand," International Conference on Power System Technology (POWERCON), pp. 1-6, 2010.

[59] I. Grau, S. Skarvelis-Kazakos, P. Papadopoulos, L. M. Cipcigan, and N. Jenkins, "Electric Vehicles support for intentional islanding: A prediction for 2030," North American Power Symposium (NAPS), pp. 1-5, 2009.

[60] Market Transformationg Programme, "UK Household and Population Figures 1970 - 2030," 2010 [Online]: www.mtprog.com.

[61] "Low Carbon Networks Fund: Screening Submission Pro-forma," [Online]:https://www.ofgem.gov.uk/ofgem-publications/46025/enwl-capacity-customers-isp-proforma.pdf.

[62] Y. Zhang, C. Gu and F. Li, "Evaluation of investment deferral resulting from microgeneration for EHV distribution networks," IEEE Power and Energy Society General Meeting, pp. 1-5, 2010.

[63] C. Lin, W. Hsieh, C. Chen, C. Hsu, T. Ku, and C. Tsai, "Financial Analysis of a Large-Scale Photovoltaic System and Its Impact on Distribution Feeders," IEEE Transactions on Industry Applications, vol. 47, pp. 1884-1891, 2011.

[64] Ofgem report, "Project Discovery: Energy Market Scenarios Update," 2010.

[65] J. Zhu, "Uncertainty analysis in power systems," John Wiley & Sons, Inc. : Hoboken, NJ, USA. pp. 545-596, 2009.

[66] A. S. Dobakhshari and M. Fotuhi-Firuzabad, "A Reliability Model of Large Wind Farms for Power System Adequacy Studies," IEEE Transactions on Energy Conversion, vol. 24, pp. 792-801, 2009.

[67] C. D'Annunzio and S. Santoso, "Wind power generation reliability analysis and modeling," in IEEE Power Engineering Society General Meeting, Vol. 1, pp. 35-39, 2005.

[68] R. Billinton and A. A. Chowdhury, "Incorporation of wind energy conversion systems in conventional generating capacity adequacy assessment," IEE Proceedings- Generation, Transmission and Distribution, vol. 139, pp. 47-56, 1992.

[69] S. Wang and M. E. Baran, "Reliability assessment of power systems with wind power generation," IEEE Power and Energy Society General Meeting, pp. 1-8, 2010.

[70] R. Billinton and H. Dange, "Effects of Load Forecast Uncertainty on Bulk Electric System Reliability Evaluation," IEEE Transactions on Power Systems, vol. 23, pp. 418-425, 2008.

[71] H. Dange and R. Billinton, "Load forecast uncertainty considerations in bulk electric system reliability assessment," 40th North American Power Symposium, pp. 1-8, 2008.

[72] R. Billinton and H. Dange, "Aleatory and Epistemic Uncertainty Considerations in Power System Reliability Evaluation,"10th International Conference on Probabilistic Methods Applied to Power Systems, pp. 1-8, 2008.

[73] M. Q. Wang and H. B. Gooi, "Effect of uncertainty on optimization of microgrids," IPEC, pp. 711-716, 2010.

[74] M. A. Ortega-Vazquez and D. S. Kirschen, "Estimating the spinning reserve requirements in systems with significant wind power generation penetration," IEEE Power & Energy Society General Meeting, 2009.

[75] I. Ziari, G. Ledwich, A. Ghosh, and G. Platt, "Integrated Distribution Systems Planning to Improve Reliability Under Load Growth," IEEE Transactions on Power Delivery, vol. 27, pp. 757-765, 2012.

[76] V. F. Martins and C. L. T. Borges, "Active Distribution Network Integrated Planning Incorporating Distributed Generation and Load Response Uncertainties," IEEE Transactions on Power Systems, vol. 26, pp. 2164-2172, 2011.

[77] R. Rubinstein and D. Kroese, "Simulation and the Monte Carlo Method, 2nd Edition", February 2008, Hoboken: NJ: Wiley.

[78] B. Borkowska, "Probabilistic Load Flow," IEEE Trans. Power Apparatus and Systems, vol. PAS-93(3), pp. 752-759, 1974.

[79] R. N. Allan, B. Borkowska, and C. H. Grigg, "Probabilistic analysis of power flows," the Institution of Electrical Engineers, vol. 121, pp. 1551-1556, 1974.

[80] A. M. Leite da Silva, S. M. P. Ribeiro, V. L. Arienti, R. N. Allan, and M. B. Do Coutto Filho, "Probabilistic load flow techniques applied to power system expansion planning," IEEE Transactions on Power Systems, vol. 5, pp. 1047-1053, 1990.

[81] R. N. Allan, A. M. Leite da Silva, and R. C. Burchett, "Evaluation Methods and Accuracy in Probabilistic Load Flow Solutions," IEEE Transactions on Power Apparatus and Systems, vol. PAS-100, pp. 2539-2546, 1981.

[82] R. N. Allan and M. R. G. Al-Shakarchi, "Probabilistic a.c. load flow," the Institution of Electrical Engineersvol. 123, pp. 531-536, 1976.

[83] R. N. Allan and A. M. Leite da Silva, "Probabilistic load flow using multilinearisations," IEE Proceedings-Generation, Transmission and Distribution, vol. 128, pp. 280-287, 1981.

[84] A. M. Leite da Silva, V. L. Arienti, and R. N. Allan, "Probabilistic Load Flow Considering Dependence Between Input Nodal Powers," IEEE Transactions on Power Apparatus and Systems, vol. PAS-103, pp. 1524-1530, 1984.

[85] R. N. Allan, C. H. Grigg, D. A. Newey, and R. F. Simmons, "Probabilistic power-flow techniques extended and applied to operational decision making," the Institution of Electrical Engineers, vol. 123, pp. 1317-1324, 1976.

[86] P. Zhang and S. Lee, "Probabilistic load flow computation using the method of combined cumulants and Gram-Charlier expansion", IEEE Transactions on Power Systems, Vol. 19(1): p. 676-682, 2004.

[87] J. Usaola,, "Probabilistic load flow with wind production uncertainty using cumulants and Cornish-Fisher expansion," PSCC, July 2008.

[88] E. Rosenblueth, "Two-point estimates in probability," Applied Mathematical Modelling, vol. 5, pp. 329-335, 1981.

[89] C. Su, "Probabilistic load-flow computation using point estimate method," IEEE Transactions on Power Systems, vol. 20, pp. 1843-1851, 2005.

[90] J. Yu and W. Dong, "Voltage Security Analysis on the Distribution Network Integrated with Wind Power Using Probabilistic Load Flow," International Conference on E-Product E-Service and E-Entertainment (ICEEE), pp. 1-4, 2010.

[91] T. Kim, J. Choo, S. Lee, J. Kim and K. Kim, "Security assessment for bus voltages using probabilistic load flow," International Conference on Probabilistic Methods Applied to Power Systems, pp. 888-893, 2004.

[92] M. Cortes-Carmona, R. Palma-Behnke, and G. Jimenez-Estevez, "Fuzzy Arithmetic for the DC Load Flow," IEEE Transactions on Power Systems, vol. 25, pp. 206-214, 2010.

[93] S. Bhat, "Discussion of "Bibliography on the fuzzy set theory applications in power systems (1994-2001)"", IEEE Transactions on Power Systems, vol. 19, pp. 2117-2118, 2004.

[94] M. A. Matos and E. Gouveia, "The fuzzy power flow revisited," IEEE Power Tech, pp. 1-7, 2005.

[95] S. Naaz, "Effect of different defuzzification methods in a fuzzy based load balancing application," International Journal of Computer Science vol. 8(5), September 2011.

[96] P. Jorion, "Financial risk manager handbook plus test bank : FRM Part I/Part II", Series: Wiley finance. 2011: Hoboken, N.J. : Wiley.

[97] W. Sharpe, "The sharpe ratio", The Journal of Portfolio Management, p. Fall: 49-58, 1994.

[98] R. Brown, "Exponential smoothing for prediction demand", Cambridge, Massachusetts: Arthur D. Little Inc. , 1956.

[99] [Online]: http://en.wikipedia.org/wiki/Exponential_smoothing.

[100] NIST, "NIST/SEMATECH e-Handbook of Statistical Methods," 2010.

[101] duke.edu., "Averaging and Exponential Smoothing Models," September 2011.

[102] S. Wang. G. Wang, H. Liu, Y. Xue, P. Zhou, "Self-adaptive and dynamic cubic ES method for wind speed forecasting," Power System Protection and Control, vol. 42(15), pp. 117-122, 2014.

[103] C. Kang, Q. Xia and N. Xiang, "Sequence operation theory and its application in power system reliability evaluation," Reliability Engineering and System Safety, vol. 78(2), pp. 101-109, 2002.

[104] N. Zhang, "Clustered Wind Power Analysis and Decision Making Methodology Considering Spatial Dependency," PhD, Tsinghua University, 2012.

[105] C. Kang, Q. Xia, N. Xiang and L. Bai, "Sequence operation theory and its applications," Tsinghua University Press, 2003.

[106] F. X. Diebold, N. A. Doherty, and R. J. Herring, "The Known, the Unknown, and the Unknowable in Financial Risk Management: Measurement and Theory Advancing Practi," Princeton, N.J: Princeton University Press, 2010.

[107] [Online]: http://en.wikipedia.org/wiki/Risk-adjusted_return_on_capital.

[108] P. Jorion, "Value at Risk: The New Benchmark for Managing Financial Risk (3rd ed.)," McGraw-Hill, 2006.

[109] G. A. Holton,"Value-at-Risk: Theory and Practice second edition,"e-book, 2014.

[110] D. Harper," An Introduction To Value at Risk (VAR)," [Online]: http://www.investopedia.com/articles/04/092904.asp

[111] A. M. Leite da Silva and V. L. Arienti, "Probabilistic load flow by a multilinear simulation algorithm," IEE Proceedings-Generation, Transmission and Distribution, vol. 137, pp. 276-282, 1990.

[112] A. Schellenberg, W. Rosehart, and J. Aguado, "Cumulant-based probabilistic optimal power flow (P-OPF) with Gaussian and gamma distributions," IEEE Transactions on Power Systems, vol. 20, pp. 773-781, 2005.

[113] H. Mori and W. Jiang, "A New Probabilistic Load Flow Method Using MCMC in Consideration of Nodal Load Correlation," 15th International Conference on Intelligent System Applications to Power Systems, pp. 1-6, 2009,.

[114] R. Nelsen, "An Introduction to Copulas", New York: Springer, 1998,.

[115] S. Demarta and A. McNeil, "The t copula and related copulas," International Statistical Review, vol. 73, pp. 111-129, 2004.

[116] J. Rodríguez-Lallena and M.ú.-F.,, "Distribution functions of multivariate copulas," Statistics and Probability Letters, vol. 64(1), pp. 41-50, 2003.

[117] V. D. E. Bouyé, A. Nikeghbali, G. Riboulet, and T. Roncalli, "Copulas for finance: a reading guide and some applications," Working Paper of Financial Econometrics Research Centre, Working Paper of Financial Econometrics Research Centre, City University Business School, London2000.

[118] G. Papaefthymiou and D. Kurowicka, "Using Copulas for Modeling Stochastic Dependence in Power System Uncertainty Analysis," IEEE Transactions on Power Systems, vol. 24, pp. 40-49, 2009.

[119] H. Valizadeh Haghi and et al., "Using Copulas for analysis of large datasets in renewable distributed generation: PV and wind power integration in Iran," Renewable Energy, vol. 35, pp. 1991-2000, Sep. 2010.

[120] B. Stephen, S. J. Galloway, D. McMillan, D. C. Hill, and D. G. Infield, "A Copula Model of Wind Turbine Performance," IEEE Transactions on Power Systems, vol. 26, pp. 965-966, 2011.

[121] R. J. Bessa, J. Mendes, V. Miranda, A. Botterud, J. Wang, and Z. Zhou, "Quantile-copula density forecast for wind power uncertainty modeling," IEEE

PowerTech., 2011.

[122] [Online]: http://en.wikipedia.org/wiki/Kendall_tau_rank_correlation_coefficient.

[123] M. Kendall, "A new measure of rank correlation," Biometrika, vol. 30, pp. 81-89, 1938.

APPENDIX A

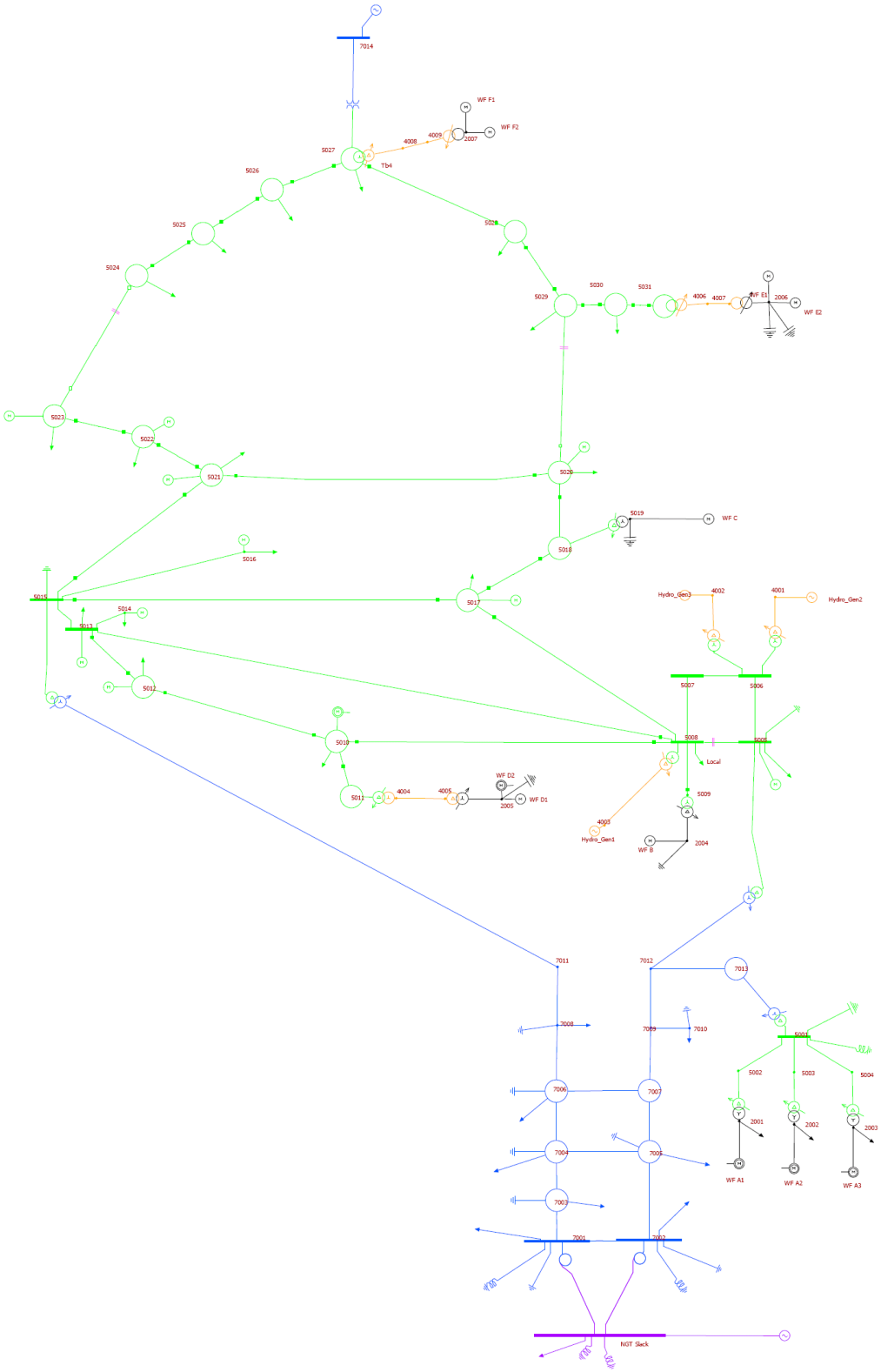

Figure A-1 Diagram of the 132/33kV Aberystwyth Network

APPENDIX B

Three assumptions are made in DC power flow:

1) Branches can be considered lossless, i.e. branch resistor R_m and charging capacitances B_m are negligible. The simplified expression of admittance Y_m on branches is shown in (B-1):

$$Y_m=\frac{1}{R_m+jX_m}\approx\frac{1}{jX_m} \tag{B-1}$$

where, X_m is the reactance.

2) The voltage magnitude of all busbars is close to 1 p.u. as shown below.

$$|V_i| \approx 1.0 \text{ p.u.} \tag{B-2}$$

3) Voltage angle θ differences across branches are very small so that

$$\sin(\theta_a-\theta_b) \approx \theta_a-\theta_b \tag{B-3}$$

Based on the intelligent EV charging model proposed in Chapter 4, in each trail T, the calculation of DC power flow at each timeslot k consists of following three steps:

1) Determine the active power injection $P_{T,k,i}$ at node i:

$$P_{T,k,i} =G_{T,k,i}-L_{T,k,i} \tag{B-4}$$

where, $P_{T,k,i}$ is the active power injection, $G_{T,k,i}$ is the forecasted generation, and $L_{T,k,i}$ is the deterministic load.

2) Calculate the voltage angle matrix θ of the network:

$$\theta=Y^{-1}\cdot P \tag{B-5}$$

where, Y is the admittance matrix of the network, and P is the matrix of active power injection on all busbars in the network.

3) Calculate the active power flows in branches:

$$PF_{T,k,m}=\frac{\theta_a-\theta_b}{X_m} \tag{B-6}$$

where, $PF_{T,k,m}$ is the power flow on line m between node a and b, X_m is the reactance of the line connecting node a and b.

According to (B-4)-(B-6), the relationship between injected power on each node and the power flow on each branch can be derived as below:

$$\frac{dPF_{T,k,m}}{dP_{T,k,i}} = \frac{Y_{am}^{-1} - Y_{bm}^{-1}}{X_m} \quad \text{(B-7)}$$

where, Y_{am}^{-1} and Y_{bm}^{-1} are elements in admittance matrix Y^{-1}.

Equation (B-7) indicates that the relationship between nodal injected power and branch power flow is linear. The linear relationship can be reflected in a sensitivity matrix called Power Transfer Distribution Factor (PTDF). Element PTDF(m,i) indicates the change of active power flow on line m when one unit of injected power is added on busbar

PUBLICATIONS

L. Zhou, F. Li, C. Gu, Z. Hu, and S. L. Blond, "Cost/Benefit Assessment of a Smarter Distribution System with Intelligent Electric Vehicle Charging," IEEE Transactions on Smart Grid, Vol. 5(2), pp.839 – 847, 2013.

L. Zhou, and F. Li, "Active Network Management considering Wind Forecasting Error," IEEE Transactions on Smart Grid, 2015 (under review).

J. Li, L. Zhou and F. Li, "Statistical Probability Based Transmission Congestion Cost Increasing Tendency Analysis," 48th International Universities' Power Engineering Conference (UPEC), 2013.